MULTI-LAYER ELECTROSPUN POEGMA HYDROGELS

ENGINEERING NANOFIBER MORPHOLOGY IN ELECTROSPUN POLY(OLIGOETHYLENE GLYCOL METHACRYLATE)-BASED TISSUE SCAFFOLDS

By CHLOE DAWSON, B.ENG,BIOSCI.

A Thesis submitted to the School of Graduate Studies in Partial Fulfillment of Requirements for the Degree Master of Applied Science

McMaster University

Master of Applied Science (2022) McMaster University

Chemical Engineering Hamilton, Ontario

TITLE: Engineering Nanofiber Morphology in Electrospun Poly(Oligoethylene Glycol Methacrylate)-Based Tissue Scaffolds

AUTHOR: Chloe Dawson, B.Eng.Biosci. (McMaster University)

SUPERVISOR: Dr. Todd Hoare

NUMBER OF PAGES: xviii, 117

Lay Abstract

Successful regeneration of diseased tissues relies first on understanding the healthy tissue structures and functions that currently exist within the body, and second, how to synthetically replicate those structures using biomaterials. Re-creating the natural networks that cells use to attach and grow has many challenges, including the challenge of creating nano-scale structures, controlling any immune response to the biomaterial(s) used, and ensuring the correct response of cells to the fabricated structures. One method of generating suitable nano-scale structures is through a process called electrospinning, specifically when it is used to produce hydrogel-based nanofibers which can bind large amounts of water. When implanted, hydrogels swell to form a hydrated environment suitable for cells. These nanofibers are generated on a scale that is smaller than the encapsulated cells to allow for guided cell responses to the material. Furthermore, the use of cell-friendly polymer solutions allows for cells to be in contact with the biomaterial without resulting in high cell death. In this thesis, aligned and/or multi-layered nanofiber structures are generated to replicate the naturally existing support structures seen in the body. These fibers are also loaded with cells to create semi-functional body tissues that in the future can serve to replace non-functional tissues or used to better understand cell interactions with their environment.

Abstract

Soft tissue engineering has become increasingly relevant in efforts to create complex, functional tissues for tissue replacement in tissue engineering applications or for the development of more complex tissue models for drug screening or fundamental research. Tissue engineering of micro- and nano-scale structures has been explored through a number of biofabrication techniques but most successfully on the nano-scale through electrospinning. Electrospun nanofibers represent one of the most similar structures to natural extracellular matrix (ECM), while electrospinning of hydrogel nanofibers is particularly relevant given that such nanofibers support the high water content environment required by cells to survive. Herein, a reactive cell electrospinning process is demonstrated based on dynamic hydrazone-crosslinked poly(oligoethylene glycol methacrylate (POEGMA) hydrogel nanofibers that can be electrospun from an aqueous solution, allowing for the generation of cell-loaded hydrogel nanofibers in a single fabrication/cell-seeding step. Using the proper collectors, the fabrication of aligned and/or multi-layered scaffolds is demonstrated without the risk of layer delamination due to the dynamic crosslinking of POEGMA hydrogels. Co-electrospun NIH 3T3 fibroblasts and Psi2 12S6 epithelial cells were found to proliferate over 14 days within the networks, while electrospun C2C12 myoblasts were found to align along the direction of aligned fibers. POEGMA hydrogels provide a suitable environment for cells and can be expanded to multi-layer, multi-cellular networks with tunable micro-architectures to better mimic more complex aligned (e.g. muscle) and/or multi-layer (e.g. smooth muscle vasculature, esophageal) tissues.

Acknowledgements

I would first like to thank my supervisor, Dr. Hoare - your guidance, knowledge, and encouragement has been extremely valuable and has taught me many lessons in and out of the lab. Thank you for the opportunity to begin researching and for always searching for new ways to innovate. Thank you to my committee, Dr. Grandfield and Dr. Latulippe - I have enjoyed having you both as professors over my time McMaster and am grateful for your guidance. Thank you also to our lab tissue engineering crew, Fei, Eva, Samaneh, Norma, Laura, Afshin - your support, answering of endless questions and collaboration has been one of my favourite parts of graduate school. I have learned so much from each of you and am truly thankful that you have been a part of my learning at McMaster. I cannot wait to see where each of you go next and I know you will be the best team members wherever that is. To the rest of the Hoare Lab, thank you for all your support, questions, guidance and fun times over the past few years. To everyone within McMaster, at CALM, CCEM, Paul Gatt and Justin Bernar, thank you for your support and help learn new techniques. Thank you to Dr. Shelir Ebrahimi and Dr. Vince Leung for the opportunities to be a teaching assistant with you especially through navigating the return virtual learning throughout COVID-19.

Thank you to my grandparents - your support of education and the importance of it passed onto your children has shaped the course of all of our lives. To all of my siblings, thank you for offering your perspective on the world. Your well-rounded knowledge inspires and encourages me to always continue learning in and out of my field and to listen to others. To my parents and their partners, your unwavering support of education has always made me feel like the options and opportunities available to me were only limited by my imagination. Thank you for listening and always trying to understand what I have been trying to do, hopefully this thesis helps. To my

lovely friends, thank you for making McMaster a home for so long. The times we shared here and challenges we sorted through together will always be some of the most special memories of my life. It is such a joy to watch each of you move forward and I cannot wait to join you over the next phases of our lives. Finally, to my partner, you make life more enjoyable in every way. Three degrees between us in 2 years has created a challenging environment that has been made infinitely better by your support. You bring a balance to my life that is invaluable and as we grow let us keep adding to our favourite memories with more adventures together.

Table of Contents

List of Figures

List of Tables

List of Abbreviations and Symbols

AA	Acrylic acid
ADH	Adipic acid dihydrazide
AFG	Aligned fibrin nanofiber hydrogel
AIBMe	2,2 azo-bis-isobutryic acid dimethyl ester
BHT	Butylated hydroxytoluene
BSA	Bovine serum albumin
CFSE	Carboxyfluorescein diacetate succinimidyl ester
CLSM	Confocal laser scanning microscopy
CNC	Cellulose nanocrystals
COA	Coefficient of alignment
CY5	Cyanine 5
Đ	Dispersity
DAPI	4′,6-diamidino-2-phenylindole
DexMA	Methacryalated dextran
DHT	Dehydrothermal treatment
DIW	distilled deionized water
DMEMAm	N,N-dimethylaminoethyl methacrylate
DMEM	Dulbecco’s Modified Eagle’s Medium
DRG	Dorsal root ganglia
ECM	Extracellular matrix
EDC	N′-ethyl-N-(3-(dimethylamino)propyl)-carbodiimide
FBS	Fetal bovine serum
Gel-HPA	Gelatinhydroxyphenylpropanoic acid
Gel-MA	Methacrylated gelatin
GPC	Gel permeation chromatography
GTA	Glutaraldehyde
FITC	Fluorescien isothiocyanate
HA	Hyaluronic acid
HCEC	Human corneal epithelial cells

HCl	Hydrochloric acid
HMSC	Human mesenchymal stem cells
HFIP	Hexafluoroisopropanol
HUVEC	Human umbilical vein endothelial cell
LUT	Look-up tables
$M(EO)_2MA$	Di(ethylene glycol) methyl ether methacrylate
MEHQ	Methyl ether hydroquinone
MHC	Myosin heavy chain
M_n	Number average molecular weight
NaOH	Sodium hydroxide
NMR	Nuclear magnetic resonance
$OEGMA_{500}$	Oligo (ethylene glycol) methyl ether methracrylate
PAAm	Polyacrylamide
PBS	Phosphate buffered saline
PCL	Poly (ε-caprolactone)
PCU	Poly(carbonate-urethane)
PEG	Poly (ethylene glycol)
PEGDA	Poly (ethylene glycol diacrylate)
PEO	Poly (ethylene oxide)
PHBV	Poly(hydroxybutyrate-co-hydroxyvalerate)
PLA	Poly (lactic acid)
PLLA	Poly (L-lactic acid)
PLLA-CL	Poly (L-lactic acid-co-caprolactone)
POA	Aldehyde-functionalized POEGMA
POEGMA	Poly (oligoethylene glycol methacrylate)
POH	Hydrazide-functionalized POEGMA
PS	Polystyrene
PVA	Poly (vinyl alcohol)
PVDF	Poly (vinylidene fluoride)
PVP	Poly (vinyl pyrrolidone)
RFG	Random fibrin nanofiber hydrogels

RGD	Arginylglycylaspartic acid
RHC	Recombinant human collagen
SC	Schwann cell
SEM	Scanning electron microscopy
SPION	Superparamagnetic iron oxide nanoparticles
TGA	Thioglycolic acid
UV	Ultraviolet

Declaration of Academic Achievement

The work presented below was written by the author in consultation with Dr. Todd Hoare with the exception of the following:

Chapter 1: Section 1.2 was re-purposed from a published review paper written by the author, Chloe Dawson, in collaboration with Dr. Fei Xu: Xu, F. *et al.* Hydrogels for Tissue Engineering: Addressing Key Design Needs Toward Clinical Translation. *Front Bioeng Biotechnol* **10**, 849831 (2022).

Chapter 2: Experiments, writing, and editing were carried out as a collaboration between Dr. Fei Xu and the author, Chloe Dawson. Meghan Kostashuk assisted with NMR and GPC polymer characterization results.

Chapter 3: All experimental and written work was planned, performed, and analyzed by the author, Chloe Dawson, with the exception of the following: Zheng Fu Zhou assisted with polymer synthesis, Meghan Kostashuk and Eva Mueller assisted with NMR data collection and analysis, Gurpreet Randhawa assisted with GPC data collection, and Paul Gatt assisted with the design and fabrication of the cell electrospinning drum.

1 Chapter 1: Introduction and Objectives

1.1 Hydrogels for Tissue Engineering & Tissue Modelling

Tissue engineering and regenerative medicine encompass both the replacement of older tissues for *in vivo* use and the creation more complex tissue models for *in vitro* screening[1,2]. Tissue engineering focused on extracellular matrix (ECM) replication prioritizes the fabrication of an environment suitable for cell attachment and proliferation, while other techniques of complex tissue fabrication more specific to tissue modeling (e.g. lab-on-a-chip platforms) recognize the importance of nutrient and waste flow within the tissue[3]. Organoid cell culture has also been explored to create cell models that enhance the replication of 3D body tissues when compared to 2D cell culture. The ability to create more accurate 2D and 3D cell models furthers our understanding of cell behaviours that are relevant for applications in tissue regeneration and drug screening[4-6].

The use of hydrogels for tissue engineering has been previously explored with promising results and increasing interest in soft tissue engineering. Hydrogels can be prepared from a wide range of synthetic and/or natural polymers and have a high capacity for water binding, including a capacity to swell in aqueous environments[7-9]. The high water content of hydrogels coupled with the structural support provided by polymeric materials can reproduce the mechanics of soft tissues, sparking increased research interest in hydrogels for soft tissue engineering. Natural hydrogel matrices pose advantages due to their inherently low cytotoxicity, while tunable properties such as stimulus responsiveness (temperature, pH, or magnetic response), degradation rate, or mechanical properties can be introduced through the use of synthetic polymers or the combination of both natural and synthetic polymers within the hydrogel[7]. Natural polymers commonly used in hydrogel

formation include collagen, hyaluronic acid (HA), dextran, gelatin, alginate, and chitosan, while commonly incorporated synthetic polymers include poly(ε-caprolactone) (PCL), poly (vinyl alcohol) (PVA), poly (vinyl pyrrolidone) (PVP), and poly (ethylene glycol)(PEG)-derivatives[7,10].

Structured hydrogels, defined as hydrogels that have defined micro/macro porosities in addition to the inherent nanoscale porosity of conventional hydrogels, offer particular advantages when exploring ECM replication for tissue regeneration, with the engineered deposition of hydrogel structures providing a more accurate structural replication of natural ECM. In particular, native ECM has a highly fibrous structure primarily as a result of the high contents of collagen, elastin, and fibronectin, which collectively represent the key ECM structural components that allow for cell re-modelling of the ECM, provide sites for cell attachment, and define the mechanical and elastic properties of all varieties of body tissues[11]. While decellularizing native ECM has been explored as a starting matrix for regenerative medicine given that it already contains such structures (Figure 1.1), decellularized ECM still requires a source of donor tissue and requires extensive purification processes to remove cells and other components that may stimulate immunorejection. As such, multiple nano and micro-fiber fabrication techniques have been developed to process natural and/or synthetic polymers into networks that can better recreate the fibrous nature of ECM[12].

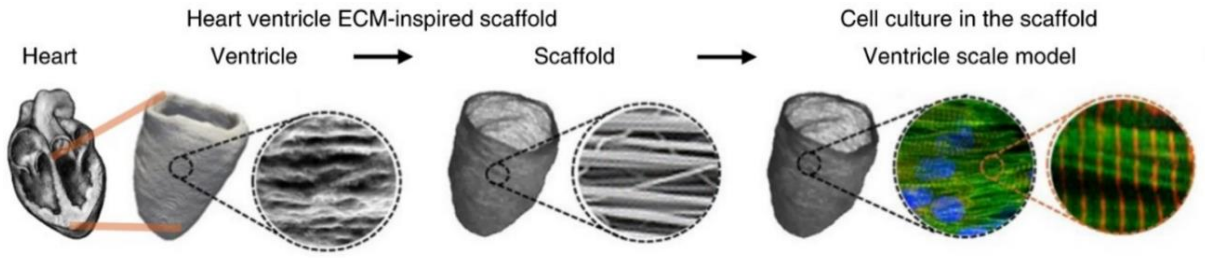

Figure 1.1. Experimental design of a ventricle model for cardiac tissue engineering with neonatal rat ventricular myocytes. Decellularized ECM was prepared as a comparison of natural ECM to the synthetic ECM prepared using nanofiber fabrication techniques. Adapted with permission from Springer Nature[12].

The fabrication of structured hydrogels can be achieved using a variety of techniques including bioprinting, freeze-casting, gas-foaming, and electrospinning[13]. Formation of structured hydrogels via bioprinting is currently the main area of structured hydrogel research given its high compatibility with cells and ability to print spatially-oriented features directly. Particular advances in this area are focused on the fabrication of new bioink formulations using a variety of polymers along with additives (i.e. growth factors) to better mimic the chemical environment of ECM[10]. Bioprinting allows for the purposeful deposition of biomaterials in an organized manner, resulting in a high level of control over hydrogel deposition. While new bioprinting techniques such as stereolithography bioprinting and digital light processing bioprinting[14] are being developed, effectively bioprinting "fiber" resolutions at scale remains a key challenge; extrusion bioprinted structures generally remain on the micron scale rather than the required nanoscale required to recreate most native ECM fibrous structures[14]. This bioprinting size resolution limitation can be related to challenges associated with tuning bioink gelation times (i.e. enabling flow during processing but not after deposition on the print platform), physical constraints when photo-crosslinking the bioink, cost[14], and the limited range of extrusion back-pressures that are printable

with small diameter nozzles, the latter being particularly problematic with high viscosity bioinks that (even if they can be printed) can introduce shear-driven cytotoxicity to encapsulated cells[10,14].

Other conventional hydrogel structuring methods also have key drawbacks for recreating ECM structures. Directional freeze-casting has been highlighted as a method of forming structured hydrogels with anisotropically aligned pores ideal for creating aligned tissues, using a temperature gradient to directionally freeze the polymer solution and thus induce alignment of ice crystal formation in the direction of the temperature gradient. After freeze-drying, the ice crystals are removed and a polymeric network is left behind with micro/macropores templated by the ice crystal development[15-18]. However, controlling morphologies on very small length scales remains challenging and the method is not relevant to the direct seeding of the cells during the fabrication process, requiring post-loading that may lead to less homogeneous cell distribtuions[15]. Alternately, gas-foaming can be used to produce macroporous hydrogels through the addition of gas-forming components such as various pore-forming agents or CO_2 generation. While the formation of pores using gas-foaming can be useful in developing porous scaffolds, control over pore size and distributions as well as the cytotoxic effects of foaming agents remains challenging[13].

1.2 Electrospun hydrogels

As an alternative, electrospinning is one of the most common and versatile nano-fiber fabrication techniques reported and has been used to fabricate many new forms of structured hydrogels. In electrospinning, a high voltage difference is applied between a needle extruding a precursor polymer solution and a conductive collector. When the electrostatic repulsion forces of the charged polymer solution overcome the surface tension of the polymer solution, a fiber is ejected [19] that can be collected on a grounded conductive collector, which may include rotating drums, flat

collectors, or parallel collectors [20-22]. The versatility and relatively low experimental complexity of the electrospinning setup makes it an accessible and feasible method of forming polymer nanofibers that have been widely used in a variety of tissue engineering applications[23,24]. The recent development of portable handheld electrospinning devices (in contrast to conventional devices that require a large power supply) has further expanded the potential of this technique[25], enabling the direct in situ application of polymeric nanofibers (to-date including PCL, polystyrene (PS), poly (lactic acid) (PLA) and poly (vinylidene fluoride) (PVDF)) in the clinic for wound healing and other applications[26].

Electrospinning requires careful tuning of several parameters including polymer concentration, solvent, relative humidity, high voltage, collector, working distance, solution viscosity, and flow rate[27]. When considering the electrospinning of hydrogels, crosslinking and gelation kinetics must also be considered, particularly relative to their effects on the polymer solution viscosity throughout the electrospinning process[21]; in particular, it is imperative to maintain a flowable solution at the needle outlet but produce a stable crosslinked fiber (or a sufficiently viscous fiber that buys time for covalent or physical crosslinking to occur) at the collector. Some methods of hydrogel electrospinning instead elect to crosslink as a postprocessing step of the nanofiber scaffold to avoid changes in viscosity to the electrospinning solution during the fabrication process itself; however, this choice adds an additional step to the process and may result in deformation of the original electrospun structure on the collector prior to the completion of the crosslinking process[28]. Electrospun hydrogels based on both natural polymers such as collagen, gelatin, dextran, alginate, HA, or chitosan as well as synthetic polymers such as POEGMA[21] have been reported, with other synthetic polymers such as poly (ethylene oxide) (PEO), PVP, or PVA also in some cases included to promote chain entanglement in the precursor polymer solution and thus nanofiber

formation instead of particle sprays. Stiffer degradable polymers such as PCL may also be added to increase the mechanical strength of the porous hydrogel scaffold, a key challenge with electrospinning[21,29-32].

Table 1.1 summarizes different materials and methods used for electrospinning hydrogels. Common crosslinking methods include chemical crosslinking through saturation of the scaffold with the chemical crosslinking agent, photocrosslinking with UV-light irradiation, and physical crosslinking such as the ionic crosslinking of calcium-alginate hydrogels[33,34], methods that will be further described in the following sections.

Table 1.1. Materials and methods used for electrospinning hydrogels for tissue engineering. Reproduced with permission[10].

	Materials	Solvent(s)	Crosslinking mechanism(s)	Voltage (kV)	Cells Incorporated	Nanofiber size (nm)	Key Biological Results	Specific Application
Natural Polymers	Collagen[35]	Hexafluoro-2-propanol	Chemical (EDC-NHS, genipin, transglutaminase, UV photo-crosslinking)	11	Human osteosarcoma MG-63 cells	106 ± 22	• Faster cell growth on EDC/NHS crosslinked scaffolds compared to TG or GP-crosslinked scaffolds over up to 21 days	Bone tissue engineering
	Collagen[36]	Hexafluoro-2-propanol and acetic acid	Chemical (EDC-NHS, glutaraldehyde, genipin)	20	Mc3T3-E1 cells	300-650	• Best cell proliferation observed using EDC-NHS as the crosslinker	Extracellular matrix model
	Collagen and chitosan[28]	Acetic acid and ethanol	Chemical (EDC)	16	HUVECs and NIH 3T3 fibroblast cells	168 ± 58	• Facilitated improved cell viability when compared to the tissue culture dish control	Wound Healing
	Gelatin[37]	Acetic acid, ethyl acetate and water	Chemical (glutaraldehyde, genipin, glyceraldehyde, reactive oxygen species)	12	MG63 osteoblastic cells	~300	• Glyceraldehyde-crosslinked nanofibers maintained highest cell viability and growth.	Tissue engineering
	Gelatin[38]	Acetic acid and water	Chemical (EDC, Genipin, GTA vapour)	15	HeLa epithelial cells	268 ± 18 nm	• EDC/NHS crosslinking resulted in the longest stability in a physiological-like environment	Tissue engineering

	Methacrylated dextran[39]	Sodium bicarbonate and HEPES	Chemical (UV photocrosslinking)	7.5	NIH 3T3 fibroblasts and human mesenchyme stem cells	<500	• Fiber scaffold stiffness did not affect cell viability, but remodeling of the scaffold occurred to a much higher degree in soft scaffolds	Extracellular matrix model
	GelMA[40]	Hexafluoro-2-propanol	Chemical (UV photocrosslinking)	15	Bone mesenchymal stem cells and hippocampal neuronal cells	~1000	• Decreased glial scar tissue formation, increased vascularization, and increased neuronal development compared to electrospun gelatin fibers crosslinked with glutaraldehyde	Spinal cord regeneration
Natural and Synthetic Polymers	Alginate and PEO[41]	Triple-distilled water	Physical (ionic crosslinking via $CaCl_2$)	10.5	C2C12 myoblast cells	250-400	• > 90% cell viability for 7 days • Cells grow along the direction of the aligned fibers	Skeletal muscle tissue regeneration
	Alginate, PEO, GelF-MA with Pluronic®F127[30]	Deionized water	Dual (ionic crosslinking with $CaCl_2$ + UV photocrosslinking)	7	Mesenchymal stem cells	183 ± 36	• <10% cytotoxicity and an 8-fold increase in cell proliferation observed over 2 weeks • Signs of maturation of the human iPSC-derived ventricular cardiomyocytes observed	Stem cell therapy and tissue regeneration

	Gelatin-hydroxyphenyl-propanoic acid (Gel–HPA) hexafluoroisoprop-anol (HFIP) and water[42]	Hexafluoro-2-propanol and water	Enzymatic (oxidation of the HPA moieties with the addition of horseradish peroxidase and H_2O_2)	18	HUVECs	~400-2000	• Full scaffold degradation observed within 4 weeks of *in vivo* implantation with good cell penetration.	Soft tissue engineering
	Thiolated hyaluronic acid (HA) and PEO[43]	DMEM cell medium	Chemical (disulfide formation + thiol-Michael addition following the post-fabrication addition of PEGDA)	18	NIH 3T3 fibroblasts	50-300	• Cells can infiltrate the scaffold up to 32 μm below the surface and showed an extended dendritic network morphology compared to 2D controls	Cell encapsulation and tissue regeneration
	Alginate and PEO[44]	Triple-distilled water	Physical (ionic crosslinking using $CaCl_2$)	10.5	HUVEC, C2C12, or H9c2 smooth muscle cells	328 ± 50-488 ± 67	• 90% cell viability maintained • Myogenic gene expression markers identified • 2154% increase in cell proliferation with HUVECs and seeded C2C12 cells	Muscle tissue regeneration
	Fibrinogen and PEO[45]	Deionized water	Chemical (thrombin-induced crosslinking)	4.5	C2C12 myoblasts	80,000-90,000	• Higher viability achieved by electrospinning aggregates and decreasing voltages • Induced myogenesis of C2C12 aggregates growing along the microfiber bundle	Mucle tissue regeneration

	Collagen and PVP[31]	Hexafluoro-2-propanol	Physical (pH-induced)	3.6	HUVECs	461 ± 129	• Altered crosslinking methods maintained the triple helical structure of collagen through the electrospinning process • HUVECs cultured on scaffolds along the fiber direction	Tissue engineering
	Chitosan and PVA[29]	Acetic acid	Physical (temperature-induced)	20	L-929 fibroblast cells	172 ±60 - 257 ± 63	• Attachment and proliferation of fibroblast cells over 5 days	Wound healing and tissue engineering
	Collagen and PVA[46]	Acetic acid and water	Dual (phosphoric acid +glutaraldehyde)	12-15	Human keratocytes (HKs) and human corneal epithelial cells (HCECs)	163-211	• HKs align to the fiber orientation • Good cell adhesion and proliferation over 4 weeks	Cornea tissue engineering
	Chitosan and PVA[47]	Acetic acid and water	Chemical (glyoxal)	15	Human normal fibroblast cells	227 ± 63	• 3.5x increased strength with 5% halloysite nanotubes (HNTs) incorporated into the fibers • HNTs-reinforced fibers exhibited better cell attachment on surface of nanofibers	Skin tissue regeneration
	Hyaluronic acid, PVA, L-arginine and cellulose	Water	Physical (citric acid)	28-30	Human normal lung fibroblast	122-222	• Increased fiber mechanical strength due to CNC addition	Wound healing and

	nanocrystals (CNCs) [48]				WI38 and skin melanocyte HFB-4 cells		• Increased ECM collagen synthesis, angiogenesis, and epithelialization	tissue engineering
Synthetic Polymers	Poly(oligoethylene glycol methacrylate) (POEGMA)and PEO[49]	DMEM cell medium and PBS	Chemical (*in situ* hydrazone crosslinking)	10	NIH 3T3 fibroblast and C2C12 myoblast cells	~400	• Cells can be encapsulated directly within POEGMA hydrogel nanofibers during electrospinning without and pre- or post-treatment • High cell viabilities after cell electrospinning and 3-4x cell proliferation over 18 days	Cell encapsulation and tissue engineering

1.2.1 Photocrosslinked Hydrogel Fibers

Methacrylated natural polymers such as alginate, gelatin and dextran have been electrospun to form photocrosslinked hydrogel scaffolds. Photocrosslinking can be used as the only crosslinking strategy or (depending on its speed) a secondary crosslinking step toward producing a multi-crosslinked hydrogel network[50]. For example, alginate, GelMA, PEO, and the photoinitiator Irgacure 2959 were electrospun, placed in a $CaCl_2$ bath (enabling rapid primary alginate-calcium ionic crosslinking) and subsequently exposed to 10 min of UV irradiation (enabling secondary GelMA photo-crosslinking). High cell viability (>90%) could be maintained coupled with an 8-fold increase of cell number in human iPSC-derived ventricular cardiomyocytes in 3D culture over 2 weeks of observation[30]. For soft tissues, photocrosslinking can be used directly to form the hydrogels. For example, GelMA dissolved in the solvent hexafluoroisopropanol (HFIP) was reported to fabricate aligned electrospun nanofibers that were subsequently submerged in anhydrous alcohol containing Irgacure 2959 and crosslinked under UV light for 60 min to form hydrogel nanofibers[40]. *In vivo* work showed that implantation of the GelMA scaffolds in rats enabled decreased glial scar tissue formation, increased vascularization, and increased neuronal development compared to electrospun gelatin fibers crosslinked with glutaraldehyde. The degree of crosslinking can also be tuned by adjusting the UV-light exposure time post-fabrication. Baker et al. (2015) similarly showed that DexMA could be electrospun to form a hydrogel scaffold with a range of scaffold moduli based on the UV exposure time. While the fiber scaffold stiffness did not affect cell viability, remodeling of the scaffold occurred to a much higher degree in the soft scaffolds[39]. However, it should be noted that there is considerable debate over the degree to which UV irradiation may impact encapsulated cells (both in the short term and the long term). While the wavelength and the total dose (intensity + time) of the irradiation certainly does influence the

degree to which UV irradiation may impact encapsulated cells, access to alternative crosslinking strategies (particularly for cells that have less robust viability in vitro) is recommended.

1.2.2 Chemically Crosslinked Hydrogel Fibers

Electrospun hydrogels can also be formed by chemically crosslinking the polymer components via covalent bond forming chemistries. Common chemical crosslinking agents include N-(3-dimethylaminopropyl)-N′-ethylcarbodiimide hydrochloride (EDC, for crosslinking proteins), genipin (for crosslinking aminated polymers), glutaraldehyde (GTA, for crosslinking hydrazide and aminated polymers), and glyoxal (for crosslinking hydroxylated polymers) [36,47]. Such crosslinking agents are typically added either in liquid or vapor form following electrospinning to crosslink the hydrogel fibers[37], with the typically rapid hydration rate of the electrospun hydrogel when exposed to a moist or saturated environment potentially deforming the fibers (via swelling) on the same time scale as crosslinking. In addition, the cytotoxicity of many of these chemical crosslinking agents is a significant concern, with many studies having been published seeking to define the optimum type and concentration of crosslinker for maintaining high cell viability[34,36,38]. For example, Deng et al. (2018) examined the use of low concentrations of EDC co-electrospun recombinant human collagen (RHC), chitosan, and PEO in an acetic acid and ethanol solution to aid in solvent evaporation and dry fiber formation. The slow gelation that occurs at the low EDC concentration used results in the fabrication of hydrogel nanofibers with diameters of 168 ± 58 nm that facilitated improved seeded NIH 3T3 and human umbilical vein endothelial cell (HUVEC) cell viability when compared to the tissue culture dish control[28]; however, the fabrication of thicker scaffolds (requiring longer electrospinning times) may be challenging when the crosslinker is added directly to the electrospinning solution. As another example, genipin, EDC-NHS, and glutaraldehyde were compared to assess which crosslinker best maintained the triple helical

structure of electrospun collagen fibers[36], with the best cell proliferation observed using EDC-NHS as the crosslinker (although all three scaffolds exhibited improved cell proliferation relative to the control) [36]. Similarly, Torres-Giner et al. electrospun collagen dissolved in HFP, post-crosslinked the fibers with EDC-NHS, and then seeded with the scaffold with MG-63 cells, enabling faster cell proliferation and far more cell growth over 21 days compared to a genipin-crosslinked scaffold[35]. Genipin, GTA vapour, and glyceraldehyde have also been specifically compared by Sisson et al. as crosslinking agents for electrospun gelatin fibers, with glyceraldehyde-crosslinked nanofibers found to maintain the highest cell viability and growth[37]. However, any small molecule crosslinker that reacts non-bioorthogonally with proteins in or secreted from cells does offer some risk in terms of promoting undesired cell or (following implantation if the crosslinker is not thoroughly removed) tissue toxicity and should be used only judiciously.

Chemical crosslinking with GTA has also been explored in comparison to the physical crosslinking method of dehydrothermal treatment (DHT) for fabricating an electrospun collagen scaffold[51]. The triple helix in the collagen fibers was better maintained when using chemical crosslinking methods, with the use of GTA avoiding the need for heat application as is required with the DHT method[51]. Ammonia treatment of the collagen electrospun scaffold after fabrication to neutralize any remaining acetic acid further improved maintenance of the triple helix collagen structure in the fibers[51]. Using a volatile crosslinker can also facilitate both penetration throughout the scaffold and post-purification of the scaffold to ensure the removal of unreacted crosslinker; for example, a PVA/collagen blend electrospun in HFIP and crosslinked under phosphoric acid vapor followed by GTA vapor promoting suitable seeded cell viabilities and transparency for corneal tissue engineering applications[46].

Covalent chemical crosslinking can also enable more efficient entrapment of additives into the electrospun hydrogels without significantly compromising the crosslinking and mechanical strength of the scaffold. For example, Hussein et al. (2020) electrospun HA, PVA, cellulose nanocrystals (CNCs), and L-arginine to form hydrogel fibers with the PVA component chemically crosslinked through the addition of anhydrous citric acid prior to electrospinning. CNC addition serves to increase the mechanical strength of the fibers while L-arginine promotes ECM collagen synthesis, angiogenesis, and epithelialization, promoting improved cell viabilities when cells were seeded on the scaffold. The scaffold also had anti-microbial properties related to L-arginine release and faster wound closure times compared to controls[48]. However, the inclusion of multiple components in the electrospinning solution that may cross-interact in multiple ways can pose challenges with controlling the precursor solution viscosity and thus the uniformity of the electrospun hydrogel.

Enzymes can also be used as chemical crosslinking agents to minimize cytotoxicity. For example, a gelatinhydroxyphenylpropanoic acid (Gel–HPA) scaffold electrospun in hexafluoroisopropanol (HFIP) was crosslinked via enzymatic oxidation of the HPA moieties with the addition of horseradish peroxidase and H_2O_2[42]. Enzymatic crosslinking scaffold preparations reported full scaffold degradation within 4 weeks of *in vivo* implantation with good cell penetration[42]; however, the specific substrates required plus the cost of most enzymatic crosslinkers may limit the broad utility of this approach in the context of a larger manufacturing platform.

1.2.3 Solvent-Free Electrospun Hydrogels

While the use of organic solvents can be a useful tool in the formation of electrospun nanofibers due to the ease of solvent evaporation between the nozzle and the collector, emerging studies have focused on electrospinning polymer solutions in water to remove the need for solvent removal

before cell seeding and do not risk exposure of the seeded cells to cytotoxic crosslinking chemicals or photoinitiators. Altered experimental setups and polymer chemistries have both been explored as methods to reduce the need for electrospinning with organic solvents. First, the use of sacrificial sheaths can be used. Wakuda et al. (2018) reported a core-shell electrospinning approach in which the outer layer contained PVP while the inner layer consisted of collagen pre-crosslinked in a basic solution[31]. Post-fabrication, the PVP layer was dissolved to leave the insoluble collagen, avoiding challenges associated with maintaining the anisotropic triple helix structure in organic solvents[35,36]. HUVECs cultured on the surface of the formed collagen fibers followed the orientation of the fibers, unlike HUVECs seeded on collagen fibers electrospun in HFIP directly[31]. Second, latent click or click-like chemistries can be used to lock the printed nanofiber in place after electrospinning. For example, Ji et al. (2006) electrospun thiolated HA with PEO as an electrospinning aid in DMEM, enabling chemical crosslinking via both disulfide formation and thiol-Michael addition following the post-fabrication addition of poly (ethylene glycol)-diacrylate (PEGDA) [43]. 3T3 fibroblasts seeded on the scaffolds were found to infiltrate the scaffold up to 32 mm below the scaffold surface and showed better morphology compared to 2D cell culture controls[43]. However, this approach still required a post-treatment of a pre-electrospun nanofiber network.

Third, reactive electrospinning techniques have been developed in which *in situ*-gelling polymer pairs are co-delivered through a double-barrel syringe directly into the electrospinning process. For example, Xu et al. (2016) electrospun aldehyde and hydrazide-functionalized POEGMA polymers from a double-barrel syringe tuned to have gelation times that ensured free flow of the polymers at the needle tip but rapid gelation upon electrospinning, leveraging the acceleration of gelation rate as water evaporates and the polymers concentrate in the emitted jet; as such, the

nanofibers are sufficiently gelled upon hitting the collector that their structure can be maintained without the need for any post-processing/post-crosslinking step[21]. Of note, conducting the process in a biosafety cabinet can also directly produce sterile scaffolds without any additional sterilization requirement. Both protein-repellent and thermoresponsive electrospun POEGMA scaffolds were prepared by varying the polymer component ratios, with the latter found to expand and contract reversibly to facilitate cell adhesion (at physiological temperature) but rapid cell delamination within 2 min upon swelling of the scaffold at 4° C that could serve as a replacement for typical trypsin-based cell delamination methods[52].

1.2.4 Cell Electrospinning

All examples described to this point required separate fabrication and cell loading steps, with the use of solvents, the drying of the scaffold, and/or the challenges with conducting electrospinning in a sterile environment all limiting cell survival in addition to the shear and electric field stress placed on cells during the electrospinning process. Relatively few examples exist of combining these steps together, which is highly beneficial to avoid the need to seed cells onto the scaffold post-fabrication and introduce more flexibility into the elec trospinning process (akin to 3D printing) in terms of structuring different cell types within a single fabricated scaffold. The reactive electrospinning technique (Figure 1.2A) offers particular advantages in this regard given that no additional post-processing is required, enabling returning cells to an incubator in sterile conditions much faster than with other techniques, and the entire process is designed to run in water. The cell-friendly and high water-binding nature of the POEGMA electrospun fibers enabled high survivals of >80% of both NIH 3T3 fibroblasts and C2C12 myoblasts, survivals maintained even following cryoprotectant-free storage of the visibly “dry” scaffolds in liquid nitrogen over a 3 week period; in addition, 3-4x increases in cell number were observed over the 18-day observation period,

showing how the otherwise cell-repellent POEGMA scaffold could support cell adhesion and proliferation due to the nanofiber structure formed *in situ* around the cells during electrospinning[49,53].

A few other examples cell electrospinning have been reported using post-crosslinked nanofiber scaffolds. In one such example, C2C12 cells were suspended in a mixture of fibrinogen and the electrospinning aid PEO and electrospun into a collection bath containing thrombin to crosslink the fibers into fibrin (Figure 1.2B) [45]. Cell viability, and ultimate differentiation of the myoblasts into mature myotubes, was promoted through the electrospinning process by decreasing the voltage applied to 4.5 kV and by using more stable C2C12 cell aggregates rather than monodispersed cells[45]. As another example (Figure 1.2C), C2C12 myoblasts were electrospun in water with alginate and PEO (electrospinning aid) and then crosslinked in a calcium ion/DMEM bath for 2 min to produce hydrogel nanofibers with aligned morphologies[41]. The C2C12 cells maintained cell viabilities above 90% for 7 days and grew along the directions of the aligned fibers, with a follow-up study showing similar efficacy with HUVEC cells[44]. Subsequent seeding of C2C12 cells on top of the alginate/PEO/HUVEC fibers resulted in faster myoblast maturation compared to the same scaffold without the HUVECs[44]. However, the design of electrospinning strategies compatible with cells is still in its infancy despite offering enormous potential to create ECM mimics that can reproduce the nanofibrous internal morphologies of native ECM.

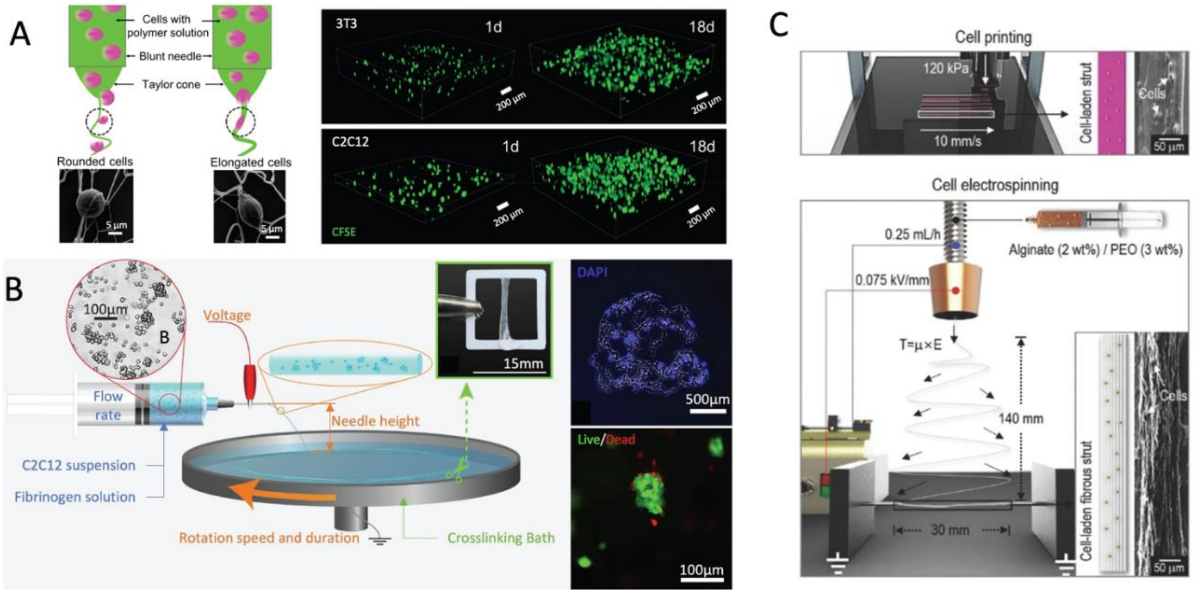

Figure 1.2. Strategies for cell electrospinning: (A) reactive electrospinning of 3T3 mouse fibroblasts and C2C12 mouse myoblasts in POEGMA hydrogel nanofibers[49]; (B) cell-laden electrospinning of C2C12 myoblasts in fibrin scaffolds[45]; (C) combining cell printing and cell electrospinning to encapsulate C2C12 myoblasts in alginate scaffolds[41]. Reproduced with permission[10].

1.3 Cell Alignment Techniques within Hydrogel Scaffolds

Aligned hydrogel networks have been increasingly investigated to provide cues to direct cell orientation to better reproduce the morphology and thus function of tissues that are natively aligned, including cardiac, smooth, and skeletal muscle as well as neural tissues[54]. The development of aligned tissues is relevant both in developing functional tissues for organ replacement as well as for tissue models that can enable more accurate drug screening and/or for moving current 2D cell culture methods towards cultures with more mature and differentiated tissues. For example, aligned fibrous networks have been demonstrated to provide key topographical cues to myoblast proliferation into elongated cell structures guided by fiber orientation, leading to highly ordered anisotropic structures of skeletal[41], cardiac[12], and smooth muscle[44] tissue that lead to simultaneous contraction of the tissue. Similar benefits have been

observed using aligned hydrogels to engineer more effective neural[40] and tendon[55] tissues. Electrospinning is the most common technique used to fabricate aligned, fibrous, hydrogel networks that replicate the natural aligned and fibrous properties of native ECM[10], although other techniques including pull-spinning[12], the application of external magnetic fields[56], micropatterning[57], directional freeze-casting[17], and templating by naturally aligned porous structures[58] have also been used. Pull-spinning, a technique similar to electrospinning but without the need for voltage, is particularly notable in that it does not require a conductive collector (increasing the flexibility of the fabrication process relative to electrospinning); however, it also requires far greater rotation speeds to generate aligned fibers which may not be suitable for cell incorporation into the fabrication solution[12,59]. As such, electrospinning is identified as the preferred method for creating aligned nanofibrous networks. Quantification of aligned structures as well as cell alignment in response to the aligned hydrogels are both crucial to allow comparison between techniques, which will be described in detail in the following section.

1.3.1 Aligned Hydrogels

Micropatterning techniques such as extrusion bioprinting have been effective in the deposition of hydrogel bioinks to fabricate microchannel collectors in which cells can be seeded within the microchannel and thus respond to the anisotropic nature of the patterned channels[60]. For example, human mesenchymal stem cells (HMSCs) seeded on soft polyacrylamide (PAAm) hydrogel films with or without aligned grooves with thicknesses of either 30 μm or 300 μm (generated by imprinting PCL fibers) indicated that the aspect ratio of the cells (i.e. the ratio of their length to width) changed when exposed to the aligned groves[57]. Higher aspect ratios were observed at four days of culture relative to one day as well as for cells cultured on aligned grooves compared to non-grooved substrates[57]. Similarly, the development of skeletal tissue models with improved

myoblast maturation was observed when C2C12 myoblasts were grown in micropatterned gelatin constructs with grooves 10 μm wide, with the C2C12 cells found to visually align with the direction of the grooves and sarcomere development found to be higher for cells grown on the patterned constructs relative to non-patterned gelatin hydrogels, plastic, or collagen-coated substrates[61].

Other templating techniques have also been examined. For example, bulk hydrogels with aligned microarchitectures were fabricated by extrusion of a cell-laden gelatin bioink through a nylon grid with varying pore sizes of 20-100 μm[62], with the bioink optionally functionalized with the cell adhesion peptide arginylglycylaspartic acid (RGD). The alignment of C2C12 myoblasts within the hydrogels was assessed by examining the elongation of the cell nucleus, which was found to be elongated in all hydrogels formed with the nylon grid but not within the bulk gels[62]. Cell-laden hydrogel bioinks have also been extruded as fibers to form anisotropic hydrogel structures with encapsulated cells. For example, a C2C12 myoblast-laden bioink comprised of PEG, fibrinogen, and alginate was extruded and post-crosslinked with $CaCl_2$ and photoirradiation (using Irgacure 2959 as a photoinitiator) to create bioprinted fibers with a diameter of 250 μm. The cells showed enhanced cell alignment relative to the direction of printing as well as enhanced expression of myoblast differentiation markers over 21 days[63]. Finally, as previously discussed, directional freeze-casting has also been used to fabricate aligned cell-laden networks in which polymer solutions are strategically frozen within a mold with a controlled temperature gradient. Upon lyophilization, the removal of ice crystals within the network leaves anisotropic pores to create an aligned structure for cell growth[17,64]. The majority of dorsal root ganglia seeded on a directional freeze-casted chitosan mold were found to align within a 10° window relative to the alignment of the fabricated grooves[17].

Across all alignment techniques, the enhanced micro-topography offered by aligned scaffold structures emphasizes the need for structured hydrogels that can guide cell proliferation on the micro-scale. Nanoscale aligned features are more difficult to fabricate but are more representative of the native nanoscale features of ECM.

1.3.2 Aligned Cells within Electrospun Hydrogels

While other techniques for producing aligned hydrogels provide suitable sites for cell adhesion, proliferation, and biomaterial response, the nanoscale features of native ECM are challenging to reproduce using most methods outside of electrospinning. Aligned electrospun fibers have been used in applications for neural, tendon, skin, and cardiac tissue engineering[65], typically enabled by designing customized electrospinning setups/collectors[20,41] or collection strategies (e.g. altering drum rotation speed, a simple but effective method of achieving aligned electrospun fibers[66]). The key to effective alignment is typically proper collector design. In the following section, the design and implementation of different collector designs for creating aligned hydrogel nanofibers will be discussed.

1.3.2.1 Rotation Speed-induced Fiber Alignment

Alteration of collector drum rotation speed (primarily with cylindrical drum or disk collectors) has been demonstrated to achieve effective alignment of a series of different electrospun hydrogel nanofibers. Higher rotation speeds generate more tightly aligned fibers when compared to lower speeds[66], introducing opportunities for creating both tunable alignment and fiber network density within the same electrospinning setup (Figure 1.3). For example, aligned POEGMA nanofibers were electrospun on top of a base POEGMA-CNC hydrogel layer already mounted to a cylindrical collector drum and then thermally wrinkled in a direction parallel and perpendicular to fiber

alignment. Cells seeded on the wrinkled substrate with electrospun fibers showed cell alignment to the sheets quantified through assessment of cell aspect ratio[67]. Alternately, aligned PCL and gelatin fibers for cardiac tissue engineering were formed by using a rotating disk which when rotated at high speeds formed aligned fibers. These fibers, when seeded with primary cardiomyocytes from rabbits, were found to align in the direction of the fibers visualized through troponin-T and α-actinin staining. Additionally, when the mechanical properties of the networks were tested in two directions both parallel and perpendicular to the fiber orientation, the scaffolds had higher mechanical strengths when tested in the same direction as fiber orientation[68].

Altering the rotation speed of a rotating platen has also been used to generate aligned methacrylated dextran (DexMA) fibers with varying degrees of stiffness based on the length of UV cross-linking post-fabrication reaction. Decreased fiber stiffness was found to increase cell interactions with the fibers and changed the degree of re-modeling of the network, confirming the need for soft hydrogel ECM options[39]. The cell-adhesion peptide RGD was also incorporated into the fibers to increase cell binding to and allow for more direct analysis of the bulk mechanical changes between the scaffolds rather than different capacities of the cells to adhere[39].

Combinations of synthetic polymers and natural ECM components have also been demonstrated to create bioactive aligned electrospun fibers. For example, polylactic acid and collagen were combined to form aligned electrospun networks using a rotating drum for tendon-fascicle tissue engineering (Figure 1.4A). Staining of the cell nucleus and F-actin filaments revealed the cell structure of seeded non-tumoral human fibroblasts that elongated over 21-days of culture[55]. Alternately, an aligned fibrin nanofiber hydrogel (AFG) made from fibrinogen, thrombin, and PEO was generated for use as a nerve guidance conduit in peripheral nerve injury repair. Post-crosslinking, unidirectional spreading of the dorsal root ganglia neurites was observed on random

fibrin nanofiber hydrogels (RFG) but oriented spreading was observed on aligned fibrin nanofiber hydrogels (Figure 1.5) [69].

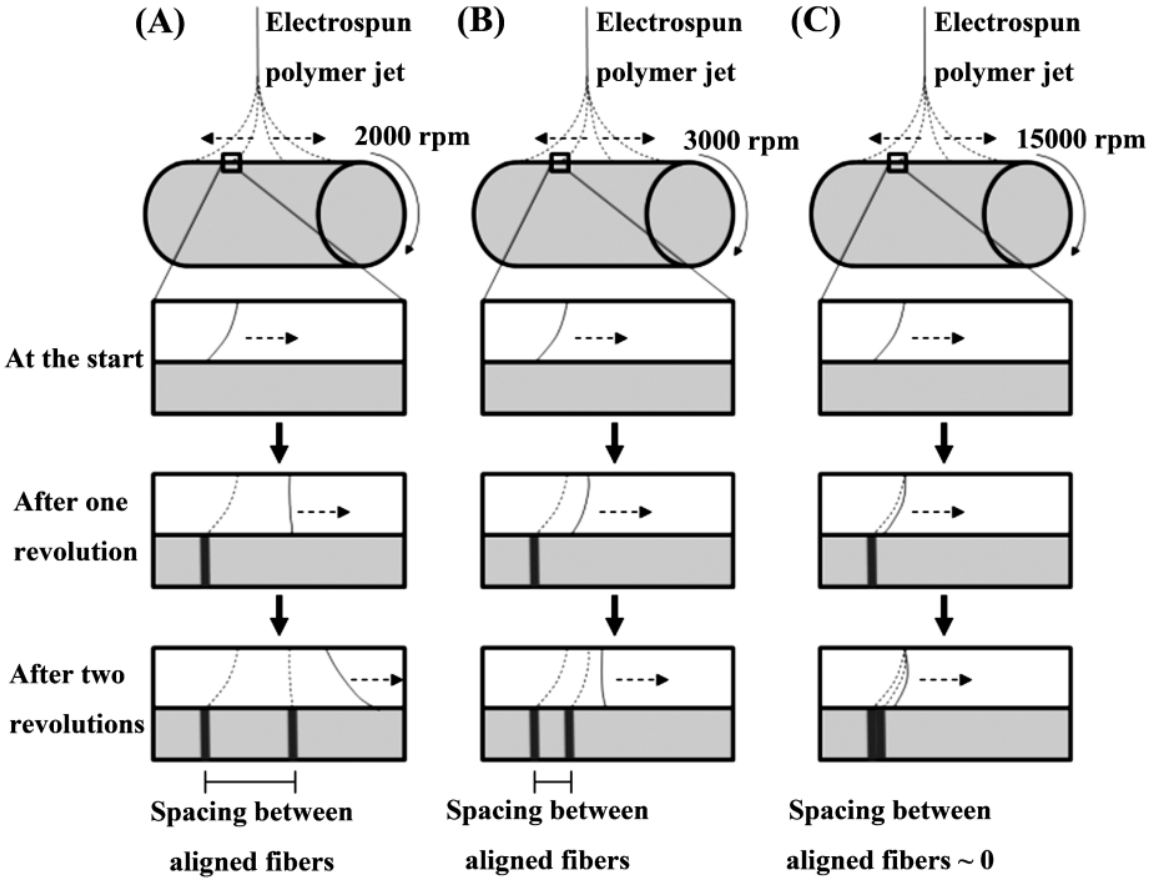

Figure 1.3. Evaluation of drum rotation speed on fiber spacing from 2000 to 15000 rpm. Reproduced from Tong et al with permission[66].

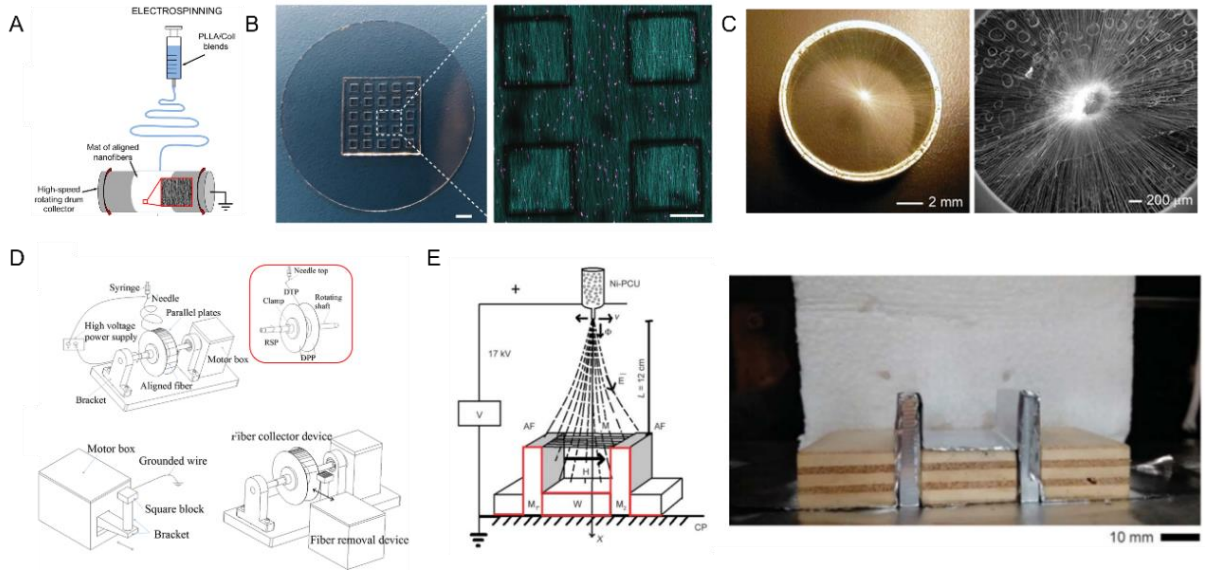

Figure 1.4. Demonstrations of a variety of collectors used to generate aligned electrospun hydrogel fibers including (A) a rotating drum[55], (B) parallel electrodes[70], (C) a ring and point electrode, adapted with permission from Xie et al. Copyright 2010 American Chemical Society[71]. (D) a parallel plate combined with a rotating drum[72], and (E) magnetic field-assisted electrospinning[56]. Adapted from with permissions[55,56,70-72].

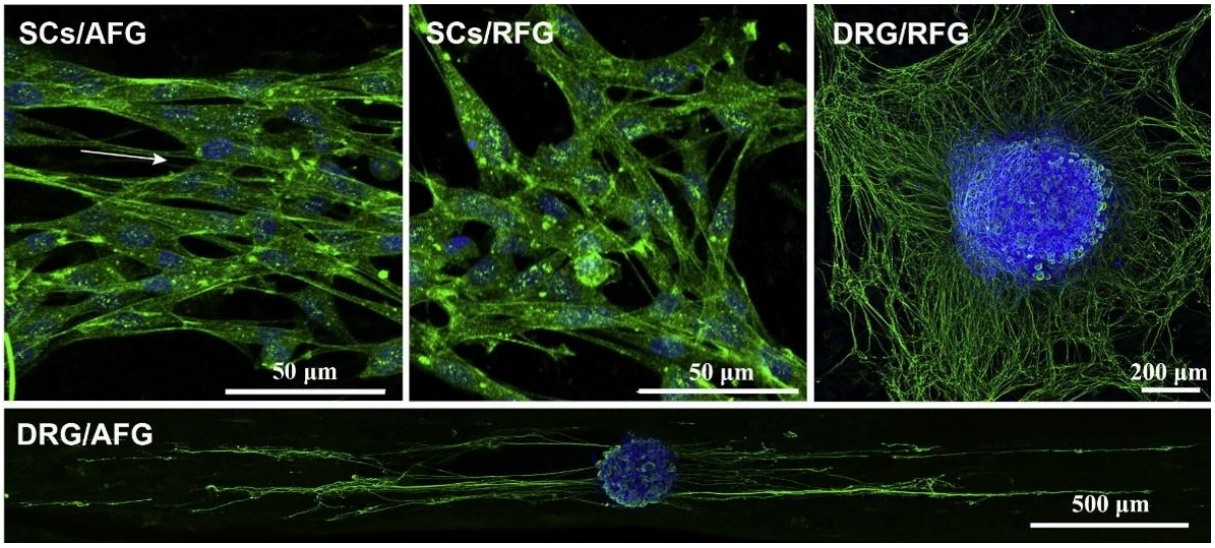

Figure 1.5. Schwann cell (SC) and dorsal root ganglia (DRG) response of aligned fibrin nanofiber hydrogels (AFG) and random fibrin nanofiber hydrogels. Adapted from Du et al. with permission[69].

1.3.2.2 Parallel Rod Collectors to Generate Aligned Fibers

Another common type of collector used to generate highly aligned fibers is the parallel rod or parallel electrode collector. These collectors used conductive rods separated by a well-defined distance (typically 0-3 cm to generate a network of fibers suspended between the rods. Similar to the aligned methacrylated dextran (DexMA) fibers generated with a rotating drum[39], re-modelling by NIH 3T3 cells of the soft and stiff aligned DexMA networks fabricated with a parallel rod collector was found to be more efficient in soft fiber environments, enabling cells in aligned networks to demonstrate increased migration and directionality (Figure 1.4B) [70]. Parallel collectors have also been used with cell electrospinning, as previously discussed with an alginate and PEO bioink[41] (Figure 1.2C); examining the C2C12 cell orientation and aspect ratio by staining the F-actin filaments of the cells with phalloidin indicated that cells within the aligned fibers enabled a 2.8-fold increase in aspect ratio compared to the same cell bioink used with a 3D printer, showing the advantages of using electrospun fibers to guide directional cell growth (Figure 1.6) [41]. Spinal cord regeneration was examined through the fabrication of aligned GelMA fibers formed using parallel electrodes, with seeded bone mesenchymal stem cells showing responses to the alignment of the fiber orientation[40]. While parallel electrodes remain a simple method of fabricating highly aligned fibers, control over alignment is relatively lower for a fixed collector (i.e. while the geometry of the collector can be altered, it is harder to alter the rest of the process). In contrast, with a rotating drum the rotation speed and/or the distance between parallel electrode collectors could be adjusted, facilitating the fabrication of non-aligned and aligned fibers with the same collector[70] to improve nanofiber alignment.

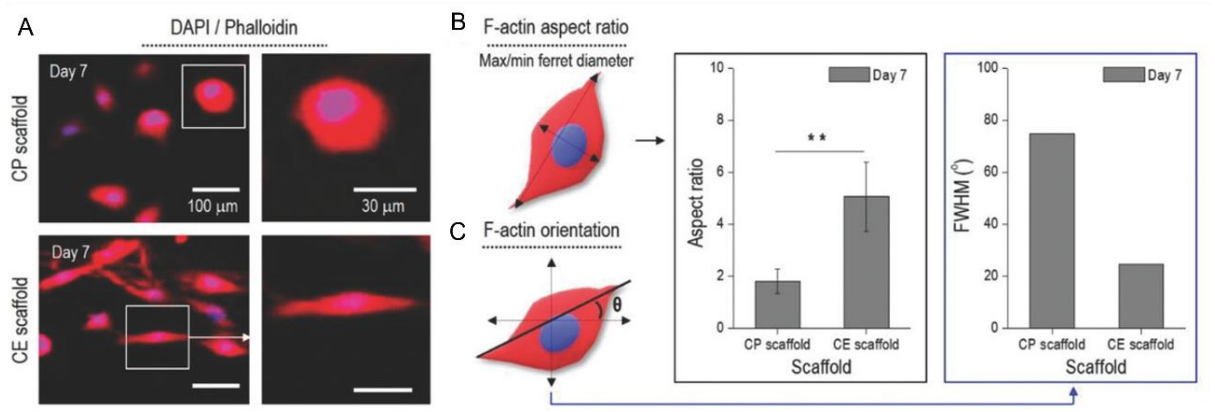

Figure 1.6. DAPI-Phalloidin staining of C2C12 myoblasts with quantitative analysis of cell elongation via F-actin aspect ratio and F-actin orientation analysis. Adapted from Yeo and Kim with permission[41].

1.3.2.3 Specialized Collectors to Generate Aligned Fibers

Specialized custom collectors, generally modifications of the previously discussed parallel electrode or rotating drum collectors, have also been explored. A modified rotating drum collector including an insulating gap in the center of the rotating drum can impart multiple alignment cues to the nanofibers; fibers would suspend across the gap, similar to a typical parallel collector, while the drum was also rotating to generate the longitudinally aligned fibers[73]. Longitudinally aligned PLGA fibers seeded with rat Schwan cells promoted enhanced cell proliferation and guided cell elongation for promoting neural cell growth. A similar combination parallel plate/rotating drum collector was used to collect nanofibers comprised of the natural/synthetic polymer combination of poly(vinyl acetate)/collagen seeded with human keratocytes and human corneal epithelial cells (HCECs) (Figure 1.4D) [46,72]. Light transmittance increased with increasing alignment, and human keratocytes could align in the direction of the fibers[46]. GelMA and PEGDA fibers have also been formed using mesh-based collectors designed to generate aligned or cross-aligned electrospun fibers, enabling the fabrication of cross-aligned fibers throughout the depth of the scaffold to

replicate the perpendicular layers present in corneal stromal tissue. When these structures were seeded with corneal stromal cells, both aligned morphologies on aligned samples and orthogonal alignment of the cells within the perpendicularly aligned layers[74] were observed. Dural fibroblasts were seeded onto aligned PCL electrospun fibers formed through the use of a ring and point electrode (Figure 1.4C) and migrated faster on aligned fibers relative to randomly aligned fibers while also showing enhanced alignment along the direction of aligned fibers[71]. Aligned fibrinogen/PEO scaffolds were also generated through the use of a custom setup with fiber collection occurring directly into the grounded, rotating cross-linking collection bath containing thrombin and $CaCl_2$ to crosslink the fibers directly upon collection (Figure 1.2B). Induced C2C12 myoblast differentiation and alignment were evaluated over 7 days of culture =, and cells were found to both align and display the mature myoblast marker, myosin heavy chain (MHC) [45]. A nerve conduit comprised of a poly (L-lactic acid) PLLA nanofiber yarn within a poly(L-lactide acid-co-caprolactone) (PLLA-CL) conduit was then formed using a modified electrospinning system with two nozzle heads with a grounded funnel-shaped collector. The resulting fibers had an aligned morphology that showed elongation of the seeded Schwann cells on the nanofiber yarn samples as well as longer axons[75]. However, the degrees of alignment achieved with these more complex collectors could be similarly achieved with a rotating drum with the added benefits of (1) more easily generating tunable degrees of alignment through rotation speed alteration and (2) the potential to generate hollow tubular structures if desired.

1.3.2.4 Magnetic Field-assisted Electrospinning to Generate Aligned Fibers

As opposed to modifying the geometry of the collector or electrospinning process, alignment of electrospun hydrogel fibers has also been explored with magnetic field-assisted electrospinning in which a magnetic field is introduced at the site of the collector and/or magnetic nanoparticles have

been introduced to the system to generate magnetic-responsive fibers that eliminate the need for collector rotation (thus reducing the mechanical shear to which cells are exposed[76,77]). Magnetic fibers have been fabricated through the incorporation of superparamagnetic iron oxide nanoparticles (SPIONs) into the electrospinning solution. The use of the magnetic field at the site of the collector or throughout the fabrication process can then lead to manipulation of the fibers as they gather on the collector. Parallel bar magnet collectors are most typically used as the collectors to enable such alignment. For example, polycarbonate-urethane (PCU) fibers containing magnetic nanoparticles and collected across two grounded bar magnets were demonstrated to increase alignment with the fibers (Figure 1.4E). The fibers were also found to be magnetically responsive for applications in stimuli-responsive applications in which scaffold deformation upon the application of a non-invasive and highly penetrative magnetic field would be useful[56].

The alignment of magnetic electrospun fibers post-fabrication has also been explored by inducing magnetic alignment of fragmented fibers after printing in a bulk hydrogel. For example, mouse tenocytes were found to show the most elongated structures when cultured in the strongest magnetic field, showing the correlation between the alignment of the magnetic fibers with the alignment of the cells in the bulk gel [78]. Alternately, superparamagnetic iron oxide nanoparticles (SPIONs) grafted to aligned PLLA fibers exposed to static, alternating, or moving magnetic fields indicated optimal rat primary dorsal root ganglia extension on the SPION-grafted fibers in an alternating magnetic field across all aligned fiber types (Figure 1.7) [79]. SPION-impregnated magnetically-responsive poly(D, L-lactide) (PLA) fibers likewise showed alignment of seeded osteoblast cells upon exposure to a static magnetic field beneath the culture surface, with alignment being responsive to both the fiber and field directions[80]. Ultimately, the incorporation of magnetic fields into the electrospinning fabrication process as well as into cell culture yield interesting

effects on fiber and cell response to the scaffolds, suggesting future alignment benefits in terms of adding other types of stimulus-responsive models and/or control measures to cell culture provided that the potential cytotoxicity of higher densities of SPIONs can be offset.

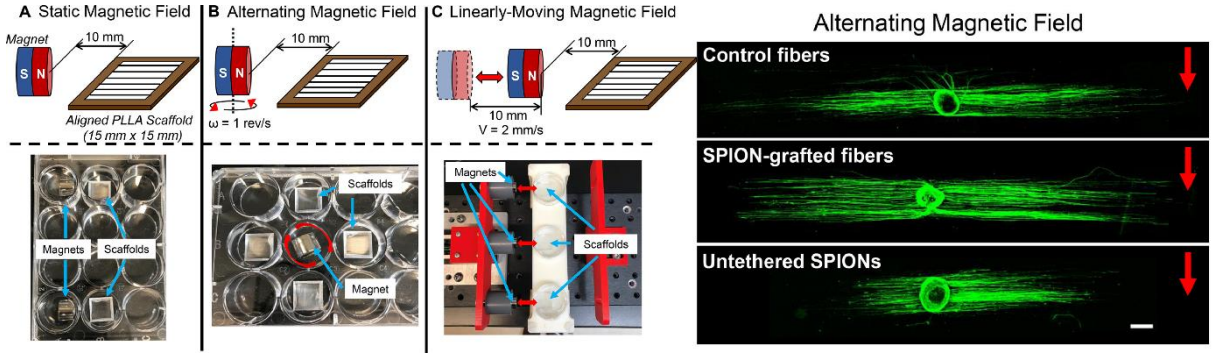

Figure 1.7. The effect of static, alternating, or linearly-moving external magnetic field on cells loaded within a magnetic nanofiber network as evaluated with rat dorsal root ganglia cells. Adapted from Funnell et al. with permission[79].

1.4 Multi-layered Electrospun Hydrogel Scaffolds

The capacity to align nanofibers using electrospinning also opens up possibilities to create more complex alignments of nanofibers within a single scaffold to replicate more complex biological tissues. Cross-alignment is a particularly relevant structure in this context. Early examples of electrospun fibers in cross-aligned scaffolds used PVP and a parallel collector, with the initially collected fibers rotated by 90° and then used as the base for further electrospinning to form a cross-aligned fiber network[22]. A similar approach was taken to fabricate a cross-aligned network based on poly(hydroxybutyrate-co-hydroxyvalerate) (PHBV), with rotation speeds greater than 3000 rpm shown to not further improve alignment while also resulting in less space between fibers leading to greater fiber density[66]. Human osteoblast-like cells (SaOS-2) seeded on these PHBV cross-aligned scaffolds showed elongation in the direction of the top layer of the scaffold; however, while some cells did penetrate the fiber networks, the possible two-way cell alignment within a

multi-layered, cross-aligned scaffold could not be fully achieved through seeding cells only on the surface of the network given the challenges cells have in diffusing through the dense electrospun layer[66]. Cross-aligned dextran fiber networks were also fabricated in a bilayer, cross-aligned network by using a glass slide between the needle and collector, rotating the collection slide by 45° or 90° between electrospinning steps to generate cross-aligned networks. NIH-3T3 cells seeded on the fibers were shown to align to the direction of the uniaxially aligned fibers, although the alignment of cells within the cross-aligned networks was not evaluated[81]. Both these examples show that a key drawback of seeding cells on cross-aligned electrospun networks is the lack of cell penetration into the networks, leading to difficulties associated with evaluating the cell alignment within each layer and/or achieving sufficiently high cell density to enable cell alignment deeper in the scaffold.

While electrospinning fibrous hydrogels has numerous applications and benefits, a common limitation to electrospinning is the production of thicker tissue structures, a result of the relatively low throughput of electrospinning as a technique. One method for combatting this limitation is the fabrication of multi-layer tissues. For example, tri-layer electrospun scaffolds have been explored for vascular applications with an interior layer of PHBV and PVA longitudinally aligned fibers, a middle layer of radially-aligned PHBV and elastin, and an exterior layer of longitudinally aligned PHBV and elastin fibers coupled with randomly aligned PHBV and PVA fibers. The combination of longitudinally and radially aligned fiber layers encouraged bidirectional elongation of cells, while mechanical testing of the scaffold found similar properties to smaller blood vessels as designed. Incorporated growth factors into the scaffold were found to increase cell infiltration into the scaffold[82]. Alternately, combining other faster biofabrication techniques with electrospinning can significantly accelerate scaffold fabrication without compromising the nanofiber formation

and alignment advantages of electrospinning[54]. For example, a combination of electrospinning and bioprinting was explored for vessel fabrication by 3D printing an interior layer of aligned PCL fibers, applying a middle layer of longitudinally aligned electrospun PCL fibers, and then depositing an outer layer of longitudinally-aligned co-electrospun PCL/PEG fibers. Including PEG as a sacrificial component in the fibers yielded a more porous outer layer to increase cell infiltration within the scaffold layers, while the 3D printed base PCL layer provided stiffer mechanics with minimal fabrication time. HUVECs seeded on the triple-layer scaffold were shown with DAPI-phalloidin staining to grow along the fiber orientation direction after only 1 day of culture[83].

Multi-layer scaffolds can also be used to better localize different cell types in different parts of more complex tissue scaffolds. For example, a multi-layer, co-culture scaffold was developed through the development of electrospun PCU fibers with an interior mesenchymal stem cell layer and an exterior layer with smooth muscle cells, targeting esophageal tissue engineering applications. A second middle layer, also comprised of PCU, was also optionally electrospun to generate a denser fiber network with decreased pore size and thus introduce a barrier to prevent either of the two cells from spreading/proliferating into the opposite layer. More cell proliferation for both cell types was seen on scaffolds fabricated with larger pores, while the addition of the narrow pores in the middle layer was sufficient to maintain the spatial arrangement of the cells in their originally designed layers over time[84]. In this way, multi-layer electrospun scaffolds can be leveraged as co-culture systems that can both control local micro-topography to guide cells in multi-layers as well as facilitate or arrest infiltration of seeded cells throughout multi-layer scaffolds by intelligent scaffold design. Both of these benefits translate to the use of the electrospun hydrogel nanofiber scaffolds as tissue engineering scaffolds for the purpose of replacing body tissues as well as in creating more complex tissue models.

1.5 Thesis Objectives

The motivation of this thesis work is to leverage the previously developed reactive cell electrospinning technique based on POEGMA hydrogels to create of multi-layer and aligned nanofiber networks that can directly incorporate cells during the electrospinning process. Hydrazone-crosslinked POEGMA hydrogels offer the advantages of low cytotoxicity when working with cell-laden polymer solutions as well as the lack of any requirement for post-crosslinking due to the dynamic covalent crosslinking of the nanofibers. The broader use of cell electrospinning remains quite limited due to the relatively few techniques available that allow for electrospinning of hydrogels in an all-aqueous solution, as required for maintaining cell viability throughout the process. This thesis offers novel insight into cell responses within co-culture systems and throughout multi-layered networks that have locally controlled micro-topographical cues. The objectives for this project are outlined in distinct chapters as follows:

(1) Chapter 2, "Multi-cellular layered nanofibrous poly (oligoethylene glycol methacrylate) (POEGMA)-based hydrogel scaffolds via reactive cell electrospinning", has been prepared for submission for publication. This chapter explores the integration of two cell types in a co-culture model into a multi-layered tissue for applications in the engineering of connective tissues. The use of the reactive cell electrospinning technique offers the unique advantage to generate multi-cellular and layered fibrous networks with directly controlled 3-dimensional cell distributions, depending on the sequence in which different cell types were added to the electrospinning process; at the same time, the dynamic covalent hydrazone crosslinking chemistry reduced risk of layer delamination.

(2) Chapter 3, “Reactive Cell Electrospinning of Anisotropically Aligned and Bilayer Hydrogel Nanofiber Networks”, has been prepared for submission for publication. This chapter explores how electrospun cells within the fibrous hydrogel network are affected by fiber alignment, including both single alignment as well as cross-aligned networks. Reactive cell electrospinning of POEGMA hydrogel nanofibers combined with simple techniques to generate aligned networks in single and bilayer scaffolds presents a novel approach to controlling not just 3-dimensional cell distribution but also 3-dimensional cell alignment throughout the scaffolds, highly beneficial to reproducing the complexity of more advanced multi-layer tissues like skin, tendon, or smooth muscle vasculature.

1.6 References

1 Chapekar, M. S. Tissue engineering: Challenges and opportunities. *Journal of Biomedical Materials Research* **53**, 617-620 (2000).

2 Lavik, E. & Langer, R. Tissue engineering: current state and perspectives. *Appl Microbiol Biotechnol* **65**, 1-8 (2004).

3 Azizgolshani, H. *et al.* High-throughput organ-on-chip platform with integrated programmable fluid flow and real-time sensing for complex tissue models in drug development workflows. *Lab on a Chip* **21**, 1454-1474 (2021).

4 Li, Y.-C. E. *et al.* Toward a neurospheroid niche model: optimizing embedded 3D bioprinting for fabrication of neurospheroid brain-like co-culture constructs. *Biofabrication* **13**, 015014 (2020).

5 Xinaris, C., Brizi, V. & Remuzzi, G. Organoid Models and Applications in Biomedical Research. *Nephron* **130**, 191-199 (2015).

6 Liu, H. *et al.* Advances in Hydrogels in Organoids and Organs-on-a-Chip. *Adv Mater* **31**, 1902042 (2019).

7 Hunt, J. A., Chen, R., Van Veen, T. & Bryan, N. Hydrogels for tissue engineering and regenerative medicine. *J. Mater. Chem. B* **2**, 5319-5338 (2014).

8 Drury, J. L. & Mooney, D. J. Hydrogels for tissue engineering: scaffold design variables and applications. *Biomaterials* **24**, 4337-4351 (2003).

9 Van Vlierberghe, S., Dubruel, P. & Schacht, E. Biopolymer-based hydrogels as scaffolds for tissue engineering applications: a review. *Biomacromolecules* **12**, 1387-1408 (2011).

10 Xu, F. *et al.* Hydrogels for Tissue Engineering: Addressing Key Design Needs Toward Clinical Translation. *Front Bioeng Biotechnol* **10**, 849831 (2022).

11 Frantz, C., Stewart, K. M. & Weaver, V. M. The extracellular matrix at a glance. *Journal of Cell Science* **123**, 4195-4200 (2010).

12 MacQueen, L. A. *et al.* A tissue-engineered scale model of the heart ventricle. *Nature Biomedical Engineering* **2**, 930-941 (2018).

13 De France, K. J., Xu, F. & Hoare, T. Structured Macroporous Hydrogels: Progress, Challenges, and Opportunities. *Adv Healthc Mater* **7**, 1700927 (2018).

14 Tan, B., Gan, S., Wang, X., Liu, W. & Li, X. Applications of 3D bioprinting in tissue engineering: advantages, deficiencies, improvements, and future perspectives. *J Mater Chem B* **9**, 5385-5413 (2021).

15 Shahbazi, M.-A., Ghalkhani, M. & Maleki, H. Directional Freeze-Casting: A Bioinspired Method to Assemble Multifunctional Aligned Porous Structures for Advanced Applications. *Advanced Engineering Materials* **22**, 2000033 (2020).

16 Chau, M. *et al.* Composite Hydrogels with Tunable Anisotropic Morphologies and Mechanical Properties. *Chemistry of Materials* **28**, 3406-3415 (2016).

17 Riblett, B. W., Francis, N. L., Wheatley, M. A. & Wegst, U. G. K. Ice-Templated Scaffolds with Microridged Pores Direct DRG Neurite Growth. *Advanced Functional Materials* **22**, 4920-4923 (2012).

18 Dewle, A., Pathak, N., Rakshasmare, P. & Srivastava, A. Multifarious Fabrication Approaches of Producing Aligned Collagen Scaffolds for Tissue Engineering Applications. *ACS Biomaterials Science & Engineering* **6**, 779-797 (2020).

19 Reneker, D. H. & Yarin, A. L. Electrospinning jets and polymer nanofibers. *Polymer* **49**, 2387-2425 (2008).

20 Katta, P., Alessandro, M., Ramsier, R. D. & Chase, G. G. Continuous electrospinning of aligned polymer nanofibers onto a wire drum collector. *Nano Letters* **4**, 2215-2218 (2004).
21 Xu, F., Sheardown, H. & Hoare, T. Reactive electrospinning of degradable poly(oligoethylene glycol methacrylate)-based nanofibrous hydrogel networks. *Chemical Communications* **52**, 1451-1454 (2016).
22 Li, D., Wang, Y. & Xia, Y. Electrospinning of Polymeric and Ceramic Nanofibers as Uniaxially Aligned Arrays. *Nano Letters* **3**, 1167-1171 (2003).
23 Greiner, A. & Wendorff, J. H. Electrospinning: A fascinating method for the preparation of ultrathin fibers. *Angewandte Chemie - International Edition* **46**, 5670-5703 (2007).
24 Sill, T. J. & von Recum, H. A. Electrospinning: Applications in drug delivery and tissue engineering. *Biomaterials* **29**, 1989-2006 (2008).
25 Brako, F., Luo, C., Craig, D. Q. M. & Edirisinghe, M. An Inexpensive, Portable Device for Point-of-Need Generation of Silver-Nanoparticle Doped Cellulose Acetate Nanofibers for Advanced Wound Dressing. *Macromolecular Materials and Engineering* **303**, 1700586 (2018).
26 Xu, S. C. *et al.* A battery-operated portable handheld electrospinning apparatus. *Nanoscale* **7**, 12351-12355 (2015).
27 Xue, J., Wu, T., Dai, Y. & Xia, Y. Electrospinning and Electrospun Nanofibers: Methods, Materials, and Applications. *Chemical Reviews* **119**, 5298-5415 (2019).
28 Deng, A., Yang, Y., Du, S. & Yang, S. Electrospinning of in situ crosslinked recombinant human collagen peptide/chitosan nanofibers for wound healing. *Biomaterials Science* **6**, 2197-2208 (2018).
29 Koosha, M. & Mirzadeh, H. Electrospinning, mechanical properties, and cell behavior study of chitosan/PVA nanofibers. *Journal of Biomedical Materials Research - Part A* **103**, 3081-3093 (2015).
30 Majidi, S. S. *et al.* Wet electrospun alginate/gelatin hydrogel nanofibers for 3D cell culture. *International Journal of Biological Macromolecules* **118**, 1648-1654 (2018).
31 Wakuda, Y., Nishimoto, S., Suye, S.-i. & Fujita, S. Native collagen hydrogel nanofibres with anisotropic structure using core-shell electrospinning. *Scientific Reports* **8**, 6248 (2018).
32 Askarzadeh, N. *et al.* Bilayer Cylindrical Conduit Consisting of Electrospun Polycaprolactone Nanofibers and DSC Cross-Linked Sodium Alginate Hydrogel to Bridge Peripheral Nerve Gaps. *Macromolecular Bioscience* **20**, 2000149 (2020).
33 Gombotz, W. & Wee, S. F. Protein release from alginate matrices. *Advanced Drug Delivery Reviews* **31**, 267-285 (1998).
34 Hennink, W. E. & van Nostrum, C. F. Novel crosslinking methods to design hydrogels. *Advanced Drug Delivery Reviews* **64**, 223-236 (2012).
35 Torres-Giner, S., Gimeno-Alcañiz, J. V., Ocio, M. J. & Lagaron, J. M. Comparative performance of electrospun collagen nanofibers cross-linked by means of different methods. *ACS Applied Materials and Interfaces* **1**, 218-223 (2009).
36 Luo, X. *et al.* Study on structure, mechanical property and cell cytocompatibility of electrospun collagen nanofibers crosslinked by common agents. *International Journal of Biological Macromolecules* **113**, 476-486 (2018).
37 Sisson, K., Zhang, C., Farach-Carson, M. C., Chase, D. B. & Rabolt, J. F. Evaluation of cross-linking methods for electrospun gelatin on cell growth and viability. *Biomacromolecules* **10**, 1675-1680 (2009).

38 Campiglio, C. E. *et al.* Cross-Linking Optimization for Electrospun Gelatin: Challenge of Preserving Fiber Topography. *Polymers* **12**, 2472 (2020).
39 Baker, B. M. *et al.* Cell-mediated fibre recruitment drives extracellular matrix mechanosensing in engineered fibrillar microenvironments. *Nature Materials* **14**, 1262-1268 (2015).
40 Chen, C. *et al.* Bioinspired Hydrogel Electrospun Fibers for Spinal Cord Regeneration. *Advanced Functional Materials* **29**, 1806899 (2019).
41 Yeo, M. & Kim, G. H. Anisotropically Aligned Cell-Laden Nanofibrous Bundle Fabricated via Cell Electrospinning to Regenerate Skeletal Muscle Tissue. *Small* **14**, 1803491 (2018).
42 Nie, K. *et al.* Enzyme-crosslinked electrospun fibrous gelatin hydrogel for potential soft tissue engineering. *Polymers* **12**, 1977 (2020).
43 Ji, Y. *et al.* Electrospun three-dimensional hyaluronic acid nanofibrous scaffolds. *Biomaterials* **27**, 3782-3792 (2006).
44 Yeo, M. & Kim, G. Micro/nano-hierarchical scaffold fabricated using a cell electrospinning/3D printing process for co-culturing myoblasts and HUVECs to induce myoblast alignment and differentiation. *Acta biomaterialia* **107**, 102-114 (2020).
45 Guo, Y., Gilbert-Honick, J., Somers, S. M., Mao, H.-Q. & Grayson, W. L. Modified cell-electrospinning for 3D myogenesis of C2C12s in aligned fibrin microfiber bundles. *Biochemical and Biophysical Research Communications* **516**, 558-564 (2019).
46 Wu, Z., Kong, B., Liu, R., Sun, W. & Mi, S. Engineering of corneal tissue through an aligned PVA/collagen composite nanofibrous electrospun scaffold. *Nanomaterials* **8**, 124 (2018).
47 Koosha, M., Raoufi, M. & Moravvej, H. One-pot reactive electrospinning of chitosan/PVA hydrogel nanofibers reinforced by halloysite nanotubes with enhanced fibroblast cell attachment for skin tissue regeneration. *Colloids and Surfaces B: Biointerfaces* **179**, 270-279 (2019).
48 Hussein, Y. *et al.* Electrospun PVA/hyaluronic acid/L-arginine nanofibers for wound healing applications: Nanofibers optimization and in vitro bioevaluation. *International Journal of Biological Macromolecules* **164**, 667-676 (2020).
49 Xu, F., Dodd, M., Sheardown, H. & Hoare, T. Single-Step Reactive Electrospinning of Cell-Loaded Nanofibrous Scaffolds as Ready-to-Use Tissue Patches. *Biomacromolecules* **19**, 4182-4192 (2018).
50 Chen, T., Bakhshi, H., Liu, L., Ji, J. & Agarwal, S. Combining 3D Printing with Electrospinning for Rapid Response and Enhanced Designability of Hydrogel Actuators. *Advanced Functional Materials* **28**, 1800514 (2018).
51 Chen, X. *et al.* Fabrication and properties of electrospun collagen tubular scaffold crosslinked by physical and chemical treatments. *Polymers* **13**, 755 (2021).
52 Xu, F. *et al.* Fast Thermoresponsive Poly(oligoethylene glycol methacrylate) (POEGMA)-Based Nanostructured Hydrogels for Reversible Tuning of Cell Interactions. *ACS Biomaterials Science & Engineering*, acsbiomaterials.0c01552 (2021).
53 Xu, F., Gough, I., Dorogin, J., Sheardown, H. & Hoare, T. Nanostructured degradable macroporous hydrogel scaffolds with controllable internal morphologies via reactive electrospinning. *Acta Biomaterialia* **104**, 135-146 (2020).
54 Lu, K. *et al.* Biofabrication of aligned structures that guide cell orientation and applications in tissue engineering. *Bio-Design and Manufacturing* **4**, 258-277 (2021).

55 Sensini, A. *et al.* Tendon Fascicle-Inspired Nanofibrous Scaffold of Polylactic acid/Collagen with Enhanced 3D-Structure and Biomechanical Properties. *Scientific Reports* **8**, 17167 (2018).
56 Guarino, V., Iannotti, V., Ausanio, G., Ambrosio, L. & Lanotte, L. Elastomagnetic nanofiber wires by magnetic field assisted electrospinning. *Express Polymer Letters* **13**, 419-428 (2019).
57 Abbasi, A., Imaichi, S., Ling, V. & Shukla, A. Mesenchymal Stem Cell Behavior on Soft Hydrogels with Aligned Surface Topographies. *ACS Appl Bio Mater* **5**, 1890-1900 (2022).
58 Modulevsky, D. J. *et al.* Plant Scaffolds Support Motor Recovery and Regeneration in Rat Spinal Cord Injury. *bioRxiv*, 347807 (2020).
59 Deravi, L. F. *et al.* Design and Fabrication of Fibrous Nanomaterials Using Pull Spinning. *Macromolecular Materials and Engineering* **302**, 1600404 (2017).
60 Tijore, A. *et al.* Contact guidance for cardiac tissue engineering using 3D bioprinted gelatin patterned hydrogel. *Biofabrication* **10**, 025003 (2018).
61 Denes, L. T. *et al.* Culturing C2C12 myotubes on micromolded gelatin hydrogels accelerates myotube maturation. *Skelet Muscle* **9**, 17 (2019).
62 Rizzo, R., Bonato, A., Chansoria, P. & Zenobi-Wong, M. Macroporous Aligned Hydrogel Microstrands for 3D Cell Guidance. *ACS Biomater Sci Eng* **8**, 3871-3882 (2022).
63 Costantini, M. *et al.* Microfluidic-enhanced 3D bioprinting of aligned myoblast-laden hydrogels leads to functionally organized myofibers in vitro and in vivo. *Biomaterials* **131**, 98-110 (2017).
64 Kroehne, V. *et al.* Use of a novel collagen matrix with oriented pore structure for muscle cell differentiation in cell culture and in grafts. *J Cell Mol Med* **12**, 1640-1648 (2008).
65 Jin, G. *et al.* Electrospun three-dimensional aligned nanofibrous scaffolds for tissue engineering. *Materials Science and Engineering: C* **92**, 995-1005 (2018).
66 Tong, H.-W., Wang, M. & Lu, W. W. Electrospun Poly(Hydroxybutyrate-co-Hydroxyvalerate) Fibrous Membranes Consisting of Parallel-Aligned Fibers or Cross-Aligned Fibers: Characterization and Biological Evaluation. *Journal of Biomaterials Science, Polymer Edition* **22**, 2475-2497 (2011).
67 De France, K. J. *et al.* Multi-scale structuring of cell-instructive cellulose nanocrystal composite hydrogel sheets via sequential electrospinning and thermal wrinkling. *Acta Biomaterialia* **128**, 250-261 (2021).
68 Kai, D., Prabhakaran, M. P., Jin, G. & Ramakrishna, S. Guided orientation of cardiomyocytes on electrospun aligned nanofibers for cardiac tissue engineering. *Journal of Biomedical Materials Research - Part B Applied Biomaterials* **98 B**, 379-386 (2011).
69 Du, J. *et al.* Prompt peripheral nerve regeneration induced by a hierarchically aligned fibrin nanofiber hydrogel. *Acta Biomaterialia* **55**, 296-309 (2017).
70 Wang, W. Y., Davidson, C. D., Lin, D. & Baker, B. M. Actomyosin contractility-dependent matrix stretch and recoil induces rapid cell migration. *Nature Communications* **10**, 1186 (2019).
71 Xie, J. *et al.* Radially Aligned, Electrospun Nanofibers as Dural Substitutes for Wound Closure and Tissue Regeneration Applications. *ACS Nano* **4**, 5027-5036 (2010).
72 Mi, S. *et al.* A novel electrospinning setup for the fabrication of thickness-controllable 3D scaffolds with an ordered nanofibrous structure. *Materials Letters* **160**, 343-346 (2015).
73 Subramanian, A., Krishnan, U. M. & Sethuraman, S. Fabrication of uniaxially aligned 3D electrospun scaffolds for neural regeneration. *Biomedical Materials* **6**, 025004 (2011).

74 Mahdavi, S. S., Abdekhodaie, M. J., Mashayekhan, S., Baradaran-Rafii, A. & Kim, K. Development and in vitro evaluation of photocurable GelMA/PEGDA hybrid hydrogel for corneal stromal cells delivery. *Materials Today Communications* **27**, 102459 (2021).
75 Li, D. *et al.* Nerve conduits constructed by electrospun P(LLA-CL) nanofibers and PLLA nanofiber yarns. *Journal of Materials Chemistry B* **3**, 8823-8831 (2015).
76 Hu, H. *et al.* Synergic effect of magnetic nanoparticles on the electrospun aligned superparamagnetic nanofibers as a potential tissue engineering scaffold. *RSC Advances* **3**, 879-886 (2013).
77 Yang, D., Lu, B., Zhao, Y. & Jiang, X. Fabrication of Aligned Fibrous Arrays by Magnetic Electrospinning. *Advanced Materials* **19**, 3702-3706 (2007).
78 Hiraki, H. L. *et al.* Magnetic Alignment of Electrospun Fiber Segments Within a Hydrogel Composite Guides Cell Spreading and Migration Phenotype Switching. *Frontiers in Bioengineering and Biotechnology* **9**, 679165 (2021).
79 Funnell, J. L. *et al.* Assessing the combination of magnetic field stimulation, iron oxide nanoparticles, and aligned electrospun fibers for promoting neurite outgrowth from dorsal root ganglia in vitro. *Acta Biomaterialia* **131**, 302-313 (2021).
80 Li, L., Yang, G., Li, J., Ding, S. & Zhou, S. Cell behaviors on magnetic electrospun poly-d, l-lactide nanofibers. *Materials Science and Engineering: C* **34**, 252-261 (2014).
81 Wang, K. *et al.* Facile Strategy to Generate Aligned Polymer Nanofibers: Effects on Cell Adhesion. *ACS Applied Materials & Interfaces* **10**, 1566-1574 (2018).
82 Deepthi, S., Nivedhitha Sundaram, M., Vijayan, P., Nair, S. V. & Jayakumar, R. Engineering poly(hydroxy butyrate-co-hydroxy valerate) based vascular scaffolds to mimic native artery. *International Journal of Biological Macromolecules* **109**, 85-98 (2018).
83 Huang, R. *et al.* Triple-Layer Vascular Grafts Fabricated by Combined E-Jet 3D Printing and Electrospinning. *Annals of Biomedical Engineering* **46**, 1254-1266 (2018).
84 Soliman, S. *et al.* A multilayer scaffold design with spatial arrangement of cells to modulate esophageal tissue growth. *Journal of Biomedical Materials Research - Part B Applied Biomaterials* **107B**, 324-331 (2019).

2 Chapter 2: Multi-cellular layered nanofibrous poly(oligoethylene glycol methacrylate) (POEGMA)-based hydrogel scaffolds via reactive cell electrospinning

2.1 Abstract

While hydrogels have been demonstrated to be effective scaffolds for soft tissue engineering, existing fabrication techniques pose limitations in terms of being able to reproduce both the micro/nanofibrous structures of native extracellular matrix as well as the spatial arrangement of different cell types inherent of more complex tissues. Herein, we describe a reactive cell electrospinning strategy using hydrazide and aldehyde-functionalized poly(oligoethylene glycol methacrylate) (POEGMA) precursor polymers that can create nanofibrous hydrogel scaffolds with controllable local cell gradients using a sequential all-aqueous process that does not require additives or external energy. Cells could be seeded directly during the fabrication process in different layers within the scaffold, enabling localized segregation of different cell types within the structures without compromising their capacity to proliferate (~4-fold increase in cell density over a 14-day incubation period). This sequential reactive electrospinning approach thus offers promise to generate co-culture fibrous hydrogel networks in which both the nano-scale architecture and the cell distribution can be controlled, as is essential to recreate more complex types of tissues.

2.2 Introduction

Hydrogels have been extensively applied for tissue engineering and tissue regeneration given their low protein adsorption, tunable mechanics, cytocompatibility, and water contents similar to native soft tissues[1-3]. As scaffolds or vehicles, hydrogels can be used to encapsulate cells, drugs, or biomolecules for different purposes in a tissue engineering context[4,5]. However, two significant challenges remain that limit the applications of hydrogel scaffolds in tissue engineering. First, cells encapsulated in 3D bulk hydrogels often do not exhibit noticeable growth or spreading[6,7], a result likely attributable to the complex microstructure of native tissues that is difficult to mimic directly using a hydrogel-based scaffold. In particular, native extracellular matrix (ECM) is composed of fibrous collagen and fibrin structures with diameters ranging from a few nanometers to micrometers that are essential for promoting cell adhesion and growth[8,9]. Second, most tissues of interest for regeneration (e.g., skin[10], bone [11], cartilage[12,13], intestine[14], liver[15], and others) contain multiple cell types as well as complex cellular microenvironments that are challenging to recreate with conventional hydrogel-based scaffolds. While cell co-culture systems have been developed to culture multiple cell types in one plate[13,16], it remains challenging to control localized cell distributions and cell densities within a hydrogel scaffold, particularly one that also mimics the micro- or nanostructures of native tissues.

Structured 3D hydrogels that contain macroporous networks or nanofibrous structures have attracted increasing interest in the context of tissue regeneration to address the challenge of mimicking native ECM[6,17]. A variety of techniques such as emulsion templating[18], salt leaching[19], gas foaming[20]and cryo-gelation[21] have been studied to fabricate structured hydrogels with internal pore networks and internal nanoscale morphologies. However, the required use of solvents, additives, or external energy to fabricate hydrogels using these techniques makes it impossible to

directly encapsulate viable cells during the scaffold fabrication process[6,22], instead requiring post-loading processes that make it very difficult to accurately spatially distribute cells within the scaffold to mimic more complex tissues[22]. In contrast, while 3D bioprinting and *in situ* tissue engineering approaches can enable the direct fabrication of scaffolds with spatially oriented cells[22], both approaches are to-date limited for creating nanofibrous internal structures that are essential cues to cells for growth, spreading, and differentiation.

Electrospinning is a versatile technique in which a high voltage is used to induce electrostatic repulsion forces that can overcome the surface tension of the polymer solution and thus enable the drawing of micro/nanofibrous structures[23,24]. Conventional hydrogel electrospinning for the purpose of generating soft tissue scaffolds is typically conducted by electrospinning polymer nanofibers, crosslinking the nanofibers post-fabrication, and then seeding cells on the surface of the resulting hydrogel nanofibers. However, these strategies typically also suffer from drawbacks in terms of maintaining the viability of co-encapsulated cells. In our previous work, we addressed this challenge by designing a "reactive cell electrospinning" technique that can not only directly prepare crosslinked hydrogel nanofibers without any post-treatment (e.g., additives, organic solvents or crosslinkers) or external energy (e.g., UV light), but also simultaneously encapsulate viable cells within these nanofibrous hydrogels during electrospinning process[25,26]. More specifically, poly(oligoethylene glycol methacrylate) (POEGMA)-based oligomers were functionalized with hydrazide and aldehyde groups (as previously demonstrated in our group) [25,27] and co-electrospun in aqueous solutions from a double barrel syringe to form a dynamic covalent crosslinked hydrogel during the electrospinning process[27]. The resulting hydrazone crosslinked network is hydrolytically degradable (over periods of days to months in cell medium or PBS[28]) while the nanoscale fibrous structures produced (coupled with the macropores maintained between

the fibers) enable better mimickry of native ECM structures. Compared to conventional "cell electrospinning" methods that use co-axial needles[29,30] or combine electrospinning with cell printing[31] or cell electrospraying[32], reactive cell electrospinning is a single-step, single-syringe, all-aqueous process that can reduce the complexity of scaffold fabrication while maintaining high cell viability. In addition, the sequential "layer-by-layer" fabrication strategy used to make electrospun scaffolds on a collector opens the potential to introduce different cell types at different times during the electrospinning fabrication process, offering a potential strategy to spatially orient cells in different locations within a single macroporous/nanofibrous ECM-mimetic network.

Herein, we apply the advantages of reactive cell electrospinning to spatially co-encapsulate two different cell types within a nanofibrous hydrogel scaffold to mimic the complexity of native tissues. Our model system aims to mimic connective tissue (e.g. cartilage or dermis) that consists of a fibroblast-containing ECM-rich layer backed by an epithelial cell layer (Figure 2.1). The layer-by-layer cell electrospinning approach designed can efficiently co-encapsulate multiple cell types in one step as well as control the cell density and cell distribution in each spatially-segregated layer, with the nanofibrous structure of the scaffolds both providing physical support for cell adhesion/proliferation even in the absence of cell adhesion ligands such as RGD. The capacity of the scaffold to support not only cell viability but also cell proliferation while largely maintaining the spatial segregation of the co-cultured cells over time offers potential to better mimic more complex multi-layered tissues using a relatively simple fabrication strategy.

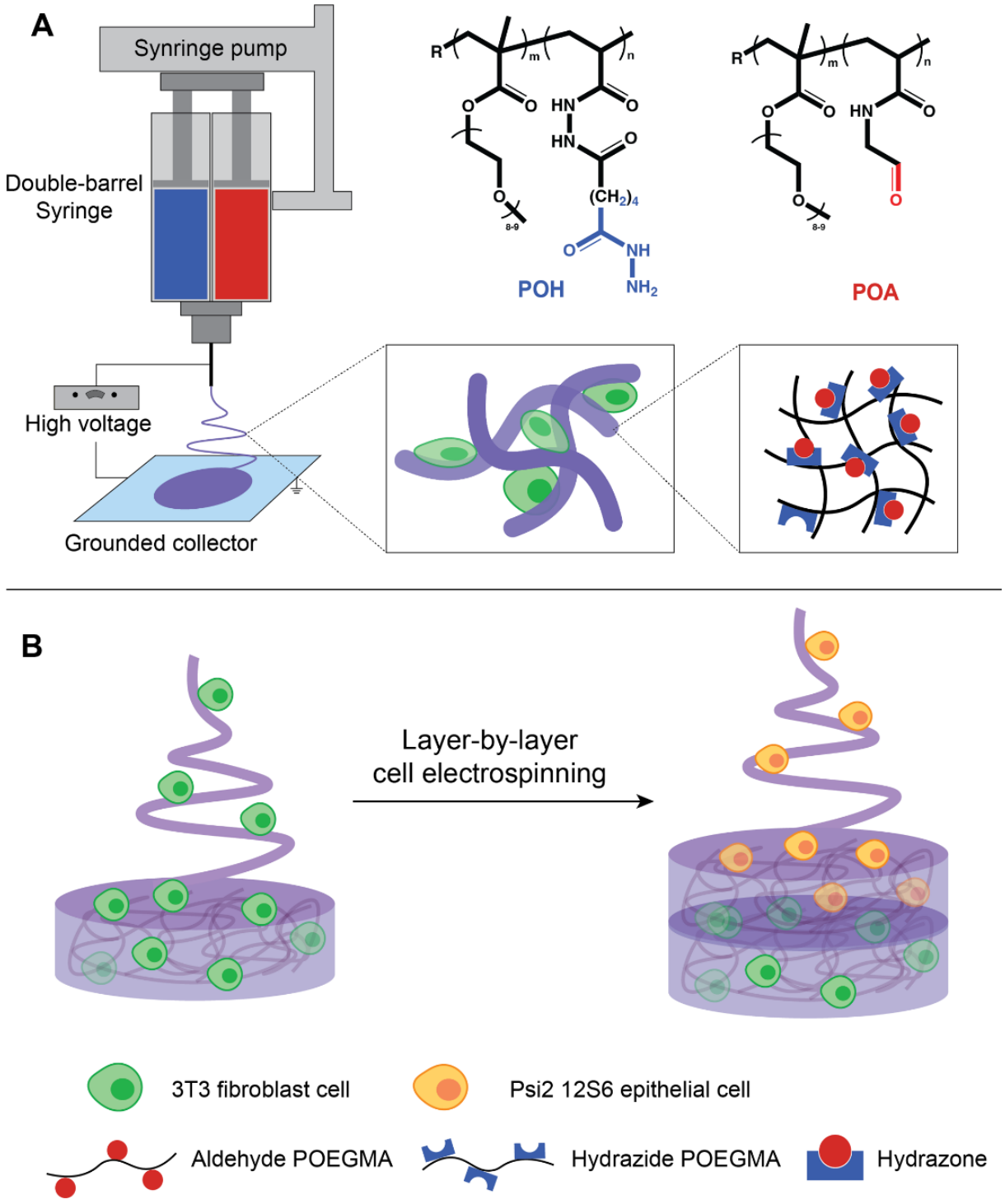

Figure 2.1. Schematics of (A) the reactive cell electrospinning process to create hydrolytically-labile dynamic hydrazone-crosslinked nanofibrous hydrogel scaffolds and (B) spatially segregated co-encapsulation of multiple cell types via layer-by-layer cell electrospinning.

2.3 Materials and Methods

2.3.1 Materials

Oligo(ethylene glycol) methyl ether methacrylate ($OEGMA_{500}$, M_n = 500 g/mol, Sigma-Aldrich, 95%) was purified to remove inhibitors prior to use with a basic aluminum-oxide-packed column (Sigma-Aldrich, type CG-20). Acrylic acid (AA, Sigma-Aldrich, 99%), 2,2-azo-bis-isobutryic acid dimethyl ester (AIBMe, Wako Chemicals), dioxane (Caledon Laboratories, 99%), thioglycolic acid (TGA, Sigma-Aldrich, 98%), adipic acid dihydrazide (ADH, Alfa Aesar, 98%), N′-ethyl-N-(3-(dimethylamino)propyl)-carbodiimide (EDC, Carbosynth, Compton CA, commercial grade), Arg-Gly-Asp (RGD, Sigma-Aldrich), sodium cyanoborohydride (Sigma-Aldrich), paraformaldehyde (Sigma-Aldrich), and poly (ethylene oxide) (PEO, M_w = 600,000 g/mol, Sigma-Aldrich) were all used as received. N-(2,2-Dimethoxyethyl) methacrylamide (DMEMAm) was synthesized in-house as previously described [33]. Milli-Q grade distilled deionized water (DIW) was used for all experiments. NIH 3T3 mouse fibroblast cells and Psi2 12S6 mouse epithelial cells were both purchased from ATCC (Cedarlane Laboratories, Burlington, ON). Dulbecco's Modified Eagle's Medium (DMEM, Wisent Inc., CA), fetal bovine serum (FBS, Wisent Inc., CA), penicillin-streptomycin (Wisent Inc., CA), trypsin−EDTA solution (Wisent Inc., CA), phosphate buffered saline (1× PBS, pH = 7.4, Wisent Inc., CA), PrestoBlue reagent (ThermoFisher), Triton-X-100 (ThermoFisher), bovine serum albumin (BSA, ThermoFisher), Pierce™ fast blocking buffer (ThermoFisher), a calcein AM/ethidium homodimer-1 (Et-D) LIVE/DEAD assay kit (ThermoFisher), rhodamine phalloidin (ThermoFisher), 4′,6-diamidino-2-phenylindole (DAPI, ThermoFisher), carboxyfluorescein diacetate succinimidyl ester (CFSE, CellTrace™, ThermoFisher) and a Far Red kit (CellTrace™, ThermoFisher) were all used as received.

2.3.2 Synthesis of hydrazide-functionalized POEGMA (POH)

Hydrazide functionalized POEGMA (POH) was synthesized by free radical polymerization followed by carbodiimide grafting as previously described[27]. AIBMe (37 mg, 0.16 mmol), $OEGMA_{500}$ (4.0 g, 8.4 mmol), AA (0.25 g, 3.5 mmol) and dioxane (20 mL) were added to a 100mL flask and polymerized at 75 °C for 4 hours under magnetic stirring to form poly(OEGMA-*co*-AA). Following purification via dialysis (6x6 hr cycles against distilled deionized water), the acrylic acid residues in poly(OEGMA-*co*-AA) was then functionalized with hydrazide groups via the addition of large excesses of ADH (2.65 g, 15.2 mmol, 5x molar excess) and EDC (1.18 g, 6.2 mmol, 2.5x molar excess) to the total -COOH groups in the polymers. The final POH polymer was then purified via dialysis (6x6 hr cycles against distilled deionized water) and was stored as a 15 w/w% solution in 1x PBS at 4°C after lyophilization for further use.

2.3.3 Synthesis of aldehyde-functionalized POEGMA (POA)

Similar to the protocol above for synthesizing POH, POA was prepared by adding AIBMe (50 mg, 0.21 mmol), $OEGMA_{500}$ (4.0 g, 8.4 mmol), N-(2,2-dimethoxyethyl) methacrylamide (DMEMAm, 0.60 g, 3.5 mmol, synthesized in-house as previously described[27]) and dioxane (20 mL) to a 100 mL flask and polymerizing at 75 °C for 4 hours under magnetic stirring to form poly(OEGMA-*co*-DMEMAm) [27]. Following purification via dialysis (6x6 hr cycles against distilled deionized water), all of the resultant poly(OEGMA-*co*-DMEMAm) polymer was dissolved in 100 mL of 0.25 M HCl to hydrolyze the acetal groups to aldehyde groups. The final POA polymer was purified by dialysis (6x6 hr cycles against distilled deionized water) and was stored as a 15 w/w% solution in 1x PBS at 4°C after lyophilization for further use.

2.3.4 Synthesis of RGD-labelled POEGMA (POA-RGD)

RGD labelled POA polymer (POA-RGD) was prepared by mixing POA (0.6 g) and RGD (10 mg, 28.9 μmol) in 50 mL distilled deionized water for 24 hours under magnetic stirring. Subsequently, sodium cyanoborohydride (18.2 mg, 0.29 mmol) was added and the solution was mixed for an additional 48 hours. The solution was then dialyzed (6x6 hr cycles against distilled deionized water) for purification and lyophilized. The final POA-RGD was stored as a 15 w/w% solution in PBS at 4°C for further use.

2.3.5 Characterization of POEGMA polymer precursors

The molar concentration of hydrazide groups in POH polymer was calculated by conductometric titration (ManTech automatic titrator, 0.1 M NaOH titrant, 1 mg/mL polymer solution). The molar concentration of aldehyde groups in POA polymer was determined using ^{1}H NMR (600 MHz, Bruker) by comparing the ratio of aldehyde proton signal at 9.52 ppm to the methyl POEGMA proton signal at 0.81 ppm. The molecular weights of POH and POA were determined by aqueous gel permeation chromatography at 30°C using the Agilent 1260 Infinity II GPC system operating with a Cytiva Superose 6 Increase 10/300 GL column and a continuous phase of 1 x PBS with 0.05% sodium azide.

2.3.6 Cell culture

NIH 3T3 fibroblasts and PSi2 12S6 epithelial cells were cultured in DMEM with 10% FBS and 1% penicillin-streptomycin in tissue culture treated flasks (Falcon) to ~80% confluency before use. Non-treated 6-well plates (Fisher Scientific) were used to culture the cells that were

encapsulated in nanofibrous hydrogels to minimize any driving force present for cells to adhere on the bottom of plates rather than within the scaffolds. All cells were incubated at 37°C and 5% CO_2.

2.3.7 Preparation of cell-loaded electrospun nanofibrous hydrogels

Poly(ethylene oxide) (PEO, M_w = 600,000 g/mol) was dissolved in sterile DMEM at a concentration of 5 wt%. Following, 0.5 mL of this PEO solution was separately added to 0.5 mL aliquots of POH or POA solutions (both at a concentration of 15 wt% in PBS) to form solutions with final concentrations of 7.5 wt% POH or POA and 2.5 wt% PEO for electrospinning. Cells were loaded into the POH+PEO precursor solution by centrifuging a 1 mL cell suspension (1×10^6 cells/mL) into a pellet, adding 1 mL of the POH+PEO precursor solution, and resuspending the cells. Subsequently, 1 mL of the POH+PEO+cells suspension and 1 mL of POA+PEO solution were loaded into separate barrels of a double-barrel syringe equipped with a static mixer (MedMix L series, 2.5 mL capacity). An 18 G blunt needle was connected to the end of the static mixer, and a 10 kV voltage was applied between the needle and a patterned collector consisting of multiple aluminum sticks separated by a 1 cm gap (Bertan High Voltage Power Supply: Output: 0-30 kV, 0.400 mA, input: 115/230V, 0.5/0.25 A). A voltage of 10 kV was used based on our previous work[26], representing the minimal voltage require to form the POEGMA hydrogel fibers with clear fiber formation. A vertical syringe pump was used to flow the precursor solutions at a rate of 15 μL/min for one hour to enable cell electrospinning. Afterwards, the electrospun scaffold (collected "dry" on the patterned collector) was immediately transferred into the DMEM growth media for re-hydration. Layer-by-layer cell electrospinning was performed using the same parameters but using POH+PEO+cells suspensions in which different cells were suspended (both using the same technique described above), with the overall electrospinning time maintained to be one hour to

maintain high cell viability. The entire protocol was conducted under a sterile environment inside a biological safety cabinet, with the humidity for all experiments maintained between 23-26% RH.

2.3.8 Microscopic analysis of cell-loaded scaffolds

Scanning electron microscopy (SEM, Tecan Vega II LSU instrument) was used to observe the morphologies of the cells and the POEGMA nanofibers after electrospinning. SEM samples were prepared by mounting the electrospun scaffolds on a SEM stub and subsequently sputter coating the scaffolds with gold to prevent charging. Confocal laser scanning microscopy (CLSM, Nikon A1R HD25) was used to track cell viability, cell proliferation, and cell morphology within the nanofibrous scaffolds following fluorescence staining using excitation/emission wavelengths as described in the following sections relevant to each assay conducted. Confocal z-stack images (3D view) were collected by scanning planes at 5 μm intervals from the bottom to the top of the electrospun scaffold, using the same imaging parameters as used to collect the 2D images for each plane.

2.3.9 Cytotoxicity of polymer precursors

3T3 fibroblast cells and Psi2 12S6 epithelial cells were seeded in a 96-well plate at a density of 10^4 cells per well and incubated in 100 μL of DMEM at 37 °C and 5% CO_2 for 24 h. The plate was then washed with fresh 1x PBS, after which 100 μL of fresh DMEM containing POH, POA, POA-RGD, and PEO at concentrations ranging from 0.1 to 1 mg/mL was added to each well. The plate was incubated for an additional 24 hours, after which the medium containing polymer precursors was removed and replaced with 90 μL of fresh DMEM and 10 μL of PrestoBlue reagent (ThermoFisher) followed by an additional 2-hour incubation step at 37 °C. Cell viabilities were

assessed using a plate reader (Biotek Cytation5) to measure fluorescence (560 nm excitation/590 nm emission), with the result normalized to a control (cells only without materials).

2.3.10 Cell viabilities during electrospinning process

For evaluating cell viability as a function of applied voltage during electrospinning, a cell suspension of 100,000 cells/mL (3T3 or Psi2 12S6 cells) in DMEM media was processed at voltages of 0, 5, 10, and 15 kV using the same cell electrospinning parameters used to fabricate the scaffolds. Cell were processed for 30s, collected in a Petri dish (60 mm × 15 mm, Fisher Scientific. Subsequently, the collected cell suspension was re-suspended and an aliquot of 100 μL was placed into each well of a 96-well plate. Cells were cultured at 37 °C for additional 24 h before assessing viability using the same PrestoBlue protocol outlined above. For evaluating effect of dehydration time on cell viability during cell electrospinning, cells (3T3 or Psi2 12S6 cells) were seeded in a 96-well plate at a density of 10,000 cells per well in 100 μL of DMEM at 37 °C for 24 h. Next, the DMEM was removed, and the plate was left open in the biological safety cabinet (under the same environment used for cell electrospinning) for defined times. Cell viability following different media-free exposure times was then evaluated using the same PrestoBlue protocol outlined above.

2.3.11 Live/dead assay

For assessing cell viability within the electrospun nanofibrous hydrogels, a calcein AM/ethidium homodimer-1 (Et-D) LIVE/DEAD assay was used following the manufacturer's protocol. PBS (1x) was used to wash off any non-bound dyes over three washing cycles before imaging. Imaging was performed using the CLSM procedures above with excitation/emission wavelengths of 488 nm/561 nm.

2.3.12 CFSE and Far Red staining for cell tracking

CellTrace™ CFSE and Far Red were used to label cells to track cell distribution and cell proliferation within electrospun nanofibrous hydrogels. 3T3 or Psi2 12S6 cells were pre-stained with CFSE and Far Red stock as described in the manufacturer's protocol and then electrospun as described previously. Imaging was performed using the CLSM procedures described previously with excitation/emission wavelengths of 492/517 nm (CellTrace™ CFSE, green) and 633/635 nm (Far Red, orange), respectively.

2.3.13 Immunofluorescent staining

For immunofluorescence staining, the cell-loaded electrospun scaffold was first washed with pre-warmed PBS (3 washes) and then fixed with 4 wt% paraformaldehyde in PBS (methanol free) for 15 mins. 0.1% Triton-X-100 was added to permeabilize the cells for 15 min, after which the cells were washed 3 times with PBS in a 24 well plate. Blocking solution containing 1% BSA was incubated with the cells for 30 mins at room temperature, after which fluorescent rhodamine phalloidin staining solution (1:1000 dilution) was then added and incubated for one-hour incubation at room temperature. After washing the sample with PBS three times, DAPI (300 nM solution in PBS) was added and incubated for 10 mins at room temperature, after which the wells were again washed with PBS to remove excess dyes. CLSM was conducted as previous description with excitation/emission wavelengths of 540/565 nm (rhodamine phalloidin, red) and 360/460 nm (DAPI, blue).

2.4 Results and Discussion

2.4.1 Cell viability for reactive electrospinning process

Hydrazide and aldehyde-functionalized POEGMA were synthesized by free radical polymerization as reported in our previous work[25,27]. Both POH and POA polymer precursors exhibited number average molecular weights less than 40 kDa (21.5 kDa for POH and 26.8 kDa for POA (Appendix A, Table S2.1), supporting their capacity to be renally cleared following the hydrolytic degradation of hydrogels. Near-quantitative incorporation of hydrazide and aldehyde functional groups was achieved, with the ~30 mol% target functionalization value resulting in a slow gelation time of 30-40 mins that ensures no significant gelation in the needle prior to fiber spinning but sufficiently fast gelation upon concentration of the polymers in the fiber jet as the water evaporates following fiber spinning to maintain independent hydrogel nanofibers on the electrospinning collector (Appendix A Table S2.1, Figure S2.1). Each precursor polymer maintained high cytocompatibility with both 3T3 fibroblasts and Psi2 12S6 epithelial cells. (Figures 2.2A and 2.2B). To model the effect of solvent evaporation during the electrospinning process, cells were plated a multi-well plate and exposed to ambient air. Both 3T3 and Psi2 12S6 cells could maintain high cell viabilities (> ~80%) in the simulated dehydration environment for 2 hours (Figure 2.2C); note that the dryness of this environment is likely significantly higher than it would be in the presence of the co-electrospun hydrogel nanofibers. In parallel, electrospinning 3T3 and Psi2 12S6 cells alone in DMEM medium (without the gel precursor materials) using voltages ranging from 0 kV to 15 kV maintains equivalent cytocompatibility to a directly plated control sample (Figure 2.2D), consistent with the low current applied during electrospinning not inducing significant cell toxicity[33,34]. As such, both the materials and electrospinning process are compatible with the target cells. To ensure optimal results based on these preliminary experiments,

all cell electrospinning experiments were limited to one hour to ensure minimal impacts on cell viability in the "dry" state prior to re-immersion in cell media.

2.4.2 Morphologies of encapsulated cells in electrospun scaffolds

3T3 fibroblast cells were co-electrospun into hydrogel nanofibrous scaffolds prepared with and without grafting of the cell adhesive ligand RGD to the POA polymer. SEM images indicated average 3T3 cell diameters of 14 ± 4 μm in POEGMA gels (POH+POA) and 11 ± 3 μm in POEGMA-RGD gels (POH+POA-RGD) (Figure 2.2E-J) and Psi2 12S6 cell diameters of 11 ± 4 μm in POEGMA gels (POH+POA) and 8 ± 5 μm in POEGMA-RGD gels (POH+POA-RGD) (Figure 2.2K-P). Both these results are consistent with the diameter of the corresponding fresh cells in DMEM suspension[26], indicating the ability of the hydrogel nanofibers (even in the "dried" state) to retain sufficient water to maintain cell hydration even in the low pressure SEM imaging environment. Additionally, two distinctive cell morphologies (round cells and elongated cells, as shown in Figures 2.2E-F, 2.2H-I, 2.2K-L, and 2.2N-O) were found in both hydrogel scaffolds, again consistent with our previous work[26], the majority of cells (> 75% in both hydrogel scaffolds) were rounded and physically entrapped between nanofibers while a subgroup (<25% in both hydrogel scaffolds) were elongated cells that were co-extruded within the Taylor cone and thus stretched within the electrospun nanofibers.

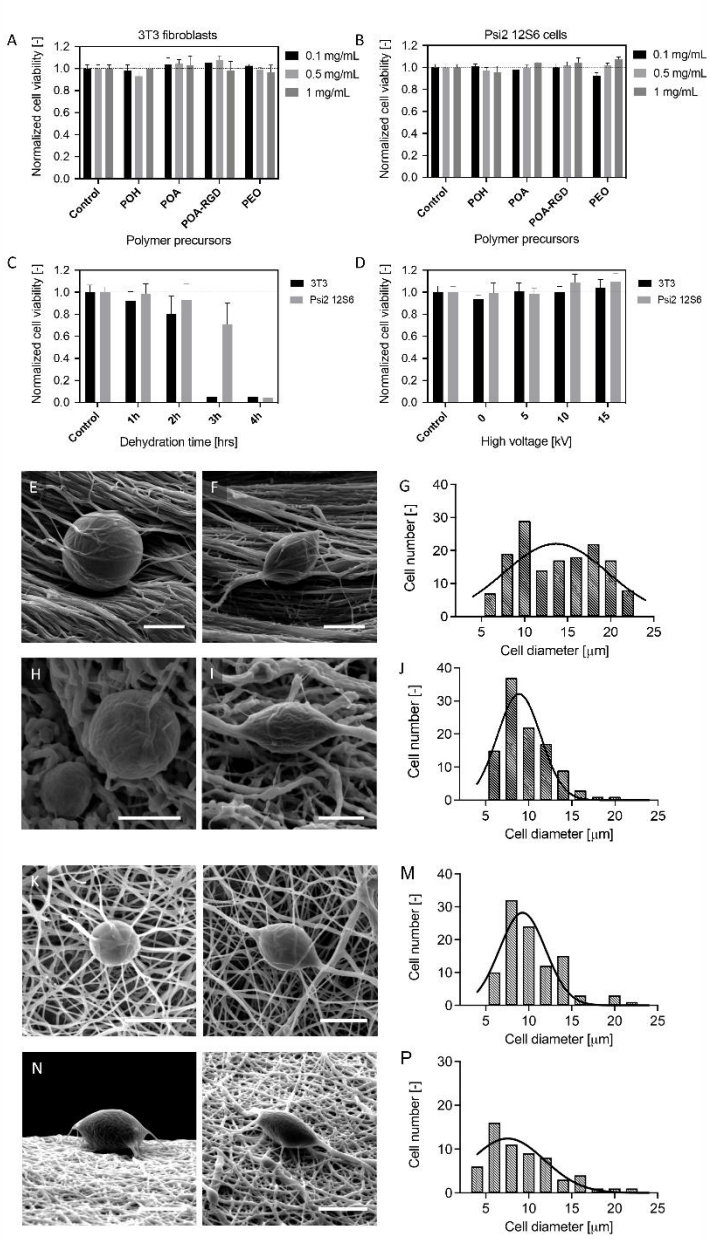

Figure 2.2. (A-B) Cell viabilities of 3T3 fibroblasts (A) and Psi2 12S6 epithelial cells (B) in the presence of polymer precursors (POH, POA, POA-RGD and PEO) for cell electrospinning. (C-D) Cell viabilities of 3T3 fibroblasts and Psi2 12S6 epithelial cells under dehydrated condition over different times following removal of media (C) and different voltages when electrospun in DMEM media only (D). Cell density is 10,000 cells per well (n = 4). (E-G) SEM images (E,F) and cell diameter distribution (G, n = 151 cells counted) of 3T3 fibroblast cells within POEGMA hydrogel nanofibers. (H-J) SEM images (H, I) and cell diameter distribution (J, n = 106 cells counted) of 3T3 fibroblast cells within POEGMA hydrogel nanofibers containing RGD. (K-M) SEM images (K,L) and cell diameter distribution (M, n = 133 cells counted) of Psi2 12S6 epithelial cells within POEGMA hydrogel nanofibers. (N-P) SEM images (N, O) and cell diameter distribution (P, n = 98 cells counted) of Psi2 12S6 epithelial cells within POEGMA hydrogel nanofibers containing RGD. Scale bars = 10 μm.

2.4.3 Cell viability and cell proliferation in nanofibrous hydrogel scaffolds

To demonstrate the viability of electrospun 3T3 fibroblast cells and Psi2 12S6 epithelial cells within the nanofibrous hydrogel scaffolds, a calcein AM/ethidium homodimer-1 LIVE/DEAD stain was used to determine cell viability within the scaffolds at 3, 7 and 14 days. (Figure 2.3A-D) Significantly more live cells (green) relative to dead cells (red) were observed in all hydrogel scaffolds after 3 days of incubation; furthermore, cell number was also observed to increased significantly from day 3 to day 14, with both 3T3 and Psi2 12S6 cells demonstrating a ~4-fold increase in cell density as analyzed by counting of live cells in both 2D (Figures 2.4A, 2.4C) and 3D (Figures 2.4B, 2.4D) confocal images. While the raw number of viable cells observed in POH+POA-RGD electrospun hydrogel scaffolds was generally higher than that observed for POH+POA scaffolds, the cell viability in the presence of RGD was only significantly improved in the 3D analysis of 3T3 cells loaded in the scaffold after 14 days (Figure 2.4B); RGD inclusion did not have a significant benefit on cell viability in any of the other analyses ($p > 0.05$ for all other pairwise comparison between the two scaffolds). This result suggests that, while the RGD tag has some benefit for promoting improved cell viability and may have some marginal benefits in promoting cell proliferation, the nanofibrous structure itself can provide sufficient physical sites and support for cell binding and adhesion even in the absence of cell adhesion peptides.

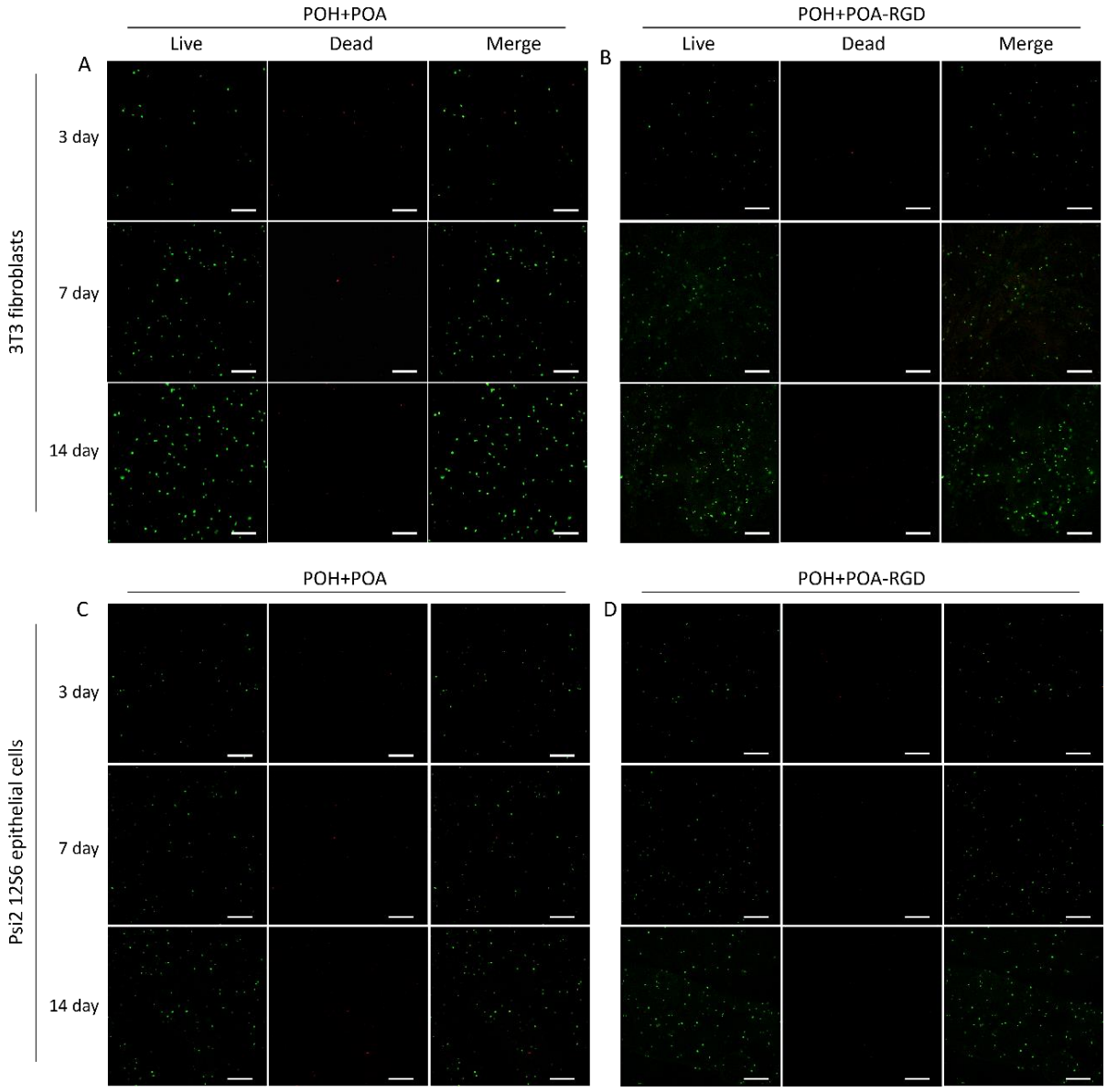

Figure 2.3. Confocal images of 3T3 fibroblasts (A,B) and Psi2 12S6 epithelial cells (C,D) cells encapsulated in nanofibrous hydrogel scaffolds fabricated without (POH+POA, panels A,C) and with (POH+POA-RGD, panels B, D) hydrogel-grafted RGD cell adhesion peptide following 3, 7, and 14 days of incubation. Live cells (green, 488 nm) and dead cells (red, 561 nm) are both shown in the images. Scale bars = 200 μm. Cell density is 10^6 cell/mL for all electrospun samples.

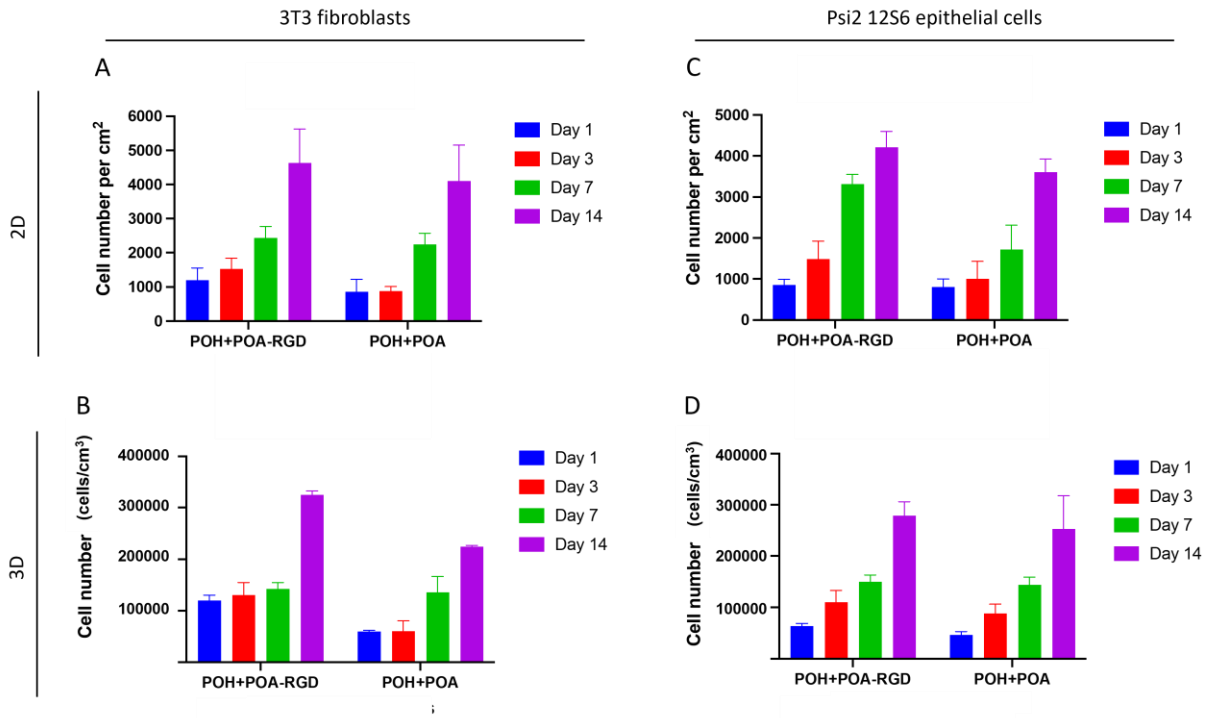

Figure 2.4. Cell densities of 3T3 fibroblasts (A,B) and Psi2 12S6 epithelial cells (C,D) co-electrospun into POH+POA or POH+POA-RGD hydrogel nanofibers as measured via ImageJ analysis of 2D (A, C) and 3D (B, D) confocal microscopy images as a function of culture time from day 1 to day 14, confirming cell proliferation within the electrospun hydrogel scaffolds. Only live cells labelled by calcein AM (green, 488 nm) were counted for analysis. (n = 4 independent scaffolds, 4 images per sample used for analysis).

2.4.4 Co-encapsulation of 3T3 and Psi2 12S6 cells via layer-by-layer cell electrospinning

To explore the potential of cell reactive electrospinning to fabricate multi-cellular tissue constructs, two types of co-culture scaffolds were fabricated: (1) a mixed-co-culture of 3T3 and Psi2 12S6 cells in which a 3:1 ratio of 3T3:Psi2 12S6 cells (to match the cell ratio in the spatially segregated sample) was suspended in the POH polymer and electrospun for 1 hour (no cell segregation – Figure 2.5A); (2) a spatially segregated co-culture of 3T3 and Psi2 12S6 cells in which a 3T3-only POH polymer solution was electrospun for 45 minutes followed by a Psi2 12S6-only POH polymer solution for an additional 15 minutes (Figure 2.5B). Depth coding of the samples prepared within NIS Elements Viewer demonstrated that, in the mixed co-culture, both 3T3 (green) and Psi2 12S6

(orange) cells were distributed throughout the full depth of the scaffold, with depth profiling images in which cells at the top of the scaffold are colored blue and cells at the bottom of the scaffold are colored pink confirming the random distribution of the two cell types (Figure 2.5D). In contrast, the sequential cell electrospinning method showed that the Psi2 12S6 cells (orange) spun on top of the scaffold remained on top while the bottom layer of 3T3 cells (green) remained on the bottom; depth coding confirms this result, with 3T3 cells visually appearing primarily pink (bottom) in colour and Psi2 12S6 cells remaining primarily blue (top) in colour (Figure 2.5C). As such, the layer-by-layer strategy can localize specific cells within a scaffold. Note that such segregation is only observed if the sequentially electrospun layers are sufficiently thick; for example, if only short electrospinning times were used (5 minutes for each layer, Appendix A, Figure S2.2), both pre-stained cells can be observed in a given 2D confocal slice (Appendix A, Figure S2.2F-H) due to the small volumes of each layer electrospun.

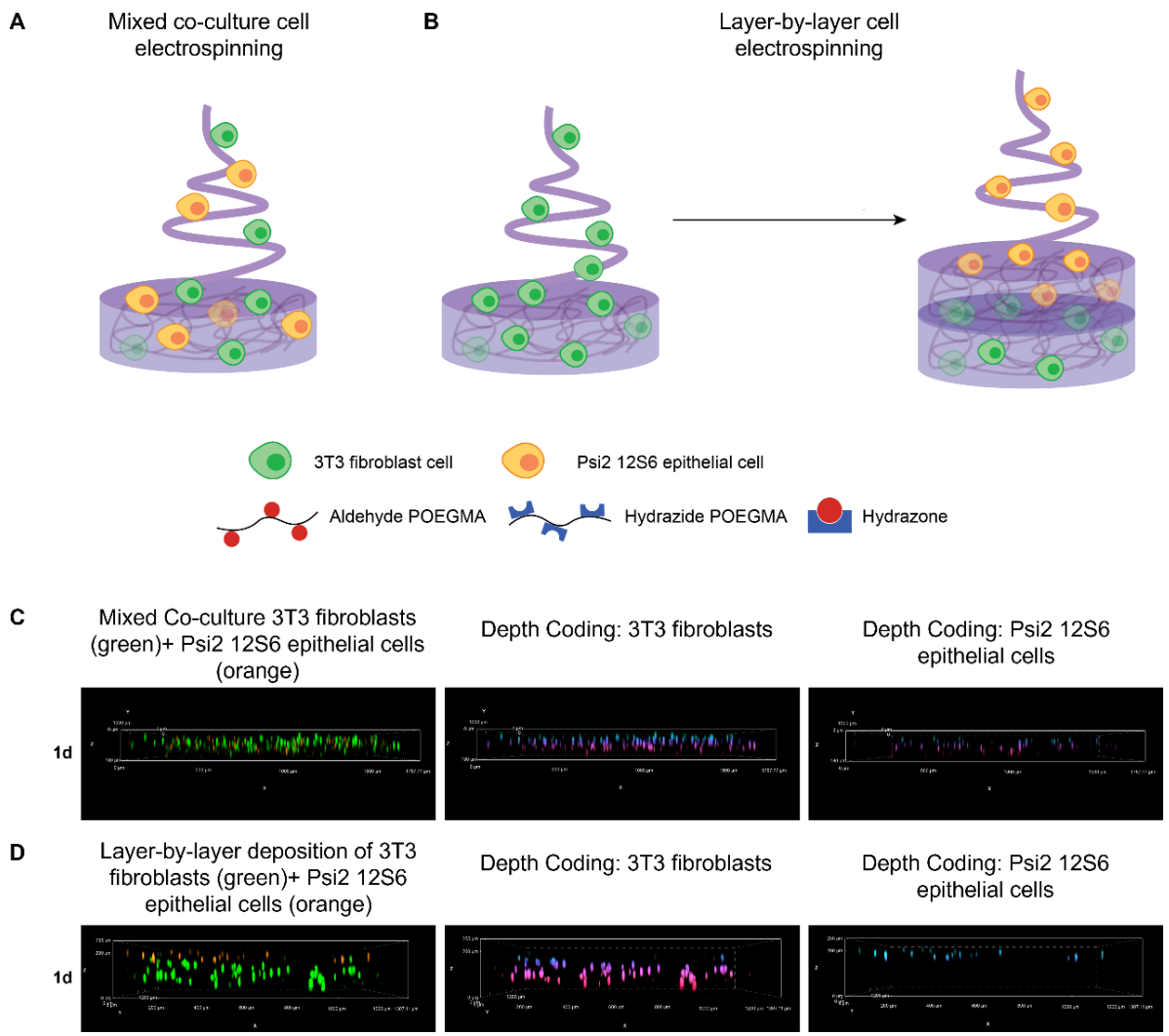

Figure 2.5. (A,B) Schematic diagrams of cell electrospinning of hydrogel scaffolds loaded with pre-stained 3T3 (green) and Psi2 12S6 epithelial cells (orange) in a mixed co-culture model (A) and using layer-by-layer deposition (B). (C,D) Experimental cross-sectional distributions (via 3D confocal imaging) of co-encapsulated cells, supplemented by depth coding (top = blue, bottom = pink) based on cell type, in POH+POA hydrogels scaffolds with mixed 3T3 and Psi2 12S6 cells (C) and POH+POA with layer-by-layer deposition of 3T3 fibroblasts for 45 minutes followed by Psi2 12S6 epithelial cells (15 minutes) (D) after 1 day of culture.

The sequentially co-encapsulated cell scaffolds were then incubated for 14 days to track the cell proliferation and/or spreading of each cell type over time. As shown in Figure 2.6A-H, significant cell proliferation was observed for both 3T3 and Psi2 12S6 cells co-encapsulated in both POH+POA and POH+POA-RGD hydrogel scaffolds, with both cell types exhibiting ~3-4 fold

population expansions over the 14-day incubation period (Figure 2.6K-O) consistent with their single-cell scaffold expansion rates (Figure 2.4); as such, the initially electrospun ratio of 3:1 (3T3:Psi2 12S6) cells is maintained even during extended incubation times. Cells loaded in the POH+POA-RGD hydrogel scaffold exhibit somewhat faster proliferation than those encapsulated in the POH+POA scaffolds, particularly the epithelial cells that are less prone to make their own ECM relative to fibroblasts[35,36] and thus would be more dependent on native ECM cues in their matrix to stimulate adhesion and/or proliferation. However, as with the single cell scaffolds in Figure 2.4, the nanofibrous scaffolds even without RGD can still provide sufficient structural cues to promote effective cell adhesion; indeed, F-actin staining demonstrates strong cell adhesion to both types of scaffolds (Appendix A Figure S2.3). Despite this proliferation, the significant majority of Psi2 12S6 cells was found to stay on the top layer while the large majority of 3T3 cells persisted in the bottom layer over the 14 day incubation period (Figure 2.6K). This result suggests that cell expansion can occur without fully compromising the beneficial spatial segregation of the two cell types that is enabled by the layer-by-layer reactive electrospinning strategy. Note that none of the multi-layer scaffolds delaminated during the cell culture period, a key benefit of the combined mechanical entanglement achieved during electrospinning coupled with the dynamic covalent chemistry of hydrazone formation that can reform hydrazone bonds[28,37] and effectively heal any interface between adjacent nanofibers.

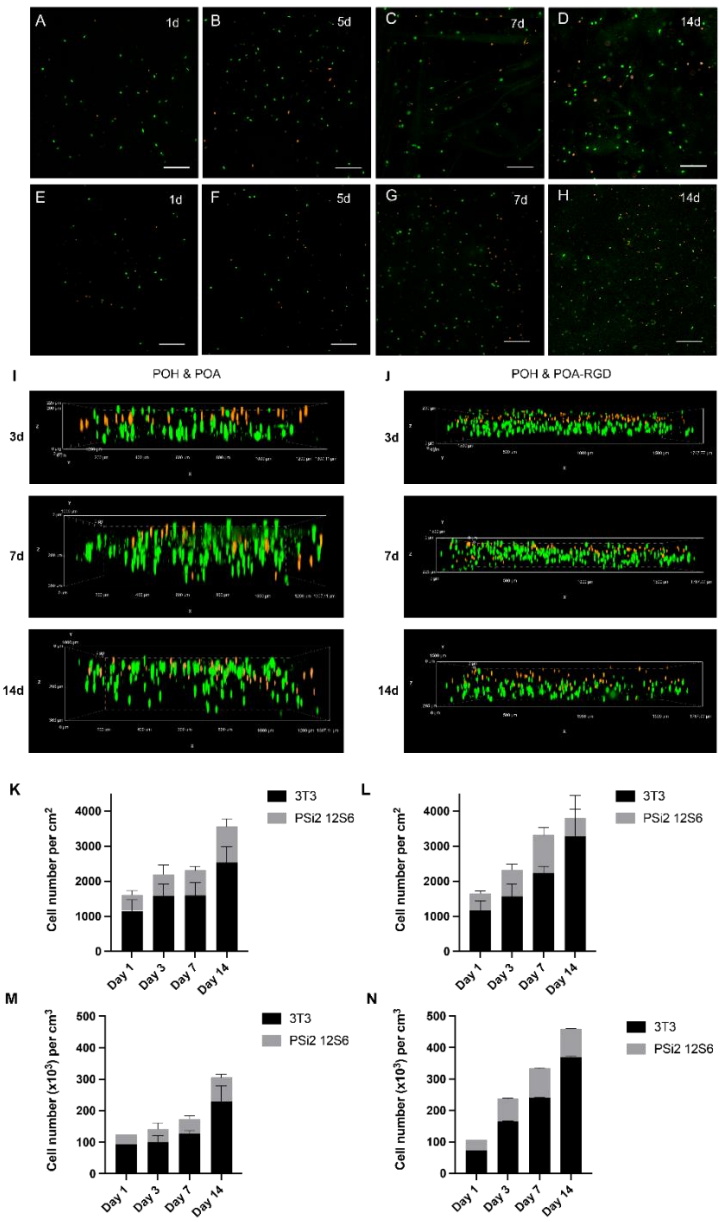

Figure 2.6. Cell proliferation in sequentially electrospun pre-stained 3T3 fibroblast (green coloration, 45 minutes electrospinning time)/Psi 12S6 (orange coloration, 15 minutes electrospinning time) hydrogel scaffolds: (A-H) 2D confocal images of co-encapsulated cells in POH+POA (A-D) and POH+POA-RGD (E-H) hydrogel scaffolds fabricated via layer-by-layer reactive cell electrospinning as a function of culture time up to 14 days. Scale bars = 200 μm. (I-J) Cross-sectional view of 3D confocal depth images of sequentially electrospun co-encapsulated cells in POH+POA (I) and POH+POA-RGD (J) hydrogel scaffolds via layer-by-layer reactive cell electrospinning over 3, 7, and 14-days. Electrospinning time was 45 mins for 3T3 cells and 15 mins for Psi2 12S6 cells. (J-M) Cell densities of sequentially electrospun 3T3 and Psi2 12S6 cells measured via ImageJ analysis of 2D (K,L) and 3D (M,N) confocal microscopy images as a function of culture time from day 1 to day 14, confirming cell proliferation of different cells within the POH+POA (K,M) and POH+POA-RGD (L,N) electrospun hydrogel scaffolds by identifying the different colours. (n = 4, 4 images per sample for analysis).

Overall, these results demonstrate that reactive cell electrospinning can be used to fabricate multi-cellular layered scaffolds in which cells are distributed throughout the depth of the scaffold. The spatial deposition of cells within the multi-cellular scaffolds adds a degree of control not typically seen in electrospun scaffolds and has not frequently been explored in conjunction with cell electrospinning techniques. While electrospinning techniques have been previously reported for cell co-culture, examples are almost entirely related to mixed co-culture models due to the increased ease of cell seeding and/or the need for further processing of the scaffold to achieve the desired scaffold architecture[38]. Spatially segregated co-culture electrospinning models face additional challenges due to the challenges inherent in post-seeding cells that are fully segregated into one layer at the exclusion of another cell-laden layer[39]. The ease of fabrication and ability to directly generate a spatially segregated co-culture without any required post-processing thus makes reactive cell electrospinning a unique approach to co-culture electrospun scaffolds. Of note, while the inclusion of the cell adhesion peptide RGD in the scaffold appeared to have some modest benefits in terms of enhancing cell adhesion and promoting cell proliferation, almost none of the statistical comparisons between RGD-grafted and RGD-free scaffolds showed significance[26]. This result is in our view notable given that the nanofibrous structure alone, even when that nanofibrous structure is fabricated with a generally protein/cell-repellent polymer (POEGMA), appears to be sufficient for providing the functional cues required for maintaining high cell activity without the inclusion of any natural ECM components. We note that fabricating larger tissues using this technique will require more complex scale-up, particularly in light of the limited electrospinning duration allowable to maintain high cell viability. However, the use of parallel nozzles and/or electrospinning on a hydrated collector (to counteract dehydration) may be potential solutions to the scale-up challenge to allow thicker scaffolds to be fabricated. The dynamic covalent hydrazone

chemistry may also allow for self-healing of independently electrospun scaffolds into a single larger scaffold as a potential alternate solution to the scale-up challenge.

2.5 Conclusions

Multi-cellular, layered hydrogel fibrous scaffolds can be generated via sequential reactive cell electrospinning using POEGMA-based precursor polymers crosslinked via dynamic covalent hydrazone chemistry. Cells were successfully electrospun with high viabilities in a bilayer scaffold that demonstrated the ability to spatially deposit cells with 3-dimensional fibrous networks of different thicknesses (based on different electrospinning times). The nanofibrous morphology promoted high cell adhesion/proliferation within the scaffold (even without inclusion of RGD cell adhesive peptides) while still largely preserving each cell type to the layer in which it was originally electrospun. The high viability and increased cell densities observed in all scaffolds over 14-days offers promise for using this strategy to fabricate more complex tissue implants and/or *in vitro* co-culture models that better mimic native ECM in addition to avoiding the challenges with post-loading multiple cell types locally in pre-fabricated gel scaffolds.

2.6 Acknowledgements

The Natural Sciences and Engineering Research Council of Canada (Discovery Grant RGPIN2017-06455 to TH, E.W.R. Steacie Memorial Fellowship to TH, and a Canada Graduate Scholarship to CD) is acknowledged for financial support The CALM institute, Dr. Harold Stover, and the CCEM are acknowledged for their help in CLSM and SEM image acquisition and analysis. Meghan Kostashuk is acknowledged for assistance in polymer synthesis and characterization.

2.7 References

1 Lee, K. Y. & Mooney, D. J. Hydrogels for Tissue Engineering. *Chemical Reviews* **101**, 1869-1880 (2001).

2 Hunt, J. A., Chen, R., Van Veen, T. & Bryan, N. Hydrogels for tissue engineering and regenerative medicine. *J. Mater. Chem. B* **2**, 5319-5338 (2014).

3 Hoffman, A. S. Hydrogels for biomedical applications. *Advanced Drug Delivery Reviews* **64**, 18-23 (2012).

4 Peppas, N. A., Hilt, J. Z., Khademhosseini, A. & Langer, R. Hydrogels in Biology and Medicine: From Molecular Principles to Bionanotechnology. *Advanced Materials* **18**, 1345-1360 (2006).

5 Caló, E. & Khutoryanskiy, V. V. Biomedical applications of hydrogels: A review of patents and commercial products. *European Polymer Journal* **65**, 252-267 (2015).

6 De France, K. J., Xu, F. & Hoare, T. Structured Macroporous Hydrogels: Progress, Challenges, and Opportunities. *Adv Healthc Mater* **7**, 1700927 (2018).

7 Tibbitt, M. W. & Anseth, K. S. Hydrogels as extracellular matrix mimics for 3D cell culture. *Biotechnol Bioeng* **103**, 655-663 (2009).

8 Yue, B. Biology of the extracellular matrix: an overview. *J Glaucoma* **23**, S20-S23 (2014).

9 Watt, F. M. & Huck, W. T. Role of the extracellular matrix in regulating stem cell fate. *Nat Rev Mol Cell Biol* **14**, 467-473 (2013).

10 MacNeil, S. Progress and opportunities for tissue-engineered skin. *Nature* **445**, 874-880 (2007).

11 Carvalho, M. S. *et al.* Co-culture cell-derived extracellular matrix loaded electrospun microfibrous scaffolds for bone tissue engineering. *Mater Sci Eng C Mater Biol Appl* **99**, 479-490 (2019).

12 Hendriks, J., Riesle, J. & van Blitterswijk, C. A. Co-culture in cartilage tissue engineering. *J Tissue Eng Regen Med* **1**, 170-178 (2007).

13 Zou, J., Bai, B. & Yao, Y. Progress of co-culture systems in cartilage regeneration. *Expert Opin Biol Ther* **18**, 1151-1158 (2018).

14 Viney, M. E., Bullock, A. J., Day, M. J. & MacNeil, S. Co-culture of intestinal epithelial and stromal cells in 3D collagen-based environments. *Regen Med* **4**, 397-406 (2009).

15 Cui, J. *et al.* Multicellular Co-Culture in Three-Dimensional Gelatin Methacryloyl Hydrogels for Liver Tissue Engineering. *Molecules* **24**, 1762 (2019).

16 Kirkpatrick, C. J., Fuchs, S. & Unger, R. E. Co-culture systems for vascularization--learning from nature. *Adv Drug Deliv Rev* **63**, 291-299 (2011).

17 Stevens, M. M. & George, J. H. Exploring and Engineering the Cell Surface Interface. *Science* **310**, 1135-1138 (2005).

18 Zhang, H. & Cooper, A. I. Synthesis and applications of emulsion-templated porous materials. *Soft Matter* **1**, 107-113 (2005).

19 Lee, S. B., Kim, Y. H., Chong, M. S., Hong, S. H. & Lee, Y. M. Study of gelatin-containing artificial skin V: fabrication of gelatin scaffolds using a salt-leaching method. *Biomaterials* **26**, 1961-1968 (2005).

20 Dehghani, F. & Annabi, N. Engineering porous scaffolds using gas-based techniques. *Curr Opin Biotechnol* **22**, 661-666 (2011).

21 Thomas, A. M. & Shea, L. D. Cryotemplation for the Rapid Fabrication of Porous, Patternable Photopolymerized Hydrogels. *J Mater Chem B Mater Biol Med* **2**, 4521-4530 (2014).

22 Xu, F. *et al.* Hydrogels for Tissue Engineering: Addressing Key Design Needs Toward Clinical Translation. *Front Bioeng Biotechnol* **10**, 849831 (2022).
23 Sill, T. J. & von Recum, H. A. Electrospinning: Applications in drug delivery and tissue engineering. *Biomaterials* **29**, 1989-2006 (2008).
24 Bhardwaj, N. & Kundu, S. C. Electrospinning: a fascinating fiber fabrication technique. *Biotechnol Adv* **28**, 325-347 (2010).
25 Xu, F., Sheardown, H. & Hoare, T. Reactive electrospinning of degradable poly(oligoethylene glycol methacrylate)-based nanofibrous hydrogel networks. *Chemical Communications* **52**, 1451-1454 (2016).
26 Xu, F., Dodd, M., Sheardown, H. & Hoare, T. Single-Step Reactive Electrospinning of Cell-Loaded Nanofibrous Scaffolds as Ready-to-Use Tissue Patches. *Biomacromolecules* **19**, 4182-4192 (2018).
27 Smeets, N. M. B., Bakaic, E., Patenaude, M. & Hoare, T. Injectable and tunable poly(ethylene glycol) analogue hydrogels based on poly(oligoethylene glycol methacrylate). *Chemical Communications* **50**, 3306-3309 (2014).
28 Mueller, E., Xu, F. & Hoare, T. FRESH Bioprinting of Dynamic Hydrazone-Cross-Linked Synthetic Hydrogels. *Biomacromolecules* **23**, 4883-4895 (2022).
29 Sampson, S. L., Saraiva, L., Gustafsson, K., Jayasinghe, S. N. & Robertson, B. D. Cell electrospinning: an in vitro and in vivo study. *Small* **10**, 78-82 (2014).
30 Townsend-Nicholson, A. & Jayasinghe, S. N. Cell Electrospinning: a Unique Biotechnique for Encapsulating Living Organisms for Generating Active Biological Microthreads/Scaffolds. *Biomacromolecules* **7**, 3364-3369 (2006).
31 Yeo, M. & Kim, G. Micro/nano-hierarchical scaffold fabricated using a cell electrospinning/3D printing process for co-culturing myoblasts and HUVECs to induce myoblast alignment and differentiation. *Acta biomaterialia* **107**, 102-114 (2020).
32 Stankus, J. J., Guan, J., Fujimoto, K. & Wagner, W. R. Microintegrating smooth muscle cells into a biodegradable, elastomeric fiber matrix. *Biomaterials* **27**, 735-744 (2006).
33 Yalcinkaya, B., Yener, F., Jirsak, O. & Cengiz-Callioglu, F. On the Nature of Electric Current in the Electrospinning Process. *Journal of Nanomaterials* **2013**, 538179 (2013).
34 Jayasinghe, S. N. Cell electrospinning: a novel tool for functionalising fibres, scaffolds and membranes with living cells and other advanced materials for regenerative biology and medicine. *Analyst* **138**, 2215 (2013).
35 Frantz, C., Stewart, K. M. & Weaver, V. M. The extracellular matrix at a glance. *Journal of Cell Science* **123**, 4195-4200 (2010).
36 Scherzer, M. T. *et al.* Fibroblast-Derived Extracellular Matrices: An Alternative Cell Culture System That Increases Metastatic Cellular Properties. *PLoS One* **10**, 0138065 (2015).
37 Mueller, E., Poulin, I., Bodnaryk, W. J. & Hoare, T. Click Chemistry Hydrogels for Extrusion Bioprinting: Progress, Challenges, and Opportunities. *Biomacromolecules* **23**, 619-640 (2022).
38 Wu, S., Wang, Y., Streubel, P. N. & Duan, B. Living nanofiber yarn-based woven biotextiles for tendon tissue engineering using cell tri-culture and mechanical stimulation. *Acta Biomaterialia* **62**, 102-115 (2017).
39 Soliman, S. *et al.* A multilayer scaffold design with spatial arrangement of cells to modulate esophageal tissue growth. *Journal of Biomedical Materials Research - Part B Applied Biomaterials* **107**, 324-331 (2019).

3 Chapter 3: Reactive Cell Electrospinning of Anisotropically Aligned and Bilayer Hydrogel Nanofiber Networks

3.1 Abstract

Structured hydrogels that incorporate nanofibrous morphologies have been demonstrated to better replicate the structures of native extracellular matrix and thus its function in guiding cell responses. However, current techniques for nanofiber fabrication are limited in their ability to create scaffolds with tunable directional alignments and cell types/densities, as required to reproduce more complex native tissue structures. Herein, we present a reactive cell electrospinning technique based on the dynamic covalent crosslinking of poly(ethylene glycol methacrylate (POEGMA) precursor polymers to fabricate aligned hydrogel nanofibers that can be directly loaded with cells during the electrospinning process. The scaffolds were found to support high C2C12 myoblast viabilities >85% over 14 days, with changes in the electrospinning collector allowing for the single-step fabrication of non-aligned, aligned, or cross-aligned nanofibrous networks. Cell aspect ratios on aligned scaffolds were found on average to be 27% higher compared to those on non-aligned scaffolds; furthermore, cell-loaded bilayer scaffolds with perpendicular fiber alignments showed evidence of enabling localized directional cell responses to individual layer fiber directions while avoiding delamination between the layers. This fabrication approach thus offers potential for better mimicking the structure and thus function of aligned and multi-layered tissues (e.g. smooth muscle, neural, or tendon tissues).

3.2 Introduction

Recent advances in soft tissue engineering have led to the development of multiple promising strategies to derive patient-specific tissues that can recapitulate the structure and cell responses of native tissues. The success of such strategies relies on adequate replication of natural extracellular matrix (ECM) functions, including its roles in supporting cell adhesion, proliferation, and nutrient transport within the tissue. While different tissue engineering techniques aim to provide a suitable environment for cell adhesion and proliferation[1-4], techniques focused on creating nanofibers or microfibers are particularly appealing given that they can imitate the fibrous structural components characterizing native ECM (e.g. collagen, elastin, or fibronectin[5,6]). The specific use of hydrogel-based fibers allows for the replication of both the natural ECM fibrous structure as well as the high-water content environment of native ECM, both of which are essential for replicating its mechanical and biological properties[7]. Fibrous hydrogels have been fabricated through electrospinning[8,9], pull-spinning[10], and bio-printing[11,12]. While bio-printing offers a high degree of control over hydrogel deposition and generally good scalability[13,14], the resolution of current scalable 3D printing methods cannot replate the length scale of native ECM fibrous structures (<1000 nm diameter) [6,15,16]. In contrast, while electrospinning and pull-spinning[10,17] offer the potential to generate such high-resolution fibrous networks due to their ability to reproducibly generate fibers with nano-scale diameters[18], enabling efficient gelation in such systems in a manner that allows for consistent nanofiber formation while also being cell-friendly remains a challenge.

Electrospinning is an adaptable fabrication method that relies on a conductive collector and a high voltage source. Frequently explored conductive collectors include stationary discs[19], parallel rods[20], or rotating drums[21,22], allowing for the fabrication of nanofibers with a range of diameters, morphologies, and alignments; custom collectors have also been explored for application-specific

requirements[23,24]. Electrospun hydrogel scaffolds have been reported based on natural polymers such as gelatin[25-27], alginate[25], dextran[28], hyaluronic acid[29,30], or collagen[31] or combinations of those polymers with synthetic polymers such as poly(ethylene glycol) (PEG)-derivatives (e.g. poly(ethylene glycol) diacrylate (PEGDA) [27] or poly(oligoethylene glycol methacrylate) [19,32] (POEGMA)), poly(ε-caprolactone) (PCL) [20,33] or poly(vinylpyrrolidone) (PVP) [34]; the synthetic polymer additive is most typically used to facilitate improved electrospinnability (e.g. by increasing polymer entanglement to enhance fiber formation) and/or provide stronger mechanics to the resulting scaffolds. The formation of hydrogel-based nanofiber networks requires cross-linking of the electrospun materials, commonly performed either simultaneously with the fabrication process or post-fabrication using techniques including photocrosslinking[28], chemical crosslinking[19], or enzymatic cross-linking[35]. Post-crosslinking methods offer advantages in terms of enhancing the range of crosslinking chemistry that is accessible, while simultaneous crosslinking offers improved efficiency in terms of not requiring further processing of the scaffold.

Structured fibrous hydrogels formed using electrospinning have shown positive results around promoting cell adhesion and interactions with the swollen fibers, demonstrating limited cell toxicity while promoting the ability of the cells to proliferate when seeded on the fibrous network[36]. Alignment of the electrospun fibers further provides key topographical cues to promote desired cell responses. While a range of electrospinning setups/collectors has been assessed to promote nanofiber alignment[23,24], altering the rotation speed of a collector drum is the simplest effective method of achieving aligned electrospun fibers[21,22]. Such an approach has been used in multiple demonstrations to enable myoblast proliferation into elongated cell structures guided by the fiber orientation, facilitating the fabrication of highly ordered anisotropic structures of skeletal[37,38], cardiac[10,39], tendon[21,40], or smooth muscle[33,37] tissues that lead to simultaneous contraction of the

tissue; alternately, directed cell signaling in neural tissue engineering applications has been achieved using aligned nanofibrous scaffolds[24,26,41,42].

Incorporating multiple layers of nanofiber alignment into a single electrospun scaffold offers additional advantages in terms of better simulating more complex tissues in which different types of cell alignment are targeted in different layers of the tissue, including blood vessels as well as stomach or esophageal tissues[33,37,43]) Bilayer cross-aligned networks that contain perpendicular nanofiber alignments in different layers are particularly biologically relevant in this context. Previous cross-aligned fibers have been fabricated using high rotation speed rotating drum collectors, pausing the fabrication process to rotate the scaffold on the collector, and then continuing the electrospinning process to generate the second layer[22,44,45]. However, such techniques have been limited in practical applications with cells due to the challenges associated with seeding cells uniformly throughout thicker, multi-layered scaffolds and/or seeding different segments of a pre-formed multi-layer scaffold with different cell types. Indeed, given the incompatibility of most hydrogel electrospinning processes with cells and thus the requirement to post-seed cells on the surface of the scaffolds after fabrication is complete, cell spreading into the deeper layers of the scaffold represents a key limitation of creating functional multi-layer tissues[33].

Cell electrospinning overcomes these challenges by directly incorporating cells into the electrospinning solutions, leading to a significantly more uniform and spatially-controlled distributions of cells within the scaffold given that cells are deposited in the scaffold at the same time as the nanofibers themselves. Cell electrospinning has been achieved via controlled electrospinning experimental designs that minimize the effects of the high voltage on the cells and use cell-compatible post-fabrication cross-linking chemistries that avoid the need for organic solvents or secondary sterilization processes. However, previous examples of cell electrospinning

are limited, with those few examples primarily applying modified collectors submerged within a crosslinking solution collection bath to immediately crosslink the cell-laden fibers (a geometry that makes simultaneous alignment extremely challenging to achieve). As an alternative, we have recently reported a dynamic covalent chemistry approach to achieving reactive cell electrospinning using hydrazone-crosslinked *in situ*-gelling POEGMA hydrogel fibers, enabling collection on a conventional "dry" collector (opening the potential to use any collector geometry) while still maintaining high electrospun cell viability and the potential to support cell adhesion and proliferation over 18 days[8]. The scaffolds can be prepared in sterile conditions by simply filtering the low viscosity precursor polymer solutions; furthermore, given that hydrazone chemistry can be performed in water without the need for any additives/catalysts, there is no need for any post-processing solvent removal or cross-linking step, improving the process compatibility with cells.

Herein, we expand on this previous work to present a combined fabrication and cell seeding technique via reactive cell electrospinning to produce highly aligned POEGMA hydrogel nanofibers that can regulate cell responses. Combining the ease of fabrication, the use of non-cytotoxic polymers, and the ability to electrospin in an all-aqueous solution, aligned reactive cell electrospinning is shown to offer significant potential to fabricate directionally orientated, soft hydrogel fiber networks. Furthermore, the reversibility of the dynamic hydrazone chemistry enables self-healing between sequentially electrospun layers containing the same or different cell types, offering a unique approach to generate bilayer scaffolds with tunable directionality in which cells can be distributed throughout the entire scaffold without supplementary cell seeding and receive topographical cues specific to each scaffold layer fiber direction.

3.3 Materials and Methods

3.3.1 Materials

Oligo(ethylene glycol) methyl ether methacrylate ($OEGMA_{500}$, 95%, M_n = 500 g/mol, Sigma-Aldrich) was purified before use to remove the inhibitors butylated hydroxytoluene (BHT) and methyl ether hydroquinone (MEHQ) inhibitors via a basic aluminum-oxide packed column (Sigma Aldrich type CG-20). AIBMe (Wako Chemicals, 98.5%), dioxane (Caledon Laboratories 99%), acrylic acid (AA, Sigma-Aldrich, 99%), thioglycolic acid (TGA, Sigma Aldrich, 98%), N'-ethyl-N-(3-(dimethylamino)propyl)-carbodiimide (EDC, Carbosynth, Compton CA, commercial grade), and adipic acid dihydrazide (ADH, Alfa Aesar, 98%) were used as received. N-(2,-dimethoxyethyl) methacrylamide (DMEMAm) was synthesized in-house using previously described methods[46]. All experiments used Milli-Q grade deionized, distilled water (DIW) when required. Poly (ethylene oxide) (PEO, M_w = 600,000 g/mol), sodium cyanoborohydride, and fluorescein isothiocyanate (FITC) were obtained from Sigma-Aldrich and used as received. Cyanine5 amine was purchased from Lumiprobe and used as received. C2C12 myoblasts were purchased from ATCC (Cedarlane Laboratories, Burlington, ON). Dulbecco's modified Eagle's medium (DMEM, ThermoFisher), phosphate-buffered saline (1 x PBS, pH = 7.4, ThermoFisher), fetal bovine serum (FBS, ThermoFisher), penicillin-streptomycin (ThermoFisher), trypsin-EDTA (Sigma-Aldrich), formaldehyde (4% in PBS, methanol-free, ThermoFisher), bovine serum albumin (BSA, ThermoFisher), Triton-X-100 (ThermoFisher), 4',6-diamidino-2-phenylindole (DAPI, ThermoFisher), carboxyfluorescein diacetate succinimidyl ester (Cell Trace CFDA-SE, ThermoFisher), Far Red (Cell Trace Far Red, ThermoFisher), PrestoBlue (ThermoFisher), rhodamine phalloidin (ThermoFisher), and a LIVE/DEAD^{TM} Cell Imaging Kit (ThermoFisher) were all used as received.

3.3.2 Hydrazide-Functionalized POEGMA Polymer Synthesis (POH)

Hydrazide-functionalized POEGMA (POH) was synthesized using previously described methods[46]. In short, POH synthesis was achieved by dissolving 42 mg of AIBMe, 4.0 g of $OEGMA_{500}$, and 0.15 g of AA in 20 mL of dioxane and polymerizing under nitrogen with magnetic stirring for 4 hours at 75 °C. The resulting polymer was then hydrazide functionalized by adding the entire polymer batch to 0.82 g EDC (2.5-fold molar excess) and 1.83 g ADH (5-fold molar excess) in 100 mL DIW and reacting at pH 4.75 for 4 hours. The resultant POH polymer was dialyzed with DIW (6 x 6 hours cycles) before lyophilization, after which the polymer was stored at 15 wt% in 1 x PBS and 4 °C.

3.3.3 FITC-Labelled POH

FITC was used to label POH to allow for contrast of the cross-aligned fiber layers. Briefly, FITC (5 mg) was reacted under magnetic stirring with 1 g POH in DIW for 12 hours, with all reaction flasks and storage containers covered in aluminum foil to minimize photobleaching (target ~1 mol% functionalization with FITC). Post-reaction, the POH-FITC solution was dialyzed for a minimum of 6 hours for 6 cycles, lyophilized, and stored at 15 wt% and 4 °C away from light.

3.3.4 Aldehyde-Functionalized POEGMA Polymer Synthesis (POA)

The POEGMA precursor aldehyde-functionalized POEGMA (POA) was synthesized using previously described methods[46]. In short, 44 mg AIBMe, 4.0 g $OEGMA_{500}$, and 0.37 g DMEMAm were dissolved in 20 mL of dioxane and polymerized under nitrogen with magnetic stirring for 4 hours at 75 °C. Aldehyde functionalization was achieved by dissolving the resulting polymer in 100 mL of 0.25 M HCl and reacting overnight to hydrolyze the acetal groups into aldehyde groups.

The resultant POA polymer was dialyzed with DIW for purification (6 x 6 hours cycles) before lyophilization and storage at 15 wt% in 1 x PBS and 4 °C.

3.3.5 Cyanine5-Labelled POA

Cy5 was used to label POA to allow for contrast of the cross-aligned fiber layers. Briefly, Cyanine5 amine (2.5 mg, Lumiprobe) was reacted under magnetic stirring with 1 g POA in DIW for 24 hours, with all reaction flasks and storage containers covered in aluminum foil to minimize photobleaching (target ~1 mol% functionalization with Cy5). After 24 hours, sodium cyanoborohydride (2.7 mg, 10 mol eq. to Cyanine5 amine) was used to reduce the imine bond, allowing the reaction to proceed for 48 hours. Post-reaction, the POA-Cy5 solution was dialyzed for a minimum of 6 x 6 hour cycles, lyophilized, and stored at 15 wt% and 4 °C away from light.

3.3.6 POEGMA Polymer Characterization

The molecular weights of the precursor polymers, POH and POA, were determined using gel permeation chromatography (GPC) using an Agilent 1260 infinity RI detector with Cytiva Superose 6 Increase 10/300 GL column. Polymer solutions were dissolved in 1x PBS with 0.05% sodium azide. The degrees of functionalization of hydrazide groups on POH and of aldehyde groups on POA was assessed using ^{1}H NMR (600 MHz, Bruker).

3.3.7 Preparation of Non-aligned, Aligned, and Cross-aligned Electrospun Hydrogel Fibers

Poly(ethylene oxide) (PEO, 5 wt% in Milli-Q water) was mixed with POH (15 wt% in PBS) or POA (15 wt% in PBS) and loaded into the respective barrels of a double-barrel syringe (MedMix L series, 5 mL capacity) fitted with a static mixer to final concentrations of 7.5 wt% POH or POA and 2.5 wt% PEO. An 18G blunt needle was fitted onto the static mixer, and fibers were

electrospun using an applied high voltage of 10 kV between the needle and the collector. The voltage used was selected based on previous work[8] and was optimized as the lowest voltage that supported formation of fiber formation rather than the production of beaded fiber morphologies. Non-aligned fiber samples were electrospun onto a grounded collector with rods separated by a 1 cm air gap. For aligned fiber samples, fibers were electrospun onto a cylindrical, rotating collector (diameter = 2.75 cm) with 6 vanes to facilitate a 6 x 1 cm air gap area for fiber collection at rotation speeds from 500-4000 rpm. Cross-aligned fiber samples were obtained by removing the first layer of aligned fibers, rotating the fiber network by 90°, and repeating the process. All non-aligned fibers were electrospun at a working distance of 10 cm, while all fibers on the rotating drum were electrospun at a working distance of 9 cm to improve fiber alignment. Both aligned and non-aligned fibers were electrospun at a relative humidity between 25-35%, with the baseline polymer solution flow rate of 15 μL/min adjusted as required with a syringe pump to accommodate for fluctuations in humidity to ensure continuous nanofiber production.

3.3.8 Scaffold Morphology

Fiber and cell morphologies were examined after electrospinning using scanning electron microscopy (SEM, Tescan Vega- II LSU) operating at a voltage of 10 kV. Collected fiber samples were mounted with double-sided tape on an SEM stub and sputter-coated with gold prior to imaging. Confocal laser scanning microscopy (CLSM, Nikon A1R HD25) was used to assess cell viability, adhesion, and morphology within the scaffold. Confocal z stack images were collected by scanning the scaffold from bottom to top at intervals of ~5 μm and then recompiling the slices to obtain 3-dimensional images. Bright-field images were also collected to track the orientation of aligned fibers within the network. Maximum intensity projections were used for live/dead cell

imaging and pre-stained cell imaging in cross-aligned scaffolds. Post-acquisition, CLSM image look-up tables (LUT) were used to process the image for optimal visualization of cell structures and removal of background noise.

3.3.9 Image Analysis

FIJI's directionality plugin was used to generate the directionality histograms and the coefficient of alignment (COA) to evaluate the alignment of the electrospun fibers. The histogram was generated with bins with a width 3° from 0° to 180°, with outputs of direction, dispersion, amount and goodness of fit. Cell aspect ratios were determined using FIJI's analyze particles plug-in with a minimum of 75 cells analyzed per scaffold and per timepoint, with the standard deviation of the aspect ratios measured reported as the error bars.

3.3.10 Mechanical Properties

Dry scaffold tensile mechanical properties were tested using the MicroSquisher (CellScale Biomaterials Testing, Waterloo, ON). Scaffolds were punctured by two tensile testing forks consisting of 5 pins (254 μm diameter per pin) spaced 7 mm across. The tensile forks with loaded scaffolds were attached to a 559 μm gauge cantilever and stretched to 10% elongation over 30 s for 15 cycles. Recovery times were held constant at 30 s with a holding time of 5 s between loading and recovery, followed by a relaxation time of 5 s used at the end of the cycle. The properties of the scaffolds respective to the orientation of the fibers were evaluated through testing in two perpendicular-oriented directions denoted by direction 1 and direction 2. For aligned samples, direction 1 correlates with tensile testing parallel to the alignment of the fibers while direction 2 correlates to tensile testing of the direction perpendicular to the alignment of the fibers.

3.3.11 Cell Culture

C2C12 myoblasts were cultured in T175 flasks in DMEM supplemented with 10% FBS, and 1% penicillin-streptomycin. C2C12 myoblasts were cultured to at least 80% confluency before use. Cell electrospun nanofibrous hydrogels were cultured for 14 days post-fabrication on non-treated Petri dishes to prevent cell adherence to the dish surface. All cells and cell scaffolds were incubated at 5% CO_2 and 37 °C.

3.3.12 Preparation of Cell-Laden Electrospun Scaffolds

PEO solutions for cell electrospinning were prepared by UV sterilizing dry PEO powder (M_w = 600,000 g/mol) for 30 minutes and then dissolving it in sterile DMEM at a concentration of 5 wt%. POH and POA solutions for cell electrospinning were prepared at a concentration of 15 wt% in a 3:1 ratio of PBS: DMEM to minimize any possible cytotoxicity and sterile filtered (0.2 μm filter) prior to use. Cells were incorporated into the precursor polymer solutions by centrifuging a C2C12 cell suspension of known cell density at 1000 rpm for five minutes and resuspending the cell pellet in equal volumes of the POH and PEO polymer precursor solutions. Electrospinning was then carried out in the same way as described above for non-aligned, aligned, and cross-aligned samples (Figure 3.1A-C). Cell densities were optimized based on the electrospinning collector used, with cell densities of 4×10^6 cells/mL used for non-aligned scaffolds and 1×10^7 cells/mL used for aligned and cross-aligned scaffolds. To account for the changes in surface area between the types of collectors (Figure 3.1C), two syringe pumps were utilized, positioned 180° away from each other, for fabricating aligned and cross-aligned fiber samples to increase the sample thickness while still electrospinning for the same amount of time as non-aligned samples. Cell electrospinning times were limited to 30 minutes for single-layer scaffolds and up to 40 minutes

for bilayer scaffolds (with the additional 10 minutes required to rotate the scaffold and re-start electrospinning) to maintain total experiment times of <1 hour, found via previous work to prevent any cell dehydration-related toxicity[8]. After fabrication, the electrospun scaffolds were immediately immersed in DMEM and cultured for up to 14 days.

3.3.13 Cell Viability Assays

3.3.13.1 Cell Viability with Polymer Precursors

Cell viability in contact with the precursor polymers POA, POH, and PEO was assessed using C2C12 myoblasts. Cells were seeded at a density of 10,000 cells per well in a 96-well plate and incubated in 100 μL DMEM for 24 hours. After 24 hours to allow for cell attachment, the cells were incubated with POH, POA, and PEO at concentrations of 1, 2, 5, and 10 mg/mL in DMEM for an additional 24 hours. Finally, the precursor polymers along with DMEM were removed was replaced with 90 μL DMEM and 10 μL of PrestoBlue reagent. After incubation at 37°C for 2 hours, cell viabilities were assessed using fluorescent readings (560 nm excitation/590 nm emission) on a plate reader (Biotek Cytation5). Results were normalized to positive control wells containing DMEM, cells, and PrestoBlue (no materials added). For each polymer and concentration, six independent replicates were performed, with the reported error bars representing the standard deviation.

3.3.13.2 Cell Viability Experimental Conditions

The cytotoxicity induced by the electrospinning process was assessed by electrospinning a cell solution with a cell density of 10^5 cells/mL in DMEM at varying high voltages between 0 and 15 kV for 30 s. The electrospun cells were collected in a Petri dish and re-suspended before plating100 μL per well in a 96-well plate to reach a final cell density of 10,000 cells per well. After a 24-hour

incubation period at 37°C and 5% CO_2, the DMEM was removed and the cell viability was assessed using the same PrestoBlue reagent protocol as outlined above. Five replicates were performed at each tested voltage, with the reported with error bars representing the standard deviation.

The effect of dehydration time on cells (i.e. the time between electrospinning and when the scaffold was placed back into media) was assessed by plating cells at a density of 10,000 cells/well and incubating for 24 hours. Following, the DMEM was removed and cells were left exposed to air (inside a biosafety cabinet) for specific time intervals ranging from 0.5-6 hours. The resulting cell viability was assessed using the same PrestoBlue protocol as outlined above. For each time point six replicates were performed, with the reported error bars representing the standard deviation.

Cell viability in contact with the precursor polymer concentrations used for cell electrospinning was tested for up to one hour to match the time over which the cells were exposed to the precursor polymer solutions during the electrospinning process. Cells were plated at a density of 10,000 cells/well in a 96-well plate and incubated for 24 hours. After 24 hours, the DMEM was removed, replaced with the precursor polymer solutions (7.5% POH + 2.5% PEO, 7.5% POA + 2.5% PEO, or 2.5% PEO), and incubated for 0.5 hour or 1 hour. Following, all polymer was removed and 90 μL fresh DMEM and 10 μL PrestoBlue were added. Cell viability was assessed using the same PrestoBlue reagent protocol as outlined above. For each set of precursor polymer solutions four replicates were performed, with error bars representing the standard deviation of the independent measurements.

3.3.13.3 Live/Dead Assay

The viability of cells electrospun into the scaffolds was assessed using a LIVE/DEAD™ Cell Imaging Kit (ThermoFisher) following the manufacturer's protocols. In short, 1 mL of live cell indicator solution (calcein AM) was added to 1 μL of lyophilized dead cell indicator (BOBO-3

iodide) before being added to the fibrous scaffolds. The scaffold was incubated with the stain for 15 minutes at 20 °C, after which it was washed with PBS over 5 x 5 minute cycles to remove non-bound dyes to minimize noise. Imaging was performed using CSLM with excitation wavelengths of 488 nm (live) and 561 nm (dead) and collecting z-stacks over the depth of the sample. Images are shown as maximum projections showing all cells throughout the volume of each scaffold.

3.3.14 Cell Adhesion Assay

C2C12 myoblast cell adhesion to the scaffolds was assessed using 4',6-diamidino-2-phenylindole (DAPI) and phalloidin staining. At each timepoint, media was removed and the scaffolds were washed twice with phosphate-buffered saline (PBS, 1x) at 5 minute intervals. The scaffolds were then fixed in 4% formaldehyde (Image-iT™ Fixative Solution, methanol-free in PBS) for 30 minutes, after which two PBS washes were conducted. The scaffolds were permeabilized with 0.1% Triton X-100 for 15 minutes and exposed to blocking solution (10% BSA in PBS) for 2 hours. Subsequently, the scaffolds were stained with rhodamine-labelled phalloidin (ActinRed™ 555 ReadyProbes, ThermoFisher) overnight at a concentration of 3 drops/mL in PBS. Immediately prior to imaging, the scaffolds were additionally stained with DAPI (300 nM in PBS) for 10 minutes, after which the scaffolds were thoroughly washed with PBS prior to imaging using CSLM at 405 nm (DAPI) and 561 nm (phalloidin) excitation. Images are represented in the form that best visualized the cell morphology as either 3D maximum projections or 2D images.

3.3.15 CFSE and Far Red Staining for Cell Tracking

Cell morphology and proliferation of C2C12 myoblast cells within cross-aligned, bilayer scaffolds over time were assessed by using carboxyfluorescein diacetate succinimidyl ester (CellTrace™ CFSE, ThermoFisher) and Far Red (CellTrace™ Far Red, ThermoFisher) dyes to differentially

pre-stain cells electrospun within each layer following the manufacturer's protocols. Following staining, the cells were centrifuged to obtain a cell pellet and re-suspended as previously described for electrospun scaffold preparation, with one type of dyed cell used to electrospin each layer to enable differentiation of when different cells were electrospun into the scaffold. Cells were imaged at 1, 3, 7, and 14 day timepoints using CSLM at 488 nm (CFSE) and 640 nm (Far Red) excitation wavelengths and collecting z-stacks over the depth of the samples. Images are shown as maximum projections showing all staining of the cell throughout the volume of each scaffold. Depth projections were generated within NIS Elements Viewer.

3.3.16 CFSE Staining

To assess cell morphology within the fibrous scaffolds at a given incubation time, scaffolds were post-stained with CFSE (CellTrace™ CFDA-SE, ThermoFisher) for 20 minutes and incubated in media for an additional 20 minutes to remove unbound dyes. Samples were fixed with 4% formaldehyde (Image-iT™ Fixative Solution, methanol-free in PBS) and washed thoroughly with PBS before imaging using CLSM using an excitation wavelength of 488 nm (CFSE).

3.3.17 Statistical Analysis

A single-factor ANOVA was performed to compare means of two or more samples. The number of replicates used for experiments and image analysis are reported for each instance with standard deviation error bars.

3.4 Results and Discussion

3.4.1 Polymer Synthesis and Characterization

Hydrazide-functionalized POEGMA (POH) and aldehyde-functionalized POEGMA (POA) polymers (Figure 3.1A) were synthesized using previously published chain transfer radical polymerization methods. POH and POA were both functionalized to 20 mol% hydrazide or aldehyde groups, with measured functionalization values (using ^{1}H NMR) of 20.7% and 18.6% respectively confirming near-stoichiometric functionalization percentages (Appendix B, Figures S3.1). Gel permeation chromatography indicated number average molecular weights of 13.5 kDa and 15.5 kDa for POH and POA respectively, both below the molecular weight threshold for kidney clearance following the degradation of the hydrogel (Appendix B, Table S3.1).

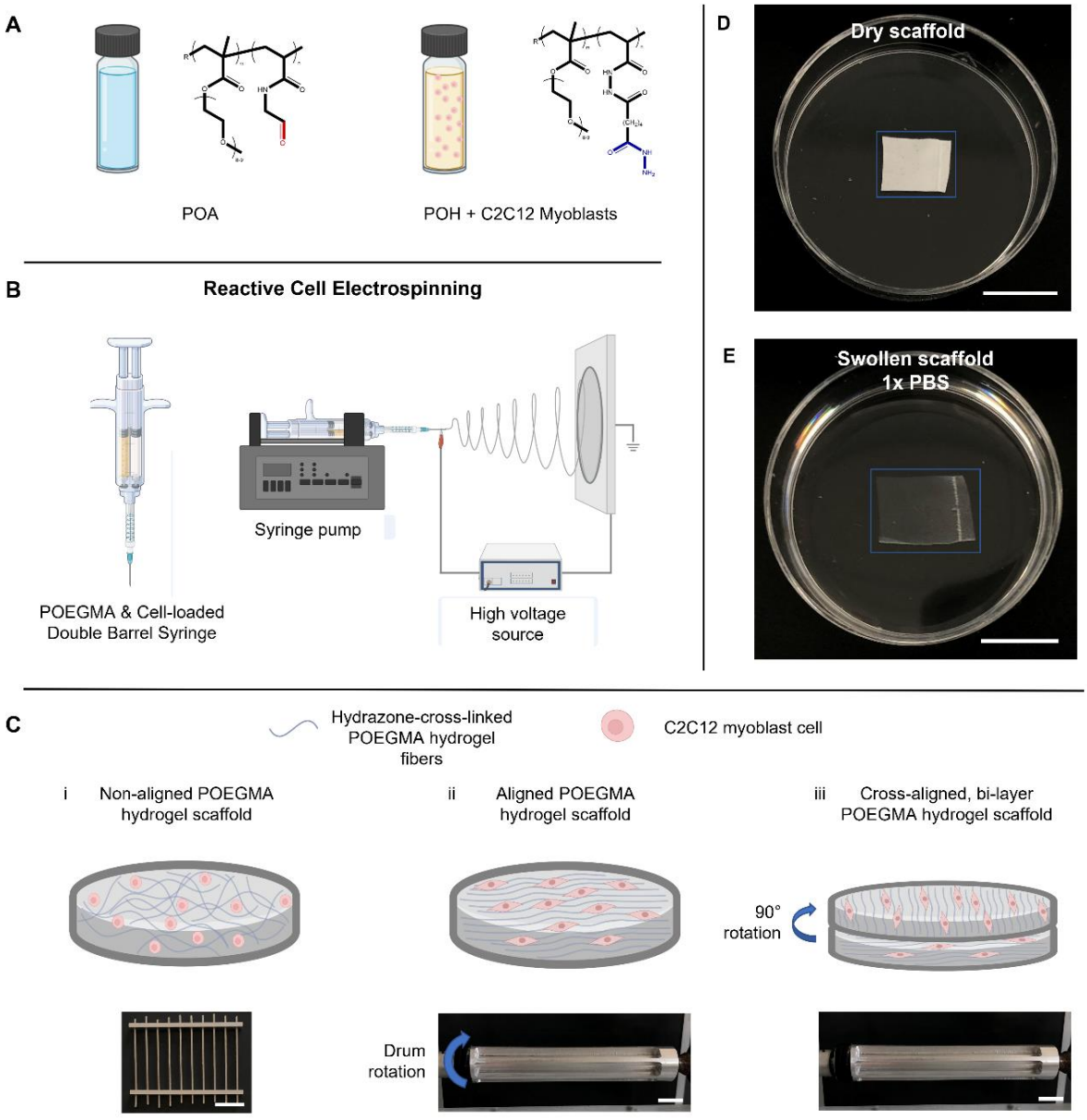

Figure 3.1. Schematic of the reactive cell electrospinning process to produce POEGMA hydrogel nanofibers loaded with C2C12 myoblasts using (A) aldehyde-functionalized POEGMA (POA), and hydrazide-functionalized POEGMA (POH) as the two reactive precursor polymers and (B) reactive cell electrospinning using a double barrel syringe loaded with POA and POH + C2C12 myoblasts to create the scaffolds; (C) (i) Schematic diagrams of non-aligned, (ii) aligned, and (iii) cross-aligned scaffolds fabricated via reactive electrospinning with encapsulated C2C12 cells by varying the collector used for fabrication. Scale bars = 2 cm; (D-E) Aligned electrospun fibers shown (D) dry and (E) immediately after swelling in 1x PBS. Scale bars = 1 cm.

3.4.2 Electrospinning of single-layer scaffolds: Assessment of fiber alignment & morphology

Non-aligned POEGMA fibers were fabricated using the reactive electrospinning strategy described in previous work[8] (Figure 3.1B) using a series of parallel rods with a 1 cm air gap as the collector (Figure 3.1C(i)). The resulting electrospun scaffolds showed hydrogel-like properties, including significant swelling and a significant reduction in their refractive index when swollen in 1 x PBS (Figures 3.1D, 3.1E). No overall direction of fiber orientation was apparent via SEM imaging (Figure 3.2A) or through use of FIJI's directionality function (Figure 3.2B), as anticipated. In contrast, tunable fiber alignment was possible using a rotating drum collector to collect radially aligned fibers (Figure 3.1C(ii); see the design in Appendix B, Figure S3.2). An increase in drum rotation speed lead to an increase in the degree of fiber alignment (Figure 3.2A). Quantification of fiber alignment at different rotation speeds (relative to non-aligned fibers) was generated using FIJI's directionality plug-in to calculate the coefficient of alignment (COA) for each electrospinning condition using the equation $COA = goodness\ of\ fit * amount$ in which "goodness of fit" and "amount" were obtained from the FIJI directionality plugin[47]. Non-aligned fibers and fibers fabricated at low rotation speeds of 500 and 1000 rpm demonstrated COA values of 0.19, 0.04, and 0.40 respectively; in contrast, for fibers collected at higher rotation speeds of 3000 and 4000 rpm, the COA values were > 0.60 (Figure 3.2C). The average fiber diameter for all sample types (irrespective of alignment) was found to be between 360-580 μm, with the broadest distribution of diameters found at higher rotation speeds of 3000 and 4000 rpm; indeed, some evidence of fiber clumping was observed particularly at 4000 rpm (Figures 3.2A and 3.2D), a result we attribute to the rotational forces on the drum enhancing contact between the fibers before they are fully dried. From these results, 3000 rpm was chosen as the standard to generate aligned fibers considering that minimal additional benefit (the same COA and some additional nanofiber

clumping) was observed by using the highest 4000 rpm speed and lower rotation speeds may be beneficial to minimize any cytotoxic effects (e.g. faster drying, higher interfacial shear).

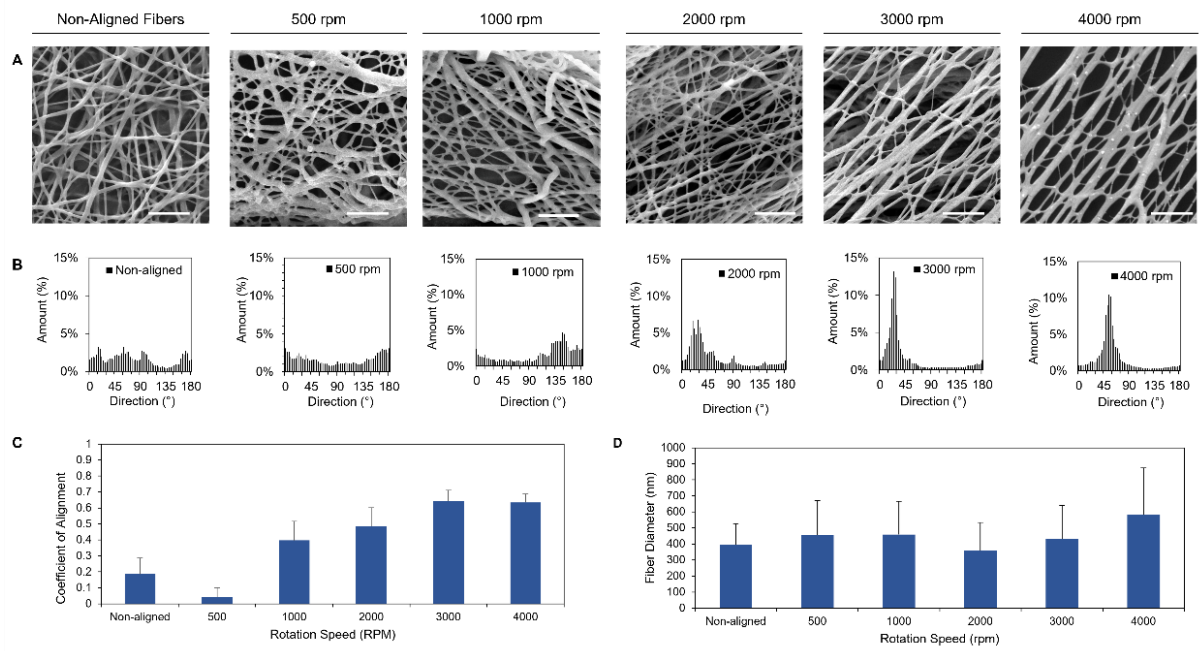

Figure 3.2. (A) SEM images of single-layer electrospun POEGMA hydrogel fibers collected with no alignment mechanism (using a parallel rod collector) compared to a drum collector rotating at speeds of 500-4000 rpm. Scale bars = 5 μm; (B) Directionality histograms generated by Image J showing the alignment of the electrospun fibers of non-aligned fibers and fibers formed at different drum rotation speeds; (C) Coefficient of alignment (COA) of electrospun fibers collected under different alignment conditions (n=5 independent samples, 5 images analyzed per rotation speed (Appendix B, Figure S3.3); error bars represent the standard deviation of the calculated COAs); (D) Diameter of the electrospun fibers collected under different alignment conditions (n=125 fibers analyzed per rotation speed, error bars represent the standard deviation).

3.4.3 Electrospinning of bilayer scaffolds

Cross-aligned, bilayer scaffolds were subsequently fabricated using the identified optimal rotation speed of 3000 rpm by electrospinning the first layer, removing the scaffolds from the drum to rotate them by 90 degrees, and then continuing electrospinning to generate the second layer with a perpendicular fiber alignment relative to the first layer (Figure 3.3A, additional images Figure S3.4). To demonstrate the successful fabrication of bilayer fiber networks, fluorescently labelled

POH/POA solutions were used to label the POEGMA fibers in each layer; FITC-labelled POH was used to fabricate layer 1 while Cy5-labelled POA was used to fabricate layer 2 (Figures 3.3B-3D). The FIJI directionality plugin demonstrated the perpendicular alignment of the fiber networks, with the peak alignments observed for the FITC-POH layer concentrated around 0 and 180° and the peak alignment of the CY5-POA layer offset by ~90° (Figure 3.3E).

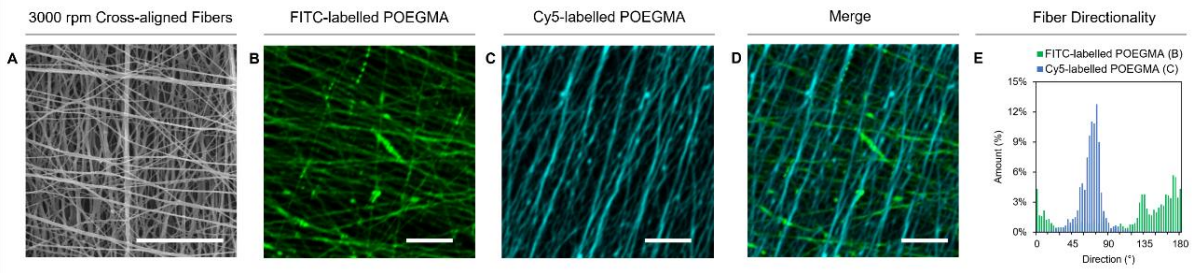

Figure 3.3. (A) SEM and (B-D) confocal microscopy of bilayer electrospun POEGMA scaffolds in which POEGMA hydrogel fibers were labelled in respective layers with (B) FITC (layer 1) and (C) Cy5 (layer 2), with (D) representing the merged images demonstrating the perpendicular alignment of the bilayer scaffold; Scale bars = 20 μm; (E) Directionality histogram generated by FIJI quantifying the alignment of the cross-aligned fluorescent electrospun fibers at 3000 rpm.

3.4.4 Mechanical properties of single-layer and bilayer scaffolds

The mechanical properties of dry single-layer scaffolds (both non-aligned and aligned at 3000 rpm) and bilayer cross-aligned scaffolds were evaluated using the CellScale Microsquisher by tensile testing in two directions offset by 90°. For aligned scaffolds, direction 1 was parallel to the direction of the fibers while direction 2 was perpendicular to the fiber alignment; for non-aligned scaffolds, the first direction was randomly chosen and the second direction was perpendicular to that initial direction. All three scaffold types could be stretched to 10% elongation and return to their original un-stretched state in both directions tested (Figure 3.4A-C), showing the high elasticity of the scaffolds consistent with the properties of native ECM. Young's modulus values for non-aligned, aligned, and cross-aligned scaffolds (calculated based on the stress-strain data and

the measured thicknesses of each scaffold, Appendix B Tables S3.2-S3.4) were found to be similar for aligned fibers tested parallel to the fiber orientation, non-aligned fibers tested in either direction, and cross-aligned fibers tested in both directions (Table 3.1). When comparing fibers tested in two perpendicular directions, neither the non-aligned scaffolds nor the cross-aligned bilayer scaffolds showed significantly different moduli (Figures 3.4D and F); in contrast, in aligned scaffolds, the Young's modulus was 245% higher in the parallel fiber direction relative to the perpendicular fiber direction (Figure 3.4E). These anisotropic mechanical properties are consistent with previous reports of aligned "hard" electrospun fibers[39] , although to our knowledge this is the first such demonstration with hydrogel-based nanofibers. Of note, while non-aligned and cross-aligned scaffolds demonstrated similar overall bulk mechanical properties, the locally controlled nanofiber alignment in the cross-aligned scaffolds compared to non-aligned scaffolds represents an advantage in terms of maintaining the same bulk scaffold mechanics while also introducing a mechanism to localize different cell types in different locations of the scaffold.

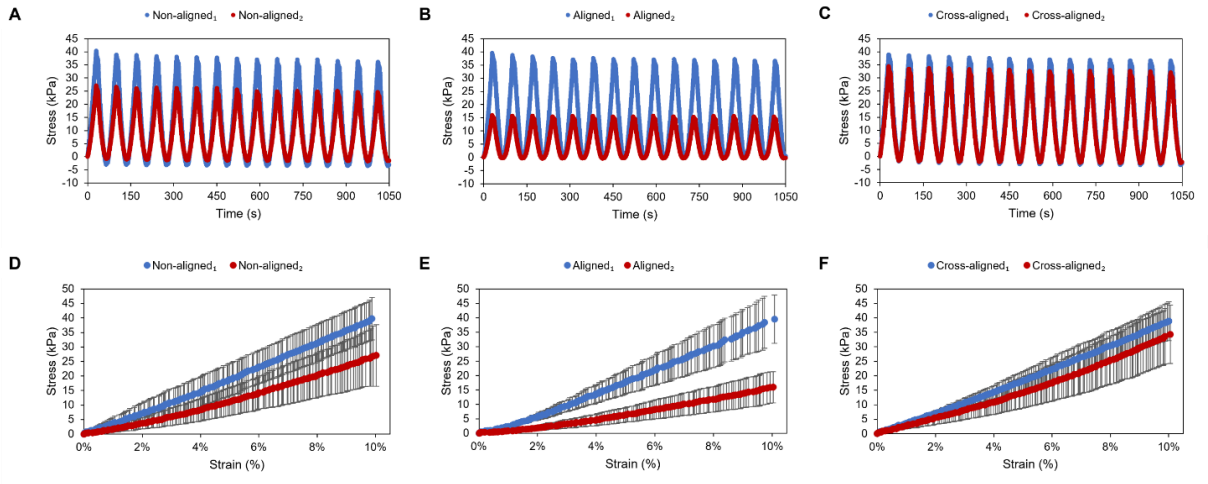

Figure 3.4. (A-C) Tensile testing of the dry PEO-POEGMA electrospun scaffolds (n=3, 3 samples tested per direction) over 15 cycles at 10% elongation for (A) non-aligned fibers, (B) single-layer aligned fibers, and (C) bilayer, cross-aligned fibers tested in two perpendicular fiber orientation directions as noted in the legend subscripts. For aligned fibers, direction 1 is parallel to the fiber direction and direction 2 is perpendicular to the fiber direction. (D-F) Stress versus strain responses for (D) non-aligned, (E) aligned, and (F) cross-aligned fiber scaffolds tested in two perpendicular directions.

Table 3.1. Young's modulus of dry electrospun POEGMA-PEO fiber scaffolds tested in two directions, oriented 90° apart (n=3, 3 samples tested for each direction, error bars represent the standard deviation). * $p < 0.05$ for pairwise comparisons within the alignment group. For the aligned scaffolds Direction 1 is parallel to the fiber direction and Direction 2 is perpendicular to the fiber direction; for the cross-aligned scaffolds Direction 1 and Direction 2 are the directions of the two cross-aligned networks.

Scaffold	Young's Modulus
	kPa
$\text{Non-aligned}_{\text{Direction1}}$	400 ± 62
$\text{Non-aligned}_{\text{Direction2}}$	270 ± 97
$\text{Aligned}_{\text{Direction1}}$	395 ± 101*
$\text{Aligned}_{\text{Direction2}}$	161 ± 57*
$\text{Cross-aligned}_{\text{Direction1}}$	386 ± 68
$\text{Cross-aligned}_{\text{Direction2}}$	331 ± 98

3.4.5 Cell electrospinning cell viability & morphology

The key cell viability concerns related to cell electrospinning were assessed prior to incorporating cells into the scaffolds. Cell viabilities after exposure to the high voltages required for

electrospinning were >79% for all voltages tested and ~84% at a voltage of 10 kV used previously for cell electrospinning[8] (Figure 3.5A), confirming the safety of the 10 kV operating voltage for cell processing. The viability of cells after exposure to air was also evaluated given that solvent evaporation during electrospinning results in at least partial drying of the hydrogel fibers on the collector over the course of the fabrication process. C2C12 cells could maintain high cell viability after both 0.5 and 1 hour of air exposure at 37°C (i.e. in the absence of media); however, at times >2 hours, viabilities dropped by >26% (Figure 3.5B). As such, electrospinning times were kept under 1 hour to maintain high cell viability in the scaffolds, after which the cellularized scaffolds were immediately immersed in DMEM. The polymer solutions were also evaluated for potential cytotoxicity by testing lower precursor polymer concentrations over 24 hours of incubation and higher precursor polymer concentrations for up to 1 hour of incubation, the latter of which was chosen to match the maximum cell electrospinning experiment times used. C2C12 myoblasts showed cell viabilities of >97% when incubated in PEO at concentrations of 0.1, 0.2, 1, and 2 mg/mL and >98% viability in POH or POA precursor polymer solutions at concentrations of 0.1, 0.2, 1, 2, 5, 10 mg/mL (Figure 3.5C). Very high cell viabilities (~100%) were also maintained in the pre-gel solutions used for electrospinning (i.e. 7.5% POH or POA + 2.5% PEO) over at least 1 hour of incubation, confirming the cytocompatibility of all parts of the electrospinning fabrication process (Figure 3.5D). SEM imaging showed that cell morphologies in cell-loaded single-layer and bilayer scaffolds immediately after cell electrospinning exhibited cell diameters similar to those observed with fresh fully hydrated cells and that cell electrospinning successful incorporates cells in the electrospun scaffolds (Figure 3.5E-G, see additional images in Appendix B Figure S3.5). This result suggests that the alignment process does not significantly alter the favorable hydration of the cells by the hydrogel scaffolds even in the vacuum chamber of an SEM, indicative

of the potential for cell viability to be maintained when the scaffolds are placed back into media following fabrication.

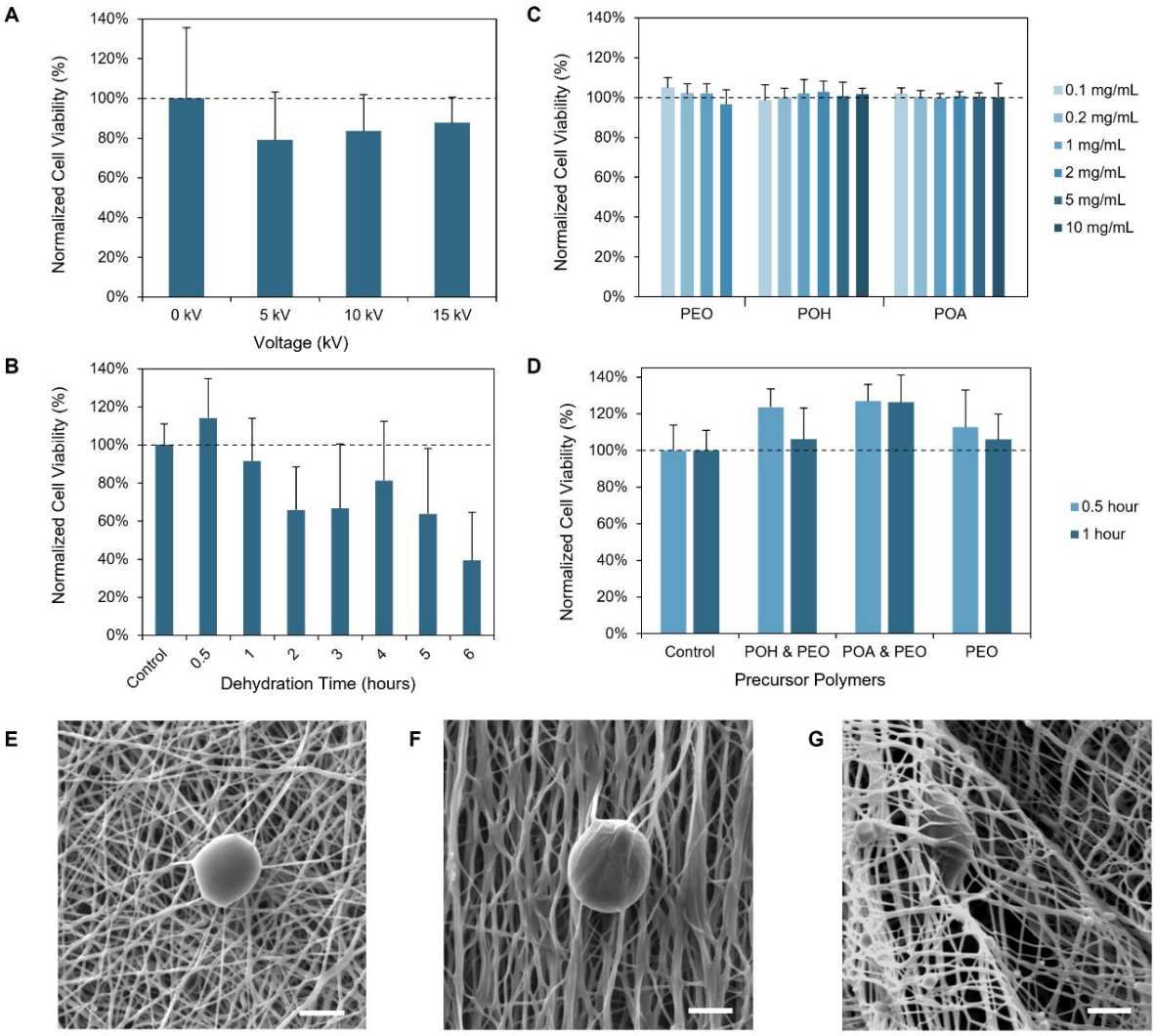

Figure 3.5. C2C12 mouse myoblast cell viability in response to different processing conditions and electrospinning precursor solutions as assessed using the PrestoBlue assay: (A) cell viability following electrospinning of cell-only suspensions using voltages of 0, 5, 10, and 15 kV (average ± std, n=5); (B) cell viability upon exposure of electrospun cell-only suspensions to air (in sterile conditions) at 37°C for 0.5, 1, 2, 3, 4, 5, and 6 hours (average ± std, n=6); (C) cell viability after 24 hours of incubation to precursor polymer solutions (PEO at concentrations of 0.1, 0.2, 1, and 2 mg/mL and POH/POA at concentrations of 0.1, 0.2, 1, 2, 5, and 10 mg/mL (average ± std, n=5); (D) cell viability upon exposure to the pre-electrospinning solutions (7.5% POH + 2.5% PEO, 7.5% POA + 2.5% PEO, and 2.5% PEO) at 0.5 and 1 hour incubation times (average ± std, n=4); (E-G) SEM images of electrospun POEGMA hydrogel fibers co-electrospun with C2C12 cells directly after electrospinning for (E) non-aligned scaffolds, (F) aligned scaffolds, and (G) cross-aligned scaffolds. Scale bars = 5 μm.

3.4.6 Cell viability within the hydrogel scaffolds

Cell-loaded scaffolds with non-aligned, aligned, and cross-aligned fibers showed successful integration of the cells into the scaffold following cell electrospinning (Figure 3.6A-C). Cell-loaded non-aligned scaffolds maintained high cell viability of >85% over each of the 3, 7, and 14 days timepoints tested, with the slightly higher cell viabilities observed at day 14 indicating not only high viability maintenance but potential proliferation of live cells within the scaffolds. Cells electrospun into aligned scaffolds at a rotation speed of 3000 rpm maintained even higher cell viabilities of >96% across all timepoints of 3, 7, and 14 days, indicating C2C12 cells can withstand the stresses of electrospinning and rotation speeds to remain viable. Similarly, cross-aligned scaffolds maintained cell viabilities >94% across each of the 3, 7, and 14 day timepoints, showing that the additional time and scaffold handling required to perform the 90° rotation of the scaffold to create the bilayer scaffold does not significantly alter the high cytocompatibility of the cell electrospinning strategy (Figure 3.6D). The volumetric densities of cells per unit volume with the scaffolds is also similar (~1 million cells/cm^3) independent of the degree of alignment (Figure 3.6E), although a limited degree of cell leaching may be observed from the non-aligned scaffold which is not apparent with the aligned scaffolds. Overall, however, high densities of cells are maintained within the non-aligned and aligned scaffolds and the retained cells within aligned scaffolds retain very high cell viabilities, showing the viability of this general approach.

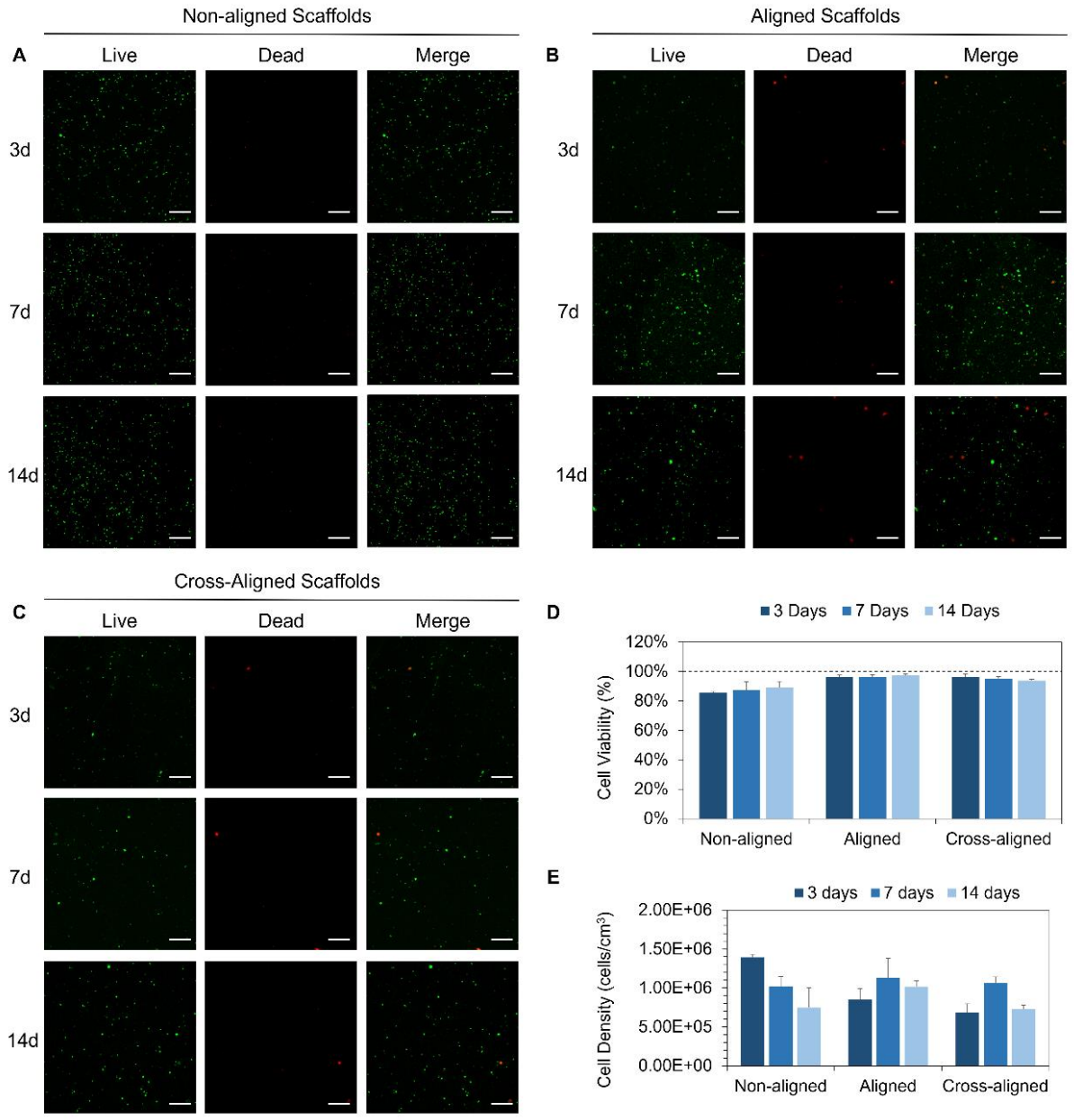

Figure 3.6. Confocal LIVE/DEAD assay imaging of electrospun cells in a single layer of (A) non-aligned, (B) aligned, or (C) cross-aligned POEGMA fiber scaffolds co-electrospun with C2C12 myoblasts after 3, 7, and 14 days of incubation in DMEM media. Scale bars = 250 μm; (D-E) Calculated (D) cell viabilities (percentage of live cells versus total cells imaged) and (E) scaffold volume-based live cell densities of the C2C12 myoblasts after electrospinning after 3, 7, and 14 days of incubation in DMEM media in non-aligned, aligned, or cross-aligned scaffolds (minimum of n=3 images analyzed per sample, Appendix B Figure S3.6, error bars represent the standard deviation).

3.4.7 Cell morphology within the hydrogel scaffolds

The morphologies of cells electrospun into non-aligned and aligned hydrogel scaffolds were assessed via staining of F-actin filaments (Figures 3.7A and 3.7C) and through staining the cell body with CFSE (Figures 3.7B and 3.7D) over the 14 day culture period. Cells in non-aligned scaffolds primarily maintained rounded morphologies over the full 14 day culture period (Figure 3.7A); in contrast, cells in single-layer aligned scaffolds showed clear evidence of alignment with the fiber direction (Figure 3.7B arrows; note that 1-day timepoints were additionally included for the aligned scaffolds to show how the alignment process proceeds over time). While the alignment observed in Chapter 2 (Figure 2.2) was specific to the capture of cells within the Taylor cone during the electrospinning process (and thus was observed immediately upon scaffold fabrication), the alignment observed in this case develops over the course of the incubation period; as such, this alignment is directed by the orientation of the fibers themselves and not an artefact of the electrospinning process. Correspondingly, CFSE staining shows that cells encapsulated within the non-aligned scaffolds remained almost entirely rounded (Figure 3.7D) while cells encapsulated in aligned scaffolds demonstrated a mix of rounded morphologies (similar to those seen in non-aligned scaffolds) and extended morphologies parallel to the alignment of the fibers that were unique to aligned scaffolds (Figure 3.7D). Cell alignment was further quantified through the analysis of cell aspect ratio using FIJI's analyze particles function. Average aspect ratios for cells in non-aligned scaffolds remained between 1.22-1.37 across all timepoints while aspect ratios for cells in aligned scaffolds were consistently between 1.48-1.60 across all timepoints; correspondingly, the maximum aspect ratios observed for non-aligned cells remained <2.2 while the maximum aspect ratios for aligned cells reached up to 4.5. Furthermore, across all timepoints evaluated, only 6% of cells in non-aligned scaffolds had aspect ratios greater than 1.6 while 29%

of cells in the aligned scaffolds maintained >1.6 aspect ratios. As such, a significant fraction of cells in the aligned scaffolds can elongate in the direction of the aligned fibers, a key benefit of this fabrication approach for directing tissue alignment.

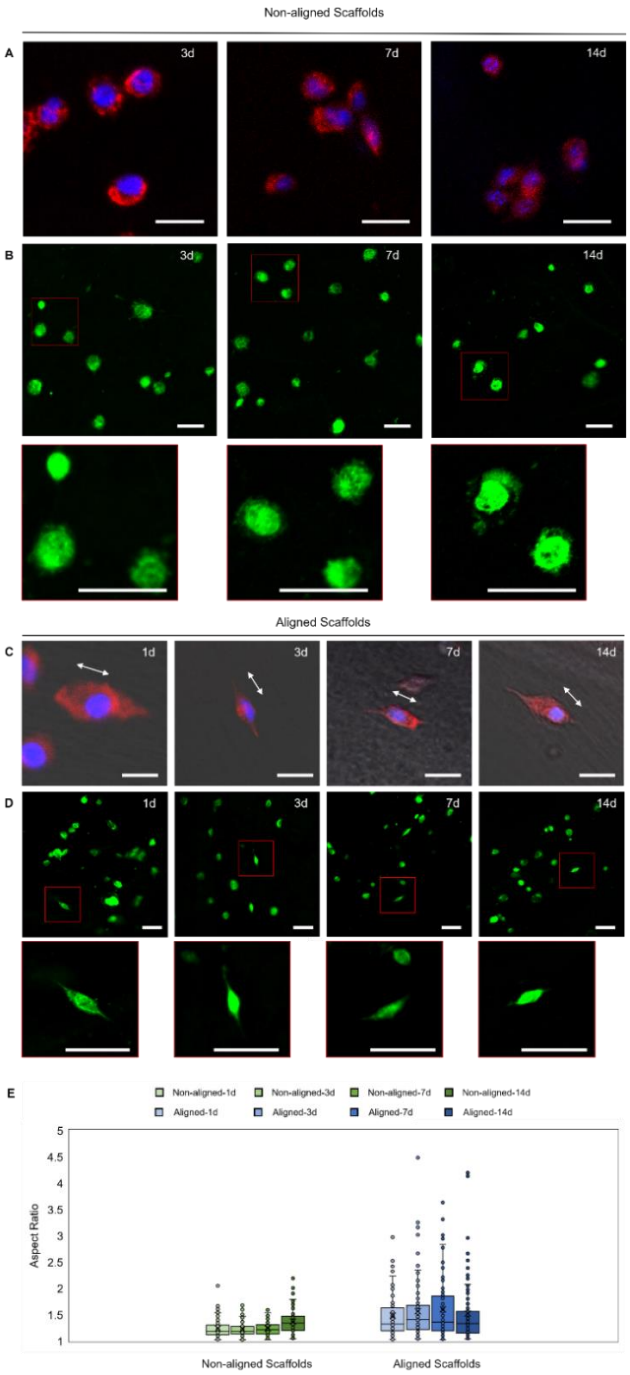

Figure 3.7. Confocal imaging of electrospun cells in a single layer of non-aligned POEGMA fibers after (A) 3, 7, and 14 days and (C) aligned POEGMA fibers after 1, 3, 7, and 14 days. Nuclei were stained with DAPI and F-actin filaments were stained with rhodamine-phalloidin. Scale bars = 20 μm; (B,D) C2C12 cells post-stained with CFSE after 1, 3, 7, and 14 days of culture for (B) non-aligned scaffolds and (D) aligned scaffolds. Scale bars = 50 μm; (E) Analysis of cell alignment in non-aligned and aligned scaffolds as quantified in FIJI using the cell aspect ratio calculation over 1, 3, 7, and 14 days (a minimum of n= 75 cells were analyzed per scaffold and per timepoint; see additional images in Appendix B Figures S3.7 and S3.8).

3.4.8 Bilayer cross-aligned scaffolds

Bilayer cross-aligned scaffolds were fabricated with CFSE-stained cells electrospun in a first layer followed by sequential electrospinning of Far Red-stained cells in a second layer. Confocal imaging of the same scaffold after 1, 3, 7, and 14 days of culture showed proliferation of the cells over 14 days as well as successful staining of the cells in separate layers (Figure 3.8A). While fewer cells were aligned in the cross-aligned scaffolds given the thin dimensions of each layer (70-90 μm, making the less aligned or even randomly aligned fibers at the interface between the two layers much more prominent in governing the overall cell responses), the perpendicular alignment of CFSE and Far Red-stained cells was still clearly visible in some images (Figure 3.8B-D). Further exploration into thicker cross-aligned constructs is likely to provide greater evidence for layer-specific cell alignment.

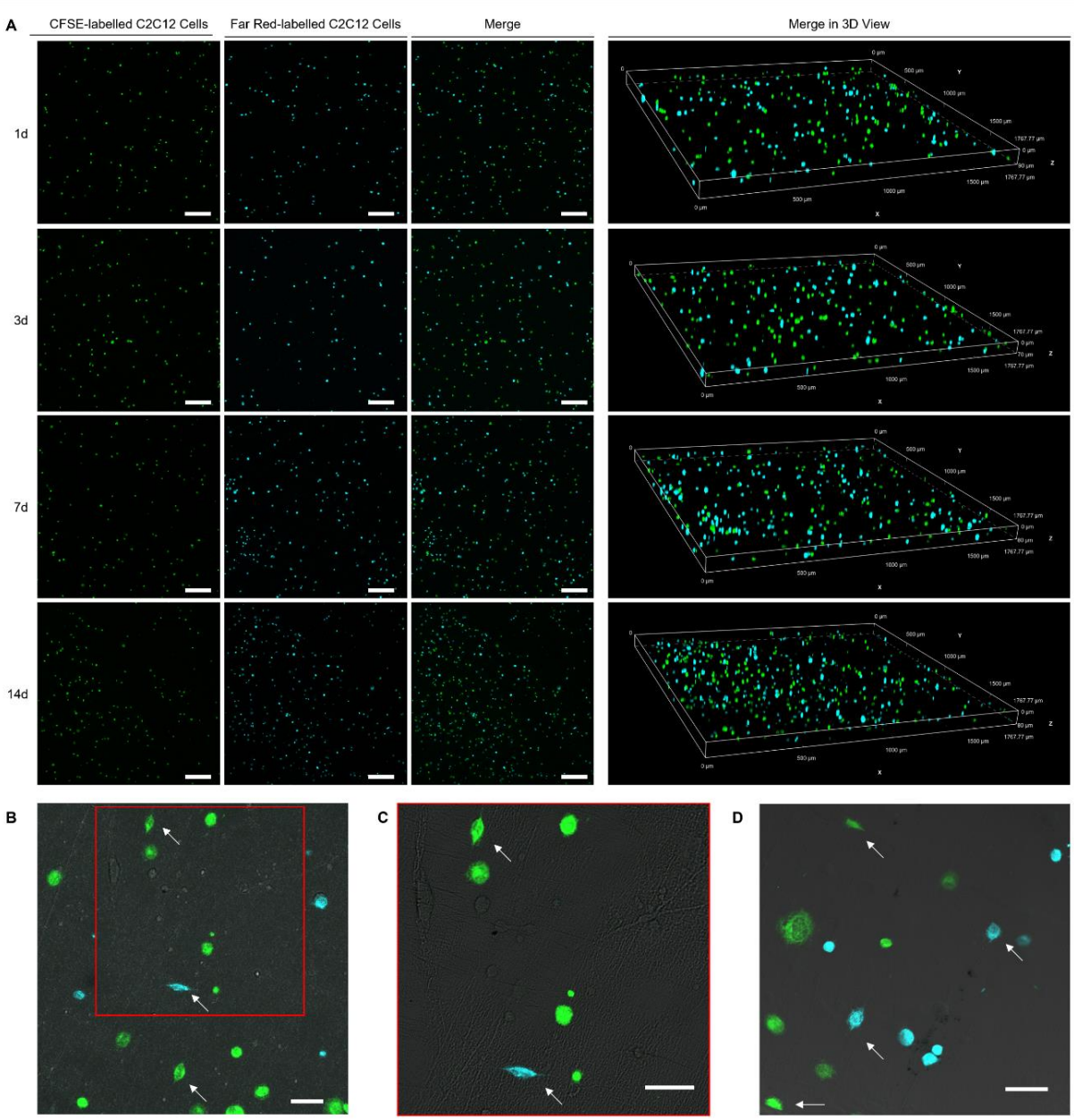

Figure 3.8. (A) Confocal imaging of electrospun C2C12 cells in bilayer cross-aligned layers, fabricated using the cylindrical drum collector rotating at 3000 rpm with CFSE-labelled cells in the first layer and Far Red-labelled cells in the second layer at 1, 3, 7, and 14-day timepoints. 3D confocal images show the merge of both FITC and Cy5 channels. Scale bars = 250 μm; (B-D) Demonstrations of orthogonal cell alignment after (B) 3-days, and (D) 7-days in a pre-stained cross-aligned scaffold; (C) close-up of (B) showing a high-resolution image after 3-days; Scale bars = 50 μm.

Overall, the fabrication of highly aligned hydrogel fibers with nano-scale diameters from an all-aqueous solution containing cells offers potential to create cellularized multi-layer scaffolds with different cells and/or different cell alignments all via a single fabrication step that can be conducted in a fully sterile environment, a key challenge with existing fabrication strategies. Previous reported aligned hydrogel fibers have required post-processing steps before cell seeding including photocrosslinking with UV light[28,48], which can introduce further process cytotoxicity concerns, or post-fabrication sterilization such as soaking scaffolds in ethanol[20] or exposure to UV light[39]. These additional processing steps for cross-linking or sterilization leave fewer options for cell integration into the scaffolds outside of cell seeding post-fabrication, resulting in significant challenges around cell infiltration from the fiber surface into the scaffold bulk due to the dense nature of electrospun fibers. Furthermore, the use of dynamic cross-linking chemistries within our scaffolds allows for the formation of multi-layer scaffolds while significantly reducing the risk of layer delamination due to the dynamic nature of the aldehyde/hydrazide chemistry[12], allowing for covalent bonding in addition to mechanical interlocking between adjacent nanofibrous layers to enhance the interfacial adhesive strength. The high cell viability achievable, coupled with the potential to align significant fractions of the co-electrospun cells in the direction of the nanofiber alignment, makes this approach promising for tissue engineering applications in which multi-cellular or layered scaffold models are required.

3.5 Conclusions

Cell-loaded POEGMA hydrogel fibers with tunable alignment can be fabricated by electrospinning non-cytotoxic, low-viscosity aqueous polymer precursor solutions in the presence of cells on to a rotating drum collector. Electrospun cells were found to effectively align in the direction of nanofiber alignment, facilitating high viability over 14 days of culture under a range of alignment

conditions and (with alignment) leading to significantly higher adhered cell aspect ratios. The introduction of aligned fibers, including the potential to create multi-layer scaffolds with different alignments by exploiting the dynamic covalent chemistry linking the fibers to prevent inter-layer fiber delamination, offers the potential to create more biomimetic and multi-cell tissue scaffolds to better mimic multi-layer complex and aligned tissues such as blood vessel smooth muscle tissue or gastrointestinal tissues such as the stomach or esophagus.

3.6 Acknowledgements

The Natural Sciences and Engineering Research Council of Canada is acknowledged for their financial support (Discovery Grant RGPIN2017-06455 to TH and a Canada Graduate Scholarship to CD). Biorender.com was used to create the Figure 3.1 graphic. We gratefully acknowledge Paul Gatt for his work in design and fabrication of our rotating drum. The CALM institute and CCEM are acknowledged for their help in CLSM and SEM image acquisition and analysis. Gurpreet Randhawa, Meghan Kostashuk, Eva Mueller, and Zheng Fu Zhou are acknowledged for their assistance in polymer synthesis and characterization.

3.7 References

1 De France, K. J., Xu, F. & Hoare, T. Structured Macroporous Hydrogels: Progress, Challenges, and Opportunities. *Adv Healthc Mater* **7**, 1700927 (2018).
2 Xu, F. *et al.* Hydrogels for Tissue Engineering: Addressing Key Design Needs Toward Clinical Translation. *Front Bioeng Biotechnol* **10**, 849831 (2022).
3 Hunt, J. A., Chen, R., Van Veen, T. & Bryan, N. Hydrogels for tissue engineering and regenerative medicine. *J. Mater. Chem. B* **2**, 5319-5338 (2014).
4 Drury, J. L. & Mooney, D. J. Hydrogels for tissue engineering: scaffold design variables and applications. *Biomaterials* **24**, 4337-4351 (2003).
5 Frantz, C., Stewart, K. M. & Weaver, V. M. The extracellular matrix at a glance. *Journal of Cell Science* **123**, 4195-4200 (2010).
6 Padhi, A. & Nain, A. S. ECM in Differentiation: A Review of Matrix Structure, Composition and Mechanical Properties. *Ann Biomed Eng* **48**, 1071-1089 (2020).
7 Van Vlierberghe, S., Dubruel, P. & Schacht, E. Biopolymer-based hydrogels as scaffolds for tissue engineering applications: a review. *Biomacromolecules* **12**, 1387-1408 (2011).

8 Xu, F., Dodd, M., Sheardown, H. & Hoare, T. Single-Step Reactive Electrospinning of Cell-Loaded Nanofibrous Scaffolds as Ready-to-Use Tissue Patches. *Biomacromolecules* **19**, 4182-4192 (2018).
9 Xu, F., Gough, I., Dorogin, J., Sheardown, H. & Hoare, T. Nanostructured degradable macroporous hydrogel scaffolds with controllable internal morphologies via reactive electrospinning. *Acta Biomaterialia* **104**, 135-146 (2020).
10 MacQueen, L. A. *et al.* A tissue-engineered scale model of the heart ventricle. *Nature Biomedical Engineering* **2**, 930-941 (2018).
11 Tijore, A. *et al.* Contact guidance for cardiac tissue engineering using 3D bioprinted gelatin patterned hydrogel. *Biofabrication* **10**, 025003 (2018).
12 Mueller, E., Xu, F. & Hoare, T. FRESH Bioprinting of Dynamic Hydrazone-Cross-Linked Synthetic Hydrogels. *Biomacromolecules* **23**, 4883-4895 (2022).
13 Tan, B., Gan, S., Wang, X., Liu, W. & Li, X. Applications of 3D bioprinting in tissue engineering: advantages, deficiencies, improvements, and future perspectives. *J Mater Chem B* **9**, 5385-5413 (2021).
14 Shrike Zhang, Y. *et al.* 3D Bioprinting for Tissue and Organ Fabrication. *Annals of Biomedical Engineering* **45**, 148-163 (2016).
15 Keshvardoostchokami, M. *et al.* Electrospun Nanofibers of Natural and Synthetic Polymers as Artificial Extracellular Matrix for Tissue Engineering. *Nanomaterials (Basel)* **11** (2020).
16 Ma, P. X. & Zhang, R. Synthetic nano-scale fibrous extracellular matrix. *Journal of Biomedical Materials Research* **46**, 60-72 (1999).
17 Deravi, L. F. *et al.* Design and Fabrication of Fibrous Nanomaterials Using Pull Spinning. *Macromolecular Materials and Engineering* **302**, 1600404 (2017).
18 Barnes, C. P., Sell, S. A., Boland, E. D., Simpson, D. G. & Bowlin, G. L. Nanofiber technology: designing the next generation of tissue engineering scaffolds. *Adv Drug Deliv Rev* **59**, 1413-1433 (2007).
19 Xu, F., Sheardown, H. & Hoare, T. Reactive electrospinning of degradable poly(oligoethylene glycol methacrylate)-based nanofibrous hydrogel networks. *Chemical Communications* **52**, 1451-1454 (2016).
20 Orr, S. B. *et al.* Aligned multilayered electrospun scaffolds for rotator cuff tendon tissue engineering. *Acta Biomaterialia* **24**, 117-126 (2015).
21 Sensini, A. *et al.* Tendon Fascicle-Inspired Nanofibrous Scaffold of Polylactic acid/Collagen with Enhanced 3D-Structure and Biomechanical Properties. *Scientific Reports* **8**, 17167 (2018).
22 Tong, H.-W., Wang, M. & Lu, W. W. Electrospun Poly(Hydroxybutyrate-co-Hydroxyvalerate) Fibrous Membranes Consisting of Parallel-Aligned Fibers or Cross-Aligned Fibers: Characterization and Biological Evaluation. *Journal of Biomaterials Science, Polymer Edition* **22**, 2475-2497 (2011).
23 Katta, P., Alessandro, M., Ramsier, R. D. & Chase, G. G. Continuous electrospinning of aligned polymer nanofibers onto a wire drum collector. *Nano Letters* **4**, 2215-2218 (2004).
24 Xie, J. *et al.* Radially Aligned, Electrospun Nanofibers as Dural Substitutes for Wound Closure and Tissue Regeneration Applications. *ACS Nano* **4**, 5027-5036 (2010).
25 Majidi, S. S. *et al.* Wet electrospun alginate/gelatin hydrogel nanofibers for 3D cell culture. *International Journal of Biological Macromolecules* **118**, 1648-1654 (2018).
26 Chen, C. *et al.* Bioinspired Hydrogel Electrospun Fibers for Spinal Cord Regeneration. *Advanced Functional Materials* **29**, 1806899 (2019).

27 Mahdavi, S. S., Abdekhodaie, M. J., Mashayekhan, S., Baradaran-Rafii, A. & Kim, K. Development and in vitro evaluation of photocurable GelMA/PEGDA hybrid hydrogel for corneal stromal cells delivery. *Materials Today Communications* **27**, 102459 (2021).
28 Baker, B. M. *et al.* Cell-mediated fibre recruitment drives extracellular matrix mechanosensing in engineered fibrillar microenvironments. *Nature Materials* **14**, 1262-1268 (2015).
29 Hussein, Y. *et al.* Electrospun PVA/hyaluronic acid/L-arginine nanofibers for wound healing applications: Nanofibers optimization and in vitro bioevaluation. *International Journal of Biological Macromolecules* **164**, 667-676 (2020).
30 Ji, Y. *et al.* Electrospun three-dimensional hyaluronic acid nanofibrous scaffolds. *Biomaterials* **27**, 3782-3792 (2006).
31 Torres-Giner, S., Gimeno-Alcañiz, J. V., Ocio, M. J. & Lagaron, J. M. Comparative performance of electrospun collagen nanofibers cross-linked by means of different methods. *ACS Applied Materials and Interfaces* **1**, 218-223 (2009).
32 Viswanathan, P. *et al.* Controlling surface topology and functionality of electrospun fibers on the nanoscale using amphiphilic block copolymers to direct mesenchymal progenitor cell adhesion. *Biomacromolecules* **16**, 66-75 (2015).
33 Huang, R. *et al.* Triple-Layer Vascular Grafts Fabricated by Combined E-Jet 3D Printing and Electrospinning. *Annals of Biomedical Engineering* **46**, 1254-1266 (2018).
34 Wakuda, Y., Nishimoto, S., Suye, S.-i. & Fujita, S. Native collagen hydrogel nanofibres with anisotropic structure using core-shell electrospinning. *Scientific Reports* **8**, 6248 (2018).
35 Nie, K. *et al.* Enzyme-crosslinked electrospun fibrous gelatin hydrogel for potential soft tissue engineering. *Polymers* **12**, 1977 (2020).
36 Chen, X. *et al.* Electrospun poly(l-lactic acid-co-ε-caprolactone) fibers loaded with heparin and vascular endothelial growth factor to improve blood compatibility and endothelial progenitor cell proliferation. *Colloids and Surfaces B: Biointerfaces* **128**, 106-114 (2015).
37 Yeo, M. & Kim, G. Micro/nano-hierarchical scaffold fabricated using a cell electrospinning/3D printing process for co-culturing myoblasts and HUVECs to induce myoblast alignment and differentiation. *Acta biomaterialia* **107**, 102-114 (2020).
38 Guo, Y., Gilbert-Honick, J., Somers, S. M., Mao, H.-Q. & Grayson, W. L. Modified cell-electrospinning for 3D myogenesis of C2C12s in aligned fibrin microfiber bundles. *Biochemical and Biophysical Research Communications* **516**, 558-564 (2019).
39 Kai, D., Prabhakaran, M. P., Jin, G. & Ramakrishna, S. Guided orientation of cardiomyocytes on electrospun aligned nanofibers for cardiac tissue engineering. *Journal of Biomedical Materials Research - Part B Applied Biomaterials* **98 B**, 379-386 (2011).
40 Wu, S., Wang, Y., Streubel, P. N. & Duan, B. Living nanofiber yarn-based woven biotextiles for tendon tissue engineering using cell tri-culture and mechanical stimulation. *Acta Biomaterialia* **62**, 102-115 (2017).
41 Miller, R. J. *et al.* Combining electrospun nanofibers with cell-encapsulating hydrogel fibers for neural tissue engineering. *J Biomater Sci Polym Ed* **29**, 1625-1642 (2018).
42 Du, J. *et al.* Prompt peripheral nerve regeneration induced by a hierarchically aligned fibrin nanofiber hydrogel. *Acta Biomaterialia* **55**, 296-309 (2017).
43 Shen, Q. *et al.* Progress on materials and scaffold fabrications applied to esophageal tissue engineering. *Mater Sci Eng C Mater Biol Appl* **33**, 1860-1866 (2013).
44 Liu, Y. *et al.* Effects of fiber orientation and diameter on the behavior of human dermal fibroblasts on electrospun PMMA scaffolds. *J Biomed Mater Res A* **90**, 1092-1106 (2009).

45 Reid, J. A. *et al.* Architected fibrous scaffolds for engineering anisotropic tissues. *Biofabrication* **13**, 045007 (2021).
46 Smeets, N. M. B., Bakaic, E., Patenaude, M. & Hoare, T. Injectable and tunable poly(ethylene glycol) analogue hydrogels based on poly(oligoethylene glycol methacrylate). *Chemical Communications* **50**, 3306-3309 (2014).
47 Mancino, C. *et al.* Electrospun electroconductive constructs of aligned fibers for cardiac tissue engineering. *Nanomedicine* **44**, 102567 (2022).
48 Wang, W. Y., Davidson, C. D., Lin, D. & Baker, B. M. Actomyosin contractility-dependent matrix stretch and recoil induces rapid cell migration. *Nature Communications* **10**, 1186 (2019).

4 Chapter 4: Conclusions and Future Outlook

4.1 Conclusions

The presented work focuses on the fabrication of tissue scaffolds for use in tissue engineering applications as well as in applications requiring tissue models with higher complexity to better mimic native tissues. The work was presented in two chapters highlighting the fabrication and characterization of cell-loaded POEGMA electrospun hydrogel fiber networks (1) in a multi-layered co-culture model and (2) in a multi-layered model with aligned microstructures.

Chapter 2 highlights the functionality of electrospinning in aqueous solution and the convenience of reactive cell electrospinning techniques. The fabricated cell-loaded POEGMA nanofibers showed cells throughout the depth of the scaffolds, a task that is hard to accomplish using typical cell seeding methods on the surface of the fibers. The ability to expand to co-culture models to either spatially segregated two or more cell types across layers or use mixed-co-cultures in which two or more cells are intimately mixed offers unique potential to study cell-cell interactions and is a key advantage of this co-culture layered model. Cells were found to show a ~4-fold increase in cell density over 14 days of proliferation, with high cell viability observed across all cell electrospinning techniques tested and the full 14 day culture period. Furthermore, when the cell adhesion peptide RGD was grafted into the scaffolds, limited benefits were observed in terms of cell adhesion, viability, or proliferation, demonstrating the potential of (otherwise cell-repulsive) POEGMA hydrogels nanofibers to provide the correct mechanical and interfacial cues to support cell adhesion and proliferation with or without modifications. Overall, cell-laden POEGMA hydrogel networks could be fabricated with controlled spatial deposition of multiple cell types without layer delamination and with successful cell seeding in three dimensions.

Within Chapter 3, the use of reactive cell electrospinning techniques with POEGMA-based hydrogels was expanded to assess the effects of incorporating directionality within the nanofiber networks. Multi-layered structures were explored through the generation of aligned fibers and cross-aligned fibers in a bilayer scaffold. The use of cell electrospinning was similarly found to produce cell-laden electrospun POEGMA hydrogel nanofibers with cells distributed throughout the depth of the generated fibers while avoiding delamination in the bilayer scaffolds, aided by the dynamic covalent cross-linking of POEGMA hydrogels. Overall, cells in non-aligned, aligned, and cross-aligned networks were found to have cell viabilities over 85% across 14 days of culture. Additionally, cells in aligned networks had on average higher aspect ratios (indicative of cell elongation) with a maximum aspect ratio 2x larger than those seen in non-aligned cell networks. The ability of cells to respond to the alignment of the fibers demonstrated the benefits of aligned networks and the potential to expand to cross-aligned networks in which alignment changes perpendicular halfway (or at any desired depth) through the scaffold. On this basis, reactive cell electrospinning provides benefits in the context of tissue engineering applications and *in vitro* cell models of tissues that are inherently aligned (e.g. smooth muscle, neural, or tendon tissues).

In conclusion, cell electrospinning of multi-layered POEGMA hydrogel fibers is shown to be an effective and simple technique capable of generating dense electrospun fiber networks with cells distributed in three dimensions, all in a single fabrication step. The multi-layered nature of these hydrogels increased the complexity of previous cell electrospinning work[1] and presented new methods of altering scaffold architecture. The culture of these models showed high cell proliferation and viability across three different cell lines (fibroblasts, epithelial cells, and myoblasts) with intended applications covering cartilage, dermis, smooth muscle, skeletal muscle, neural, and tendon tissue engineering.

4.2 Future work

The continuation of this work should aim to address three existing limitations of cell electrospinning: (1) scale-up, (2) further control over the spatial deposition of cells, and finally (3) an increased exploration of layers and cell types.

Scale-up: Scale-up of tissue engineering models remains an area of interest[2,3], including the challenge of electrospinning of thicker scaffolds[4]. The scaffolds studied in this work achieved thicknesses of ~80 μm per 30 minutes of electrospinning. The easiest method of increasing scaffold thickness is to increase the electrospinning time; however, there is a limited time over which the electrospun cells can stay on the collector (outside of media) and maintain high viability, limiting the scope of scaffold thicknesses that could be achieved by simply continuing the process for longer. However, as noted in both Chapters 2 and 3, cells in a dehydrated state (similar to those experienced throughout the electrospinning process) were found to have above ~80% viability for 3T3 fibroblasts and Psi2 12S6 epithelial cells, and ~60% for C2C12 myoblasts cell over a 2 hour duration. While 2 hours may represent the limit of electrospinning, possibly extended experiment times slightly beyond 1 hour may be explored specific to the cell types involved. An alternative would be to increase the number of nozzles used for electrospinning and thus co-electrospun the same (or optionally different) polymer solutions at the same time, as has been previously done[5-7]. This strategy was briefly explored in Chapter 3 for cell electrospun samples to increase thickness while maintaining experiment times below 30 minutes using a two-syringe system, with a further increase in syringes used beyond two remaining an option. The generation of thicker scaffolds through exploration of the expansion of the overall cell electrospinning time in addition to co-electrospinning may thus provide options to generate tissue patches with an estimated range of thicknesses from 50 μm to upwards of 200 μm.

Controlling the spatial distribution of cells: Electrospun networks with spatially deposited cells have been explored through the addition of a barrier layer to prevent cell-cell mixing or interactions[8]. Prevention of cell mixing within a co-culture scaffold was not specifically explored for POEGMA cell electrospinning, and the generation of POEGMA fibers with varying diameters has also not been closely explored; however, by directly using the techniques discussed herein, the ability to generate multi-layered networks containing a barrier middle layer remains within reach. In this sense, cell-laden networks could be explored to examine the three-dimensional migration of cells as well as the lack of migration of cells in scaffolds with barrier networks. Additionally, the benefits of co-culture models could be further studied with cell electrospinning to see the benefits of cell maturation and differentiation over time, with improved cell maturation previously observed in models with additional supporting cell types[9].

Increasing the number of layers: Finally, building off previously mentioned concepts, the ability to expand this work to fabricate scaffolds with a higher number of tissue layers can be explored. This work has focused specifically on the generation of bilayer tissue structures; however, while keeping the limiting factor of the length of electrospinning into account, any number of layers could be generated containing any desired number of cell types including a combination of layers with mixed co-cultures or single cell types. In this model, cell migration, cell-cell interactions, and functional multi-layered tissues could all be explored. Triple-layer scaffolds have been previously discussed and commonly explored for blood vessel or esophageal tissue engineering in which different layers contain different structural properties and (now) the potential for different cell types and/or alignment throughout the full depth of each layer. These multiple control factors thus

offer an opportunity to examine more complex models not yet to our knowledge seen within electrospun tissue scaffolds[5,8].

Ultimately, the generation of multi-layered, multi-cellular, and tunably aligned scaffolds via reactive cell electrospinning offers a toolbox of techniques that can be explored for fabricating novel tissues and tissue mimics. The successful generation of multi-layered structures without layer delamination, multi-cellular structures with low cytotoxicity, and the formation of new fiber structures showing cell responses highlights the novelty and functionality of POEGMA hydrogel electrospinning for tissue engineering applications and the development of complex three-dimensional cell models.

4.3 References

1 Xu, F., Dodd, M., Sheardown, H. & Hoare, T. Single-Step Reactive Electrospinning of Cell-Loaded Nanofibrous Scaffolds as Ready-to-Use Tissue Patches. *Biomacromolecules* **19**, 4182-4192 (2018).

2 Tan, B., Gan, S., Wang, X., Liu, W. & Li, X. Applications of 3D bioprinting in tissue engineering: advantages, deficiencies, improvements, and future perspectives. *J Mater Chem B* **9**, 5385-5413 (2021).

3 Xu, F. *et al.* Hydrogels for Tissue Engineering: Addressing Key Design Needs Toward Clinical Translation. *Front Bioeng Biotechnol* **10**, 849831 (2022).

4 Xue, J., Wu, T., Dai, Y. & Xia, Y. Electrospinning and Electrospun Nanofibers: Methods, Materials, and Applications. *Chemical Reviews* **119**, 5298-5415 (2019).

5 Huang, R. *et al.* Triple-Layer Vascular Grafts Fabricated by Combined E-Jet 3D Printing and Electrospinning. *Annals of Biomedical Engineering* **46**, 1254-1266 (2018).

6 Fazal, F. *et al.* A modified 3D printer as a hybrid bioprinting-electrospinning system for use in vascular tissue engineering applications. *Med Eng Phys* **94**, 52-60 (2021).

7 Yang, G., Lin, H., Rothrauff, B. B., Yu, S. & Tuan, R. S. Multilayered polycaprolactone/gelatin fiber-hydrogel composite for tendon tissue engineering. *Acta Biomaterialia* **35**, 68-76 (2016).

8 Soliman, S. *et al.* A multilayer scaffold design with spatial arrangement of cells to modulate esophageal tissue growth. *Journal of Biomedical Materials Research - Part B Applied Biomaterials* **107B**, 324-331 (2019).

9 Wu, S., Wang, Y., Streubel, P. N. & Duan, B. Living nanofiber yarn-based woven biotextiles for tendon tissue engineering using cell tri-culture and mechanical stimulation. *Acta Biomaterialia* **62**, 102-115 (2017).

Appendices

Appendix A: Chapter 2 Supplementary Information

Table S2.1. Molecular weight and degree of functionalization of POEGMA precursor polymers.

Polymer	Functional Group	Theoretical Functional Group	Actual Functional Group	M_n	Dispersity Đ
	[-]	[mol %]	[mol %]	[kDa]	[-]
POH	$NHNH_2$[a]	30	32.2	21.5	2.2
POA	CHO[b]	30	29.0	26.8	2.3
POA-RGD	CHO[b]	30	26.9	26.8	2.3
	RGD[b]	3	2.1	-	-

[a]Determined by conductometric titration. [b]Determined by ^{1}H NMR.

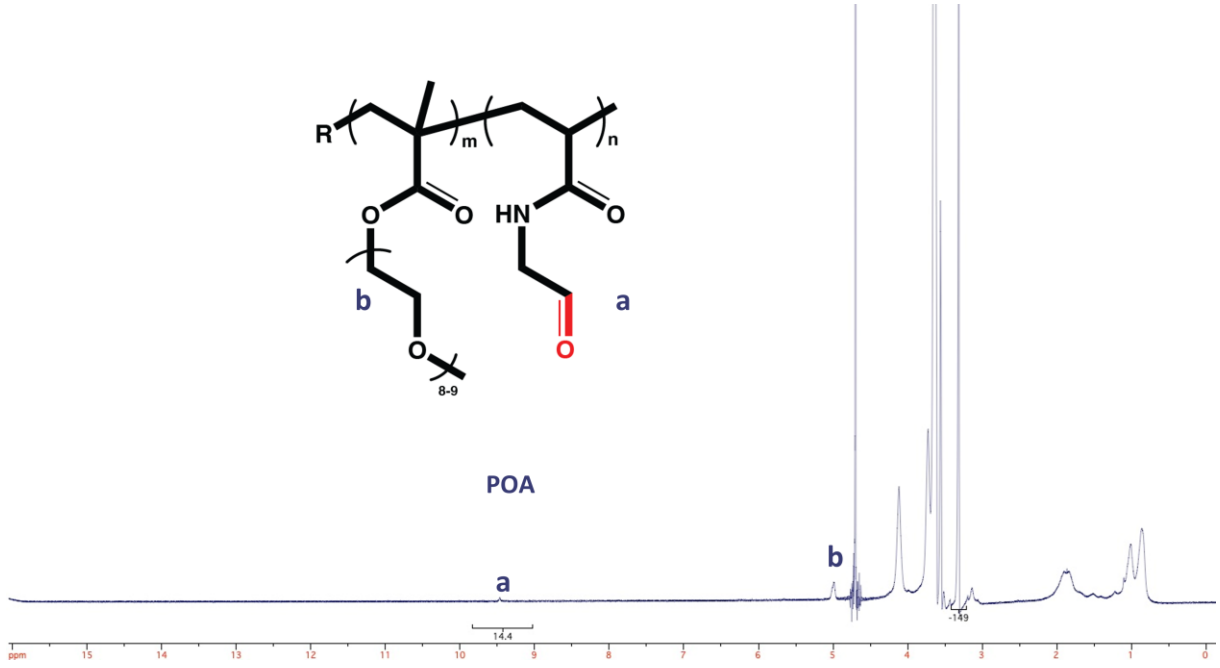

Figure S2.1. ^{1}H NMR spectrum for the precursor polymer POA used for electrospinning experiments.

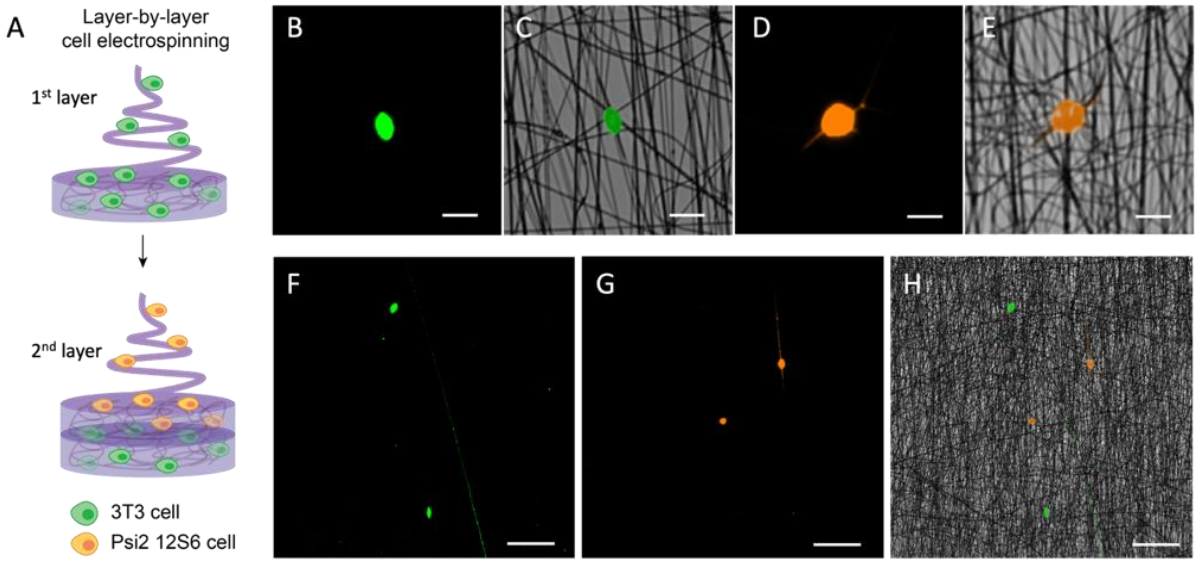

Figure S2.2. Layer-by-layer electrospinning of cellularized nanofiber scaffolds: (A) Schematic of pre-staining 3T3 and Psi2 12S6 cells for layer-by-layer cell electrospinning. (B-E) Representative confocal images of individual cells within POH+POA hydrogel scaffolds via reactive cell electrospinning by prestaining cells with CFSE (B-C, 3T3 cells, green, 488 nm) and Far Red (D-E, Psi2 12S6 cells, orange, 633 nm), respectively. Electrospinning time was 5 mins for each sample. Scale bars = 20 μm. (F-H) Confocal images of two cell types within one POH+POA hydrogel scaffold fabricated via layer-by-layer reactive cell electrospinning by prestaining cells with CFDA-SE (3T3 cells, green, 488 nm) and Far Red (Psi2 12S6 cells, orange, 633 nm), respectively. Electrospinning time was 5 mins for each cell type (total time = 10 mins). Scale bars = 100 μm. All images were taken under dry conditions after cell electrospinning.

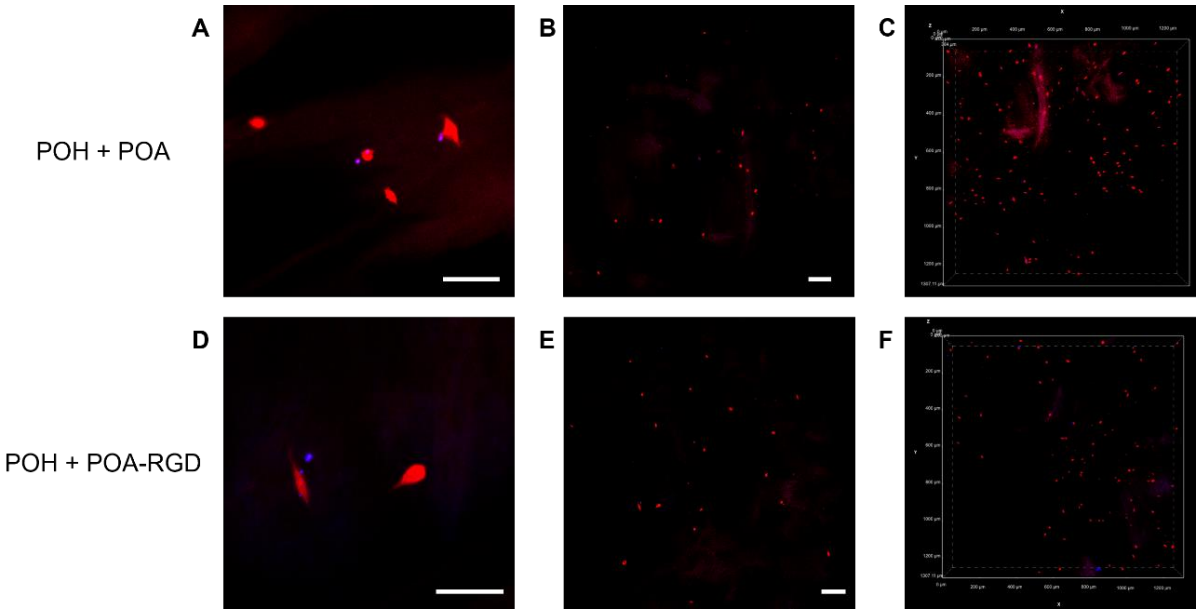

Figure S2.3. Phalloidin (red)-DAPI (blue) staining of co-cultured cells (3T3 and Psi2 12S6 cells) in POH+POA (A-C) and POH+POA-RGD (D-E) electrospun hydrogel scaffolds after 14-day incubation. (A,D) Scale bar = 50 μm. (B,E) Scale bar = 100 μ m.

Appendix B: Chapter 3 Supplementary Information

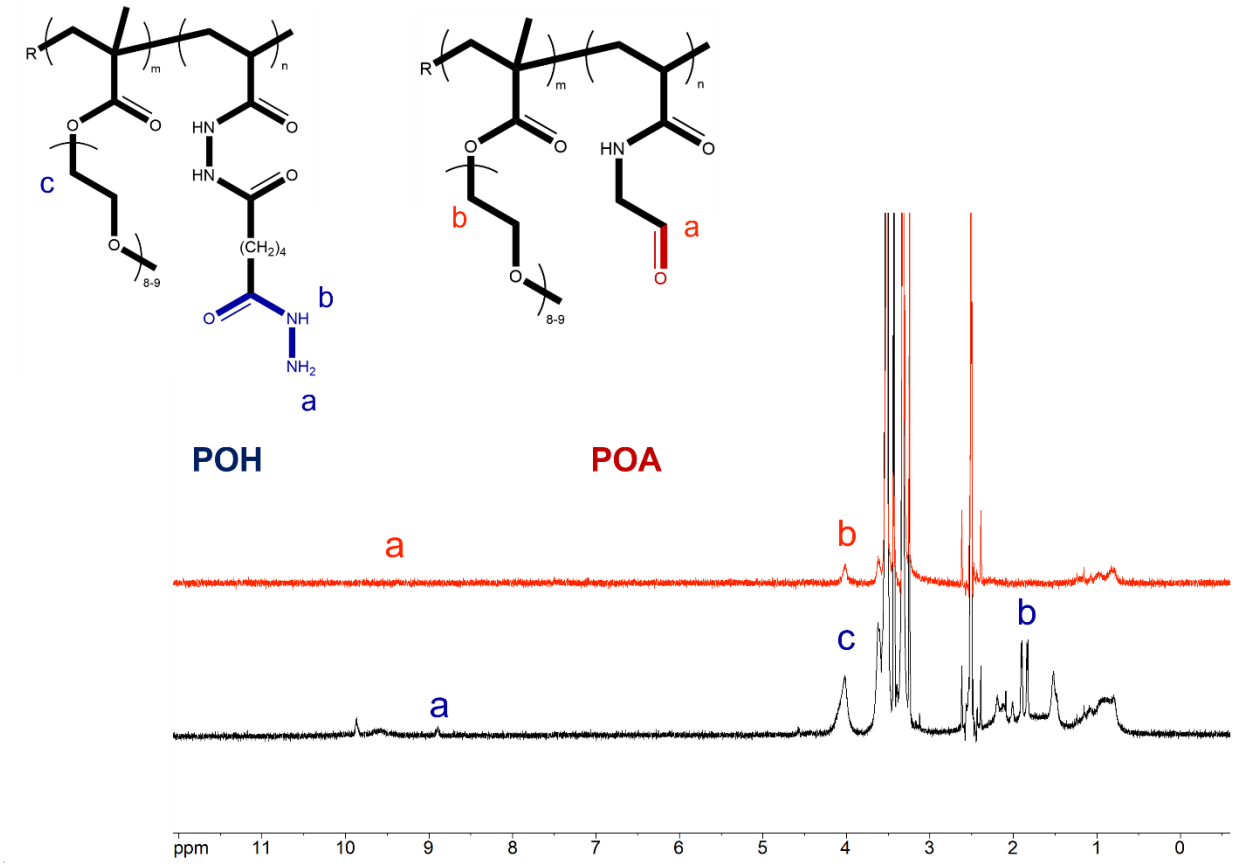

Figure S3.1. ^{1}H NMR spectra of precursor polymers POH and POA used for all electrospinning experiments.

Table S3.1. Characterization of precursor polymers POH and POA used for all electrospinning experiments.

Polymer	M_n	Dispersity	Functionalization
	Da	Đ	mol%
POH	13,500	1.5	20.7
POA	15,500	1.6	18.6

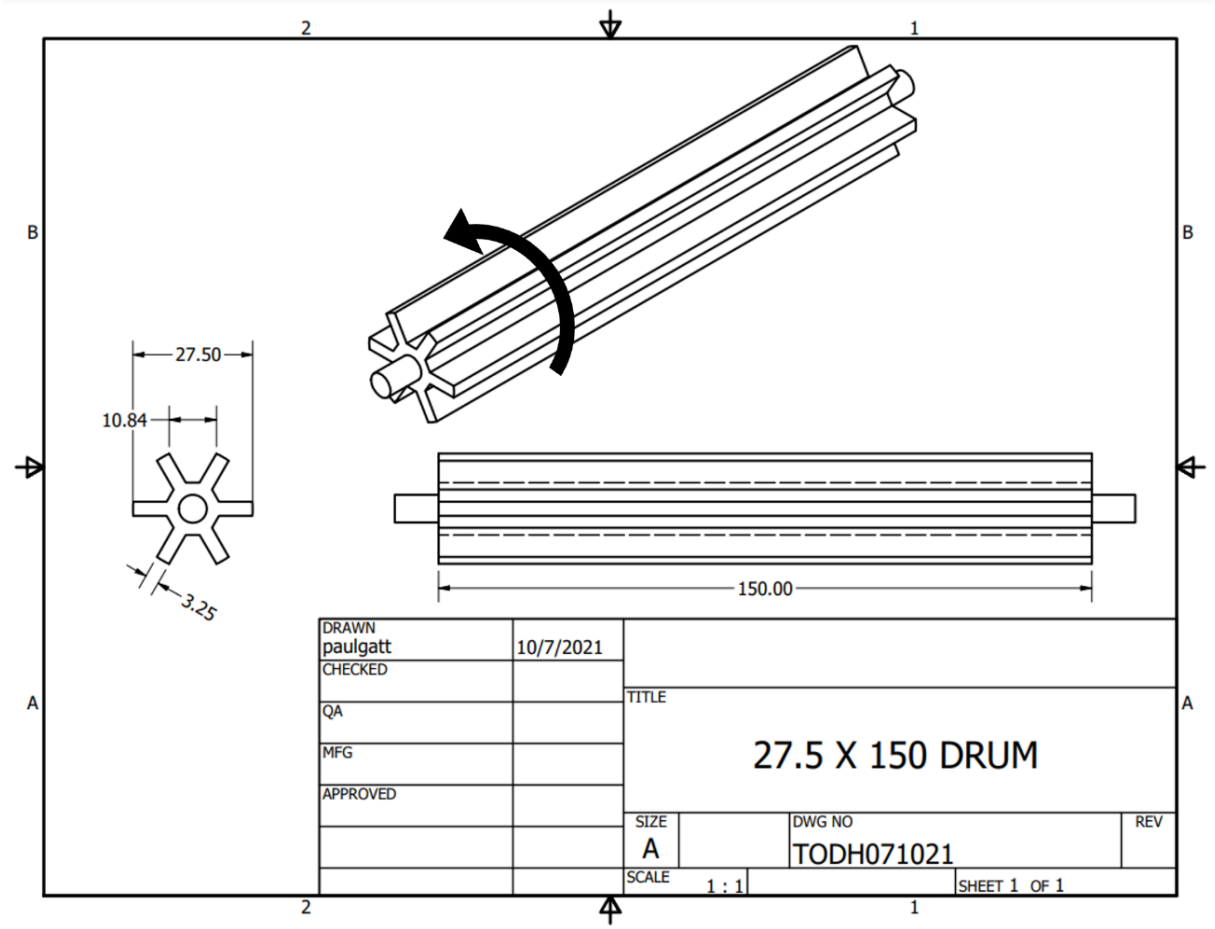

Figure S3.2. Drawings of custom-made cell electrospinning drum with six vanes separated by ~1 cm for aligned fiber collection in cell electrospinning experiments. The arrow represents the direction of drum rotation and thus the radial orientation of deposited fibers.

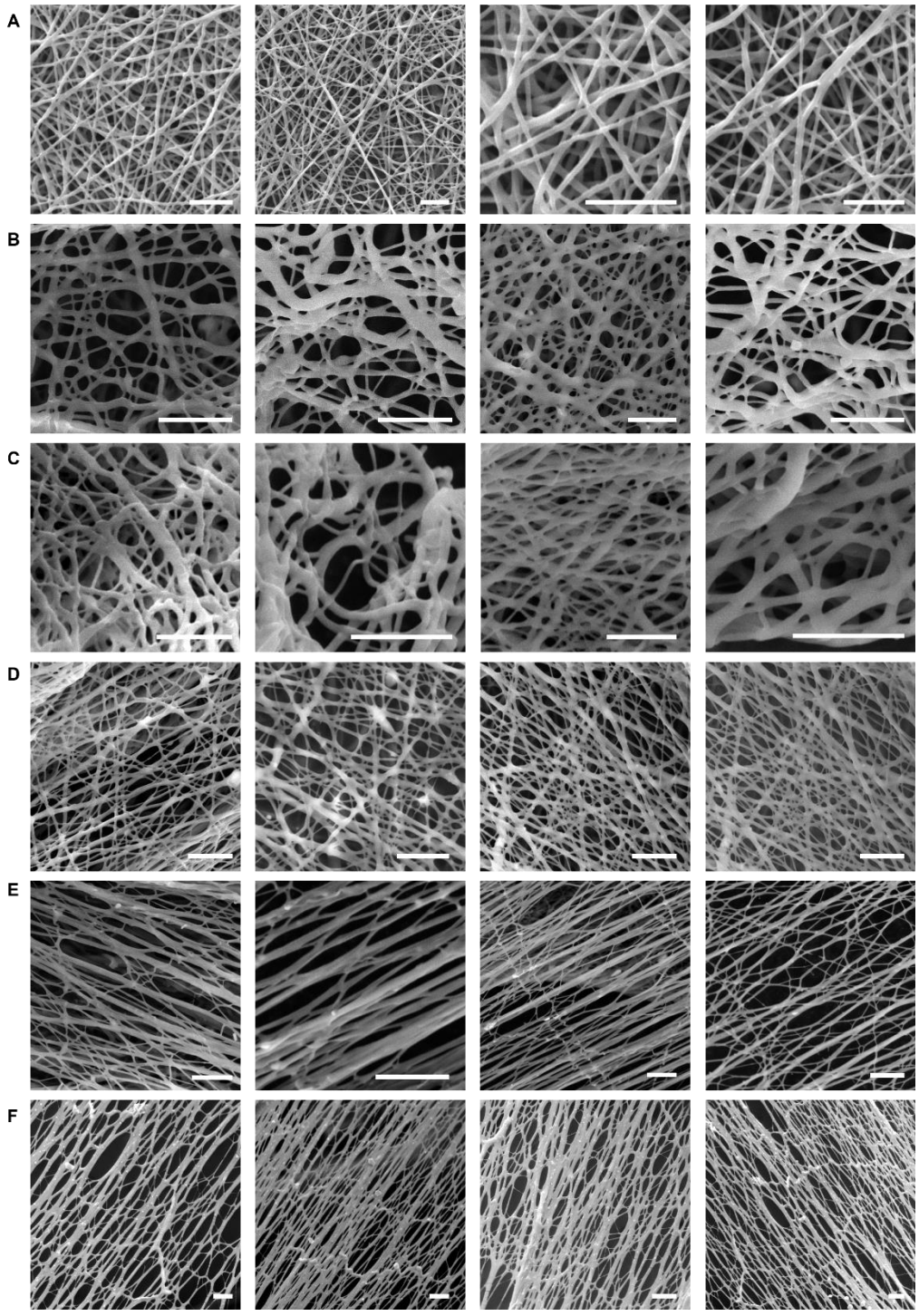

Figure S3.3. Additional SEM images for (A) non-aligned fibers and (B-F) aligned fibers collected at different rotation speeds of (B) 500, (C) 1000, (D) 2000, (E) 3000, and (F) 4000 rpm. Scale bars = 5 μm (note that all images are not at the same magnification, but the scale bars are equivalent between all images).

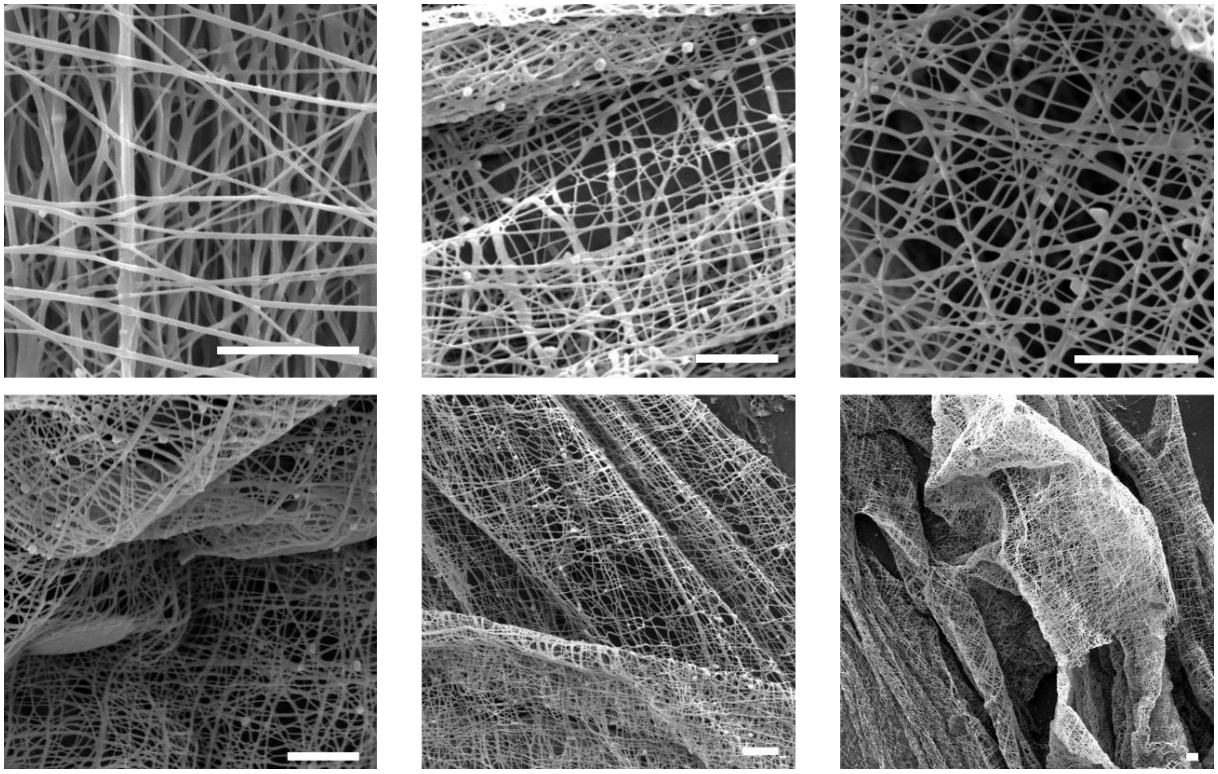

Figure S3.4. SEM images of cross-aligned scaffolds fabricated with a rotating drum at a speed of 3000 rpm. Scale bars = 10μm (note that all images are not at the same magnification, but the scale bars are equivalent between all images).

Table S3.2. Linear regression output data for mechanical tensile testing stress versus strain curves of non-aligned scaffolds analyzed in two perpendicularly oriented with three repeats per sample.

Non-aligned Scaffolds	Modulus (kPa)	Intercept Confidence Interval (kPa)		R^2
		Lower	Upper	
Direction1-1	272	-1.23	-0.90	0.996
Direction1-2	172	-2.09	-1.61	0.977
Direction1-3	366	-2.05	-1.43	0.991
Direction2-1	334	-1.22	-0.87	0.997
Direction2-2	407	-3.51	-2.66	0.987
Direction2-3	459	1.72	2.06	0.998

Table S3.3. Linear regression output data for mechanical tensile testing stress versus strain curves of aligned scaffolds analyzed in two perpendicularly oriented directions with three repeats per sample.

Aligned Scaffolds	Modulus (kPa)	Intercept Confidence Interval (kPa)		R^2
		Lower	Upper	
Direction1-1	476	-0.31	0.08	0.997
Direction1-2	428	-2.52281	-1.87789	0.993
Direction1-3	281	-2.01711	-1.46713	0.988
Direction2-1	101	-0.83356	-0.60604	0.985
Direction2-2	165	-1.77638	-1.35673	0.981
Direction2-3	216	-1.26465	-0.9316	0.992

Table S3.4. Linear regression output data for mechanical tensile testing stress versus strain curves of cross-aligned scaffolds analyzed in two perpendicularly oriented with three repeats per sample.

Cross-aligned Scaffolds	Modulus (kPa)	Intercept Confidence Interval (kPa)		R^2
		Lower	Upper	
Direction1-1	432	-1.50	-0.92	0.995
Direction1-2	236	-2.67	-1.83	0.965
Direction1-3	326	-0.60	-0.23	0.996
Direction2-1	462	-0.89	-0.621	0.999
Direction2-2	333	-0.38	-0.10	0.998
Direction2-3	364	-0.968	-0.65	0.998

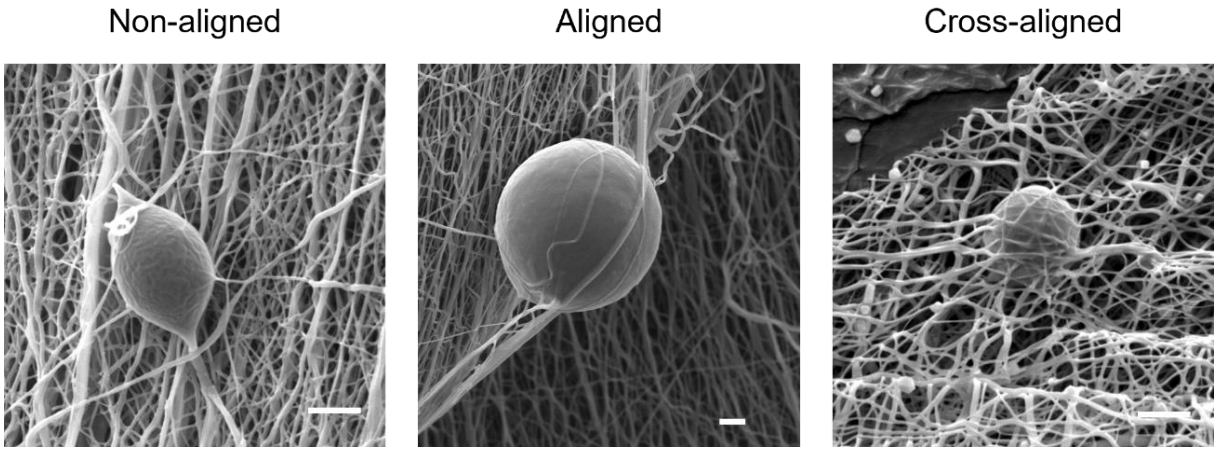

Figure S3.5. SEM images of cell-laden POEGMA hydrogel scaffolds for non-aligned, aligned and cross-aligned scaffolds immediately after electrospinning. Scale bars = 5μm.

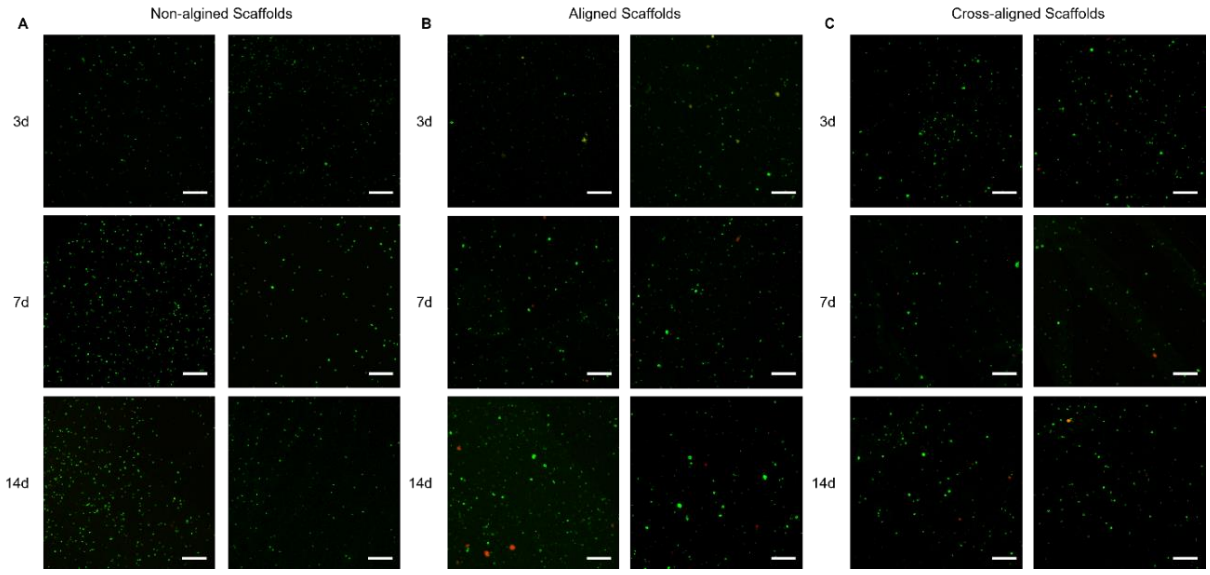

Figure S3.6. Additional confocal LIVE/DEAD assay merged images used to quantify cell viability and density within the cell-laden electrospun scaffolds for non-aligned, aligned, and cross-aligned scaffolds. Quantification was performed on n=3 images per scaffold time per timepoint, including those from Figure 3.6.

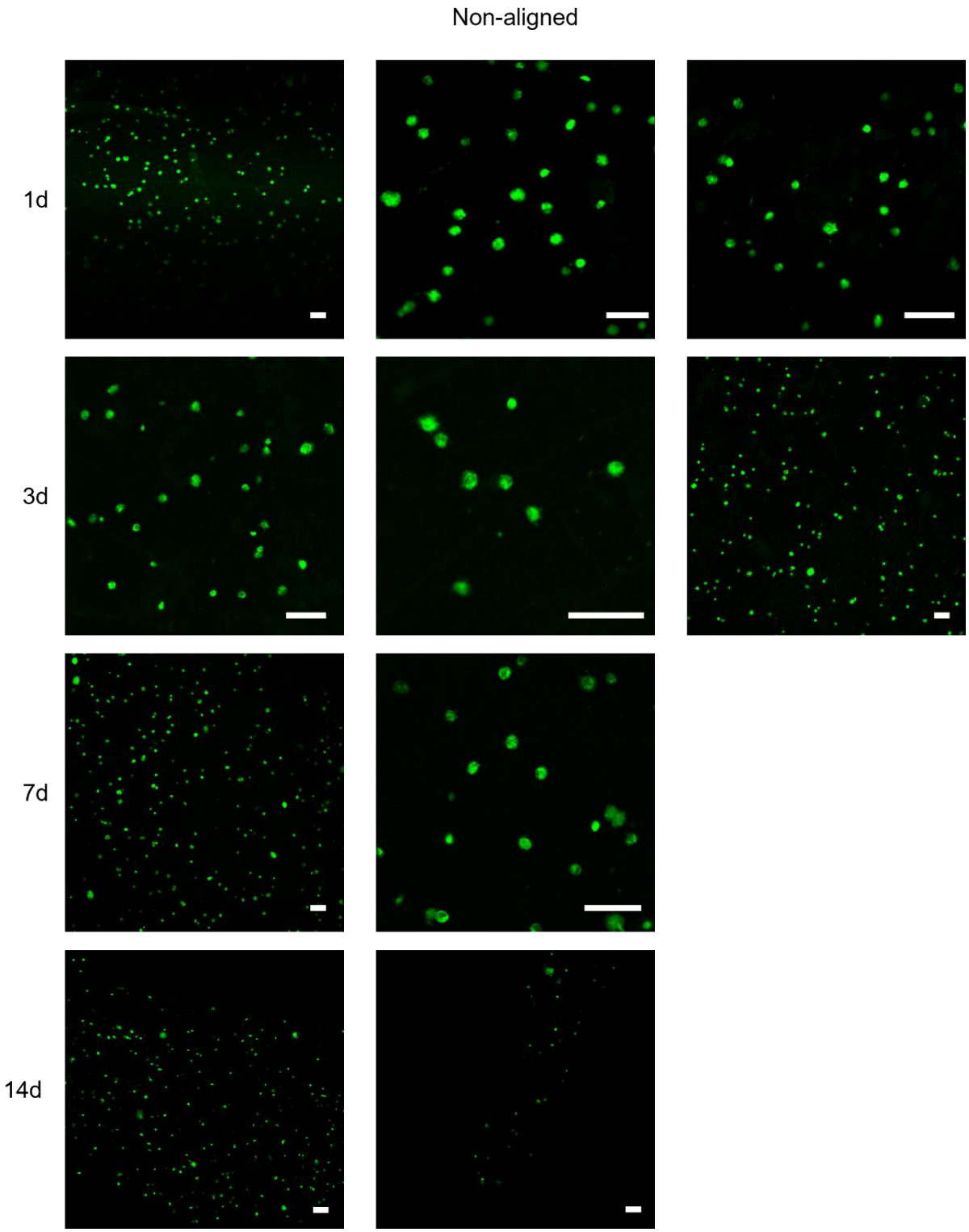

Figure S3.7. Additional images of cell-loaded non-aligned electrospun scaffolds post-stained with CFDA-SE after 1, 3, 7, and 14-days. Quantification of cell aspect ratio was determined based on the number of cells analyzed. Scale bars = 100 μm.

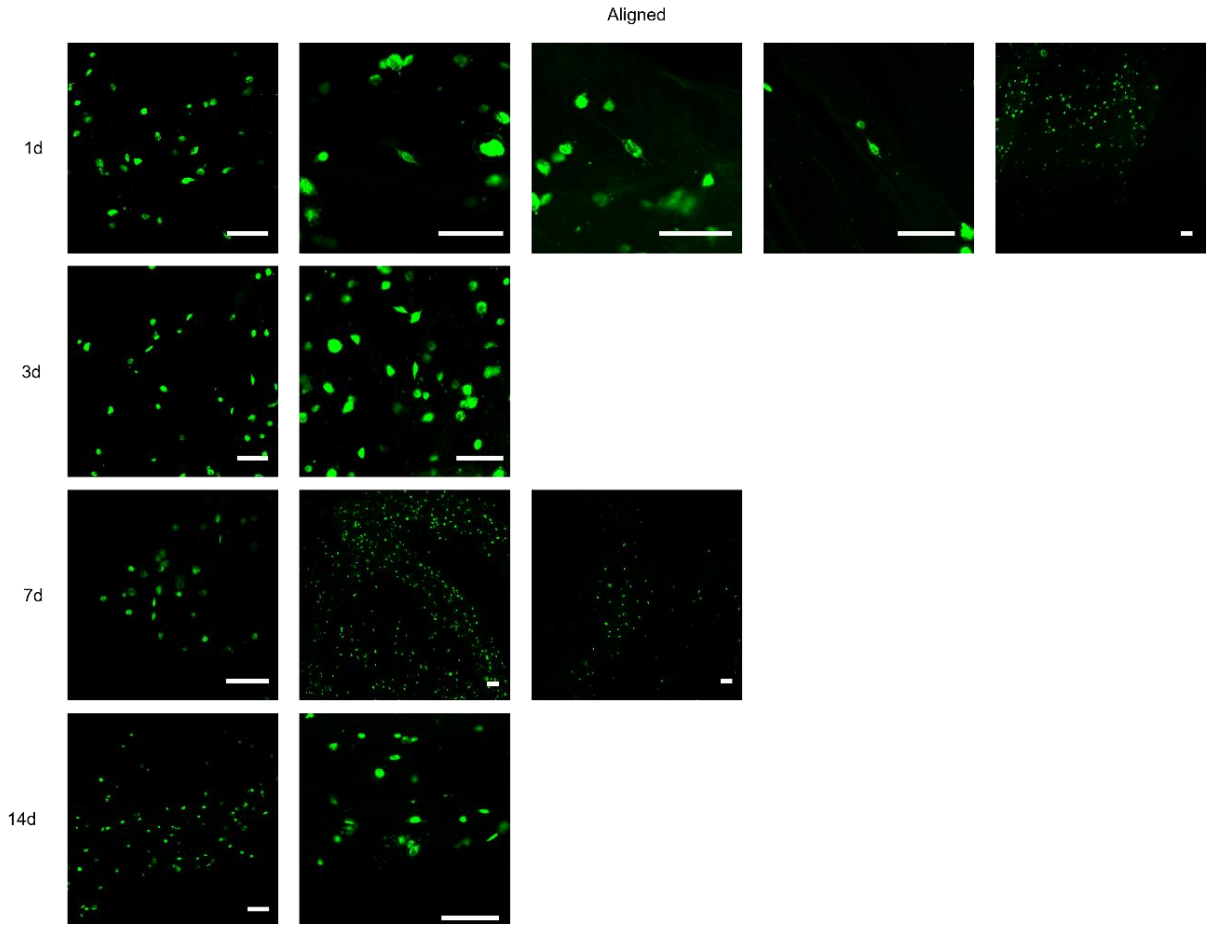

Figure S3.8. Additional images of cell-loaded aligned electrospun scaffolds post-stained with CFDA-SE after 1, 3, 7, and 14-days. Quantification of cell aspect ratio was determined based on the number of cells analyzed. Scale bars = 100 μm.